Nuclear Magnetic Resonance Studies of Dynamical Structure of One-Dimensional Hydrogen-Bonded System in the Acid Salts of Some Dicarboxylic Acids

Keisuke Miyakubo

Osaka University

March 1994

NUCLEAR MAGNETIC RESONANCE STUDIES OF DYNAMICAL STRUCTURE OF ONE-DIMENSIONAL HYDROGEN-BONDED SYSTEM IN THE ACID SALTS OF SOME DICARBOXYLIC ACIDS

by

Keisuke Miyakubo

A DISSERTATION
SUBMITTED TO THE GRADUATE SCHOOL OF
THE FUCULTY OF SCIENCE
OF OSAKA UNIVERSITY
IN PARTIAL FULFILLMENT OF THE REQUIREMENTS
FOR THE DEGREE OF
DOCTOR OF SCIENCE

Osaka University
March 1994

Doctoral Committee:

Professor	Nobuo Nakamura,	Chairman
Professor	Yoshimasa Kyougoku	
Professor	Tadasuke Matsuo	

Acknowledgements

I would like to express sincere thanks to Professor Nobuo Nakamura for his heartful encouragement, a number of valuable suggestions, and his critical reading of this manuscript.

I would like to thank Dr. Sadamu Takeda for introducing me to nuclear magnetic resonance technique, careful instructions, fruitful discussions, and encouragement during my doctral course.

I wish to express my gratitude to Assosiate Professor Taro Eguchi for his many useful comments and encouragement.

I also wish to thank Emeritus Professor Hideaki Chihara for his guidunce to physical chemistry and many helpful suggestions.

I am indebted to Emeritus Professor Hiroshi Suga and Professor Kizashi Yamaguchi for their kindness for me to continue this study. I am encouraged by Dr. Akira Inaba and his suggestion greatly impressed me. Mr. Tetsuo Yamamoto helped my X-ray diffraction experiment. Dr. Hatue Tamura instructed me with respect to crystallographic studies. Professor Tadaoki Mitani of Kanazawa University, Mr. Taro Sekikawa and the other members of Institute for Molecular Sciences collaborated with me about IR study and permitted to use data in this thesis. I would like to acknowledge to their favor.

I am grateful to all members of Condensed Matter Chemistry Laboratory of College of General Education, especially Dr. Qiang Xu and Mr. Tetsuya Kawai for their gracious assistance in my last year in the cource of this study. I am also grateful to all members of Quantum Chemistry Labolatory of Fuculty of Science. I can continue this study with joy due to their friendship and fruitful discussions with them.

Finally I greatly thank my family, especially my parents with my best regard.

Abstract

It has long been known that a number of acid salt crystals of various carboxylic acids contain one-dimensional anionic chains linked by short and symmetric hydrogen bonds. The hydrogen-bonded chain structure is thought to be essential for appearence of various interesting physical properties such as high dielectric constant, finite electrical conductivity, unusual infrared absorption spectrum, existence of phase transition, and so on, in these materials. It is important to investivagate the structure of the hydrogen bond and dynamic behavior of the acidic hydrogens in it for understanding these properties as well as possible relation of short hydrogen bond networks to some biological activities.

The present study examined the structure and dynamic properties of short hydrogen bonds, especially the possible existence of correlated motion so-called solitons, in three crystalline acid salts, *i.e.*, potassium hydrogen telephthalate (KH(tp)), potassium hydrogen acetylenedicarboxylate (KH(adc)), and α-form of rubidium hydrogen acetylenedicarboxylate (α-RbH(adc)), which contain or are believed to contain very short one-dimensional hydrogen-bonded chanis.

First of all, to investigate the detailed geometry of the hydrogen bond in these compounds single crystal X-ray diffraction experiments were carried out on KH(tp) and α-Rb(adc). The hydrogen bond in KH(tp) and α-RbH(adc) are crystallographically symmetric, and very short, *i.e.*, 2.459Å and 2.449Å, respectively. The differential Fourier synthesis map suggested two stable positions of the acidic hydrogen in the hydrogen bond for each of these compounds.

The proton NMR measurements indicated that the dynamic delocalization of the hydrogen takes place within the hydrogen bonds in all of these three compounds. The spin-lattice relaxation rate T_1^{-1} of protons increased with increase in temperature and, in the case of KH(adc), assumed a maximum at relatively high temperature. It is governed obviously by the dipolar interaction between nearby protons which are moving within the respective hydrogen bonds. However, the observed Larmor frequency dependence of T_1^{-1} cannot be interpreted by usual BPP theory for stochastic excitation of molecular or ionic motion.

A model of kink soliton, which is brought about as the limiting case of very strong interaction between the successive hydrogen bonds in the one-dimensional chain, was applied to interpret the observed T_1^{-1}. Although this model was successful to interpreting the frequency dependence of T_1^{-1} in KH(tp) to some extent, there still remains significant discrepancy in the cases of other two materials.

By a close examination of the present hydrogen bond systems, it was found that the unusual behavior of T_1^{-1} of protons in three compounds can be reproduced by a

phenomenological model based on moderately strong soliton-like interaction between the hydrogen bonds.

The models assumes that the kink defects, that is, the state in which some hydrogens are located at their "wrong" sites, in the hydrogen bonded chain are frozen at low temperatures and that the number of such defects is small as can be supposed from the energetic point of view. Providing that at some instance the kink defect proton itself or one of its neighboring protons undergoes a jump in the local double minimum potential; this jump induces fluctuation in the dipolar interaction between protons and this resultant fluctuation transmitts through the chain by the spin-diffusion mechanism, and contributes to T_1^{-1}.

At high temperatures the potential energy functions for the hydrogens in individual hydrogen bonds are strongly modulated in space and time when stochastic jump of hydrogens at or near the kink defect happens to occur. Thus at sufficiently high temperatures some correlated motions of hydrogens in the chain may be induced, responding to the instanteneous variation of their potential energy barriers. Such a situation can be phenomenologically represented by introducing a distribution of the potential energy functions at the local hydrogen bonds. In the present case the Cole-Cole type distribution function for the apparent correlation time of motion was successfully applied to interpret the frequency dependence of T_1^{-1} for each of three materials. In this model the strength of the correlation among the proton motions was evaluated by the magnitude of a parameter δ ($0 < \delta \leq 1$), where the smaller value of delta corresponds to stronger correlation.

The analysis of T_1^{-1} for the three compounds by this "pseudo soliton model" or, in other words, chaotic hydrogen motion model brought about the following results: The activation energy for proton jump near the frozen kink defect in the low temperature region is 520K for KH(tp), 100K for KH(adc), and 150K for RbH(adc); in the high temperature region the apparent activation energy (and the strength of the correlation, delta) for the hydrogen motion is 570K ($\delta = 0.65$) for KH(tp), 2000K ($\delta = 0.3$) for KH(adc), and 900K ($\delta = 0.25$) for RbH(adc). To evaluate the values of these parameters with respect to the formation energy of solitons and rate of soliton transport in other similar materials is, however, a future problem because no such data on solitons are available at the present stage.

It is noted that a linear temperature dependence of the quadrupole coupling constant of acidic deuterium in the hydrogen bond was found by ^{2}H lineshape measurement; this result suggests that the reduction of the hydrogen bond length $R_{O\cdots O}$ occurs on cooling the sample of KD(adc) and RbD(adc). The thermal contraction (or expansion) coefficient of the hydrogen bond length was estimated for KD(adc) to be $\Delta R_{O\cdots O}/\Delta T \sim 1.2\times10^{-4}$Å/K, which is of the order of the thermal expansion coefficient of usual molecular crystals. This

effect may brings about a decrease of the effective activation energy for the hydrogen on cooling and at last the potential energy function for the acidic hydrogen is expected to be pure single minimum one at extremely low temperatures.

Contents

Acknowledgements ii

Abstract iii

1 Introduction 1

2 Samples 4

2.1 Preparation 4

2.1.1 Potassium Hydrogen terephthalate, KH(tp) 4

2.1.2 Potassium hydrogen acetylenedicarboxylate, KH(adc) 4

2.1.3 Rubidium Hydrogen acetylenedicarboxylate, RbH(adc) 5

2.2 Raman spectra of KH(adc) and RbH(adc) 6

2.3 IR spectra of KH(adc) and RbH(adc) 6

2.4 Other specification of samples 14

3 Crystal structure determination 15

3.1 Introduction 15

3.2 Experimental 16

3.3 Potassium hydrogen terephthalate 18

3.3.1 Data collection 18

3.3.2 Structure solution 18

3.3.3 Bond lengths and bond angles 22

3.3.4 Hydrogen bond geometry 22

3.4 Rubidium hydrogen acetylenedicarboxylate 23

3.4.1 Data collection 23

3.4.2 Structure solution 23

3.4.3 Bond lengths and bond angles 25

3.4.4 Hydrogen bond geometry 29

4 NMR line shape 32

4.1 ^{2}H NMR 32

4.1.1 Introduction 32

4.1.2 Experimental 34

4.1.3 Results and Discussion 34

4.2 ^{1}H high-resolution spectra 41

4.2.1 Introduction 41

4.2.2 Experimental 41
4.2.3 Results and Discussion 42
4.3 ^{87}Rb NMR 44
4.3.1 Introduction 44
4.3.2 Experimental 44
4.3.3 Result and discussion 45

5 ^{1}H spin-lattice relaxation and dynamics **50**
5.1 Effect of molecular motion on T_1 50
5.2 Effect of kink soliton on ^{1}H-T_1 52
5.2.1 The concept of the kink soliton in a hydrogen bonded chain 52
5.2.2 Spin relaxation by kink-promoted hydrogen atom motion 53
5.3 Experimental 57
5.4 Results 58
5.5 Discussion 62
5.5.1 Kink soliton model 70
5.5.2 Pseudo kink soliton model 74

Bibliography **80**

Appendix **84**

A Lists of structure factors **84**

List of Tables

3.1 Experimental details of X-ray diffraction 17
3.2 Experimental details of X-ray diffraction of KH(tp) 19
3.3 Final least squares parameters of KH(tp) 20
3.4 Atomic coordinates for KH(tp). 20
3.5 Temperature factors for KH(tp). 20
3.6 Bond distances and bond angles in KH(tp) 22
3.7 Hydrogen bond geometry in KH(tp) 22
3.8 Experimental details of X-ray diffraction of RbH(adc) 24
3.9 Final least squares parameters of RbH(adc) 25
3.10 Atomic coordinates for RbH(adc) 26
3.11 Temperature factors for RbH(adc) 27
3.12 Bond distances and bond angles in RbH(adc) 27
3.13 Hydrogen bond geometry in RbH(adc) 30
4.1 Calculated of e^2Qq/h and η of ^{2}H in KD(adc) 34
4.2 ^{1}H chemical shifts of acid proton in some short symmetric hydrogen bonds in solid 43
5.1 Fitting parameters used in the fitting by pseudo kink model 75
A.1 List of structure factors for KH(tp) 84
A.2 List of structure factors for RbH(adc) $C2/c$, Half hydrogen model 91

List of Figures

1.1 Hydrogen bonded network in dicarboxylic acid and it's acid salt 2
2.1 X-ray powder diffraction pattern for KH(adc) 5
2.2 X-ray powder diffraction patterns for RbH(adc) and RbD(adc) 7
2.3 Raman spectra of KH(adc) and KD(adc) 8
2.4 Raman spectra of RbH(adc) and RbD(adc) 9
2.5 Variation of Raman spectrum of KH(adc) with deuteration ratio 10
2.6 IR spectra of KH(adc). 11
2.7 IR spectra of KD(adc). 12
2.8 IR spectra of RbH(adc). 13
3.1 ORTEP-plot of ***b***-axis projection of KH(tp). 21
3.2 ORTEP-plot of ***c***-axis projection of RbH(adc). 28
3.3 ORTEP-plot of ***b***-axis projection of RbH(adc). 29
3.4 Coordination scheme around Rb^+ in RbH(adc) 30
4.1 Some typical ^{2}H-NMR line shapes of powder sample. 33
4.2 ^{2}H line shape of KD(adc) 35
4.3 ^{2}H line shape of K($H_{0.5}D_{0.5}$)(adc) 36
4.4 ^{2}H line shape of RbD(adc) 37
4.5 Temperature dependence of e^2Qq/h and η of ^{2}H in KD(adc). 38
4.6 $\Delta\nu$ of ^{2}H line shape 39
4.7 MREV-8 pulse sequence 42
4.8 ^{1}H-CRAMPS spectrum of KH(tp). 43
4.9 Energy level diagram of $I = 3/2$ nucleus under strong magnetic field 45
4.10 NMR spectra of the central transition of a nucleus with half odd spin. . . . 46
4.11 ^{87}Rb line shape of RbH(adc) 47
4.12 Arrhenius plot of ^{87}Rb-T_1^{-1} of RbH(adc) and RbD(adc) 48
4.13 Log-log plot of ^{87}Rb-T_1^{-1} of RbH(adc) and RbD(adc) 49
5.1 A pictorial description of the concept of a kink soliton 54
5.2 Scheme on the field cycling experiment. 58
5.3 Recovery curves of ^{1}H magnetization of KH(tp) powder 59
5.4 Recovery curves of ^{1}H magnetization of KH(adc) powder 60
5.5 Recovery curves of ^{1}H magnetization of RbH(adc) powder 61
5.6 ^{1}H-T_1^{-1} of KH(tp) powder 63
5.7 ^{1}H-T_1^{-1} of KH(adc) powder 64
5.8 ^{1}H-T_1^{-1} of RbH(adc) powder 65
5.9 ω_L dependence of ^{1}H-T_1^{-1} of KH(tp) by field cycling 66

5.10 Arrhenius plot of ^{1}H-T_1^{-1} of KH(tp) in high temperature region 67
5.11 Arrhenius plot of ^{1}H-T_1^{-1} of KH(adc) in high temperature region 68
5.12 Arrhenius plot of ^{1}H-T_1^{-1} of RbH(adc) in high temperature region 69
5.13 Fitting of ^{1}H-T_1^{-1} of KH(tp) by soliton model 71
5.14 Fitting of ^{1}H-T_1^{-1} of KH(adc) by soliton model 72
5.15 Fitting of ^{1}H-T_1^{-1} of RbH(adc) by solito model 73
5.16 Fitting of ^{1}H-T_1^{-1} of KH(tp) by pseudo soliton model 76
5.17 Fitting of ^{1}H-T_1^{-1} of KH(adc) by pseudo soliton model 77
5.18 Fitting of ^{1}H-T_1^{-1} of RbH(adc) by pseudo soliton model 78

Chapter 1
Introduction

Hydrogen bond plays very important roles in many substances such as water, ice, ferroelectric crystals, protein, nucleic acid and other many molecular aggregates. In these substances it is considered that their structure and physical properties are greatly influenced by hydrogen bond between molecules or ions. Hydrogen bonds are much stronger than usual intermolecular forces and have distinctive directionality. Therefore the hydrogen bond often causes many interesting phenomena. The hydrogen bond length ($R_{O\cdots O}$) in O–H$\cdots$O varies widely from 3.0Å to 2.4Å. Physical properties of hydrogen bond also vary as the length varies. One of the most representative properties is the potential energy the hydrogen experiences. Because of these interesting nature and importance the hydrogen bond has been studied from various points of view over a long time.

In solid state hydrogen bonds often make the network of molecules or ions connected by hydrogen bonds. Such a hydrogen bonded network has been investigated actively in relation to the physical property, dielectric behavior, phase transition and so on of solid state. In one-dimensional hydrogen bonded network, especially the existence of cooperative mode has been a controversial problem for a long time. This was firstly proposed to explain the ionic conductivity of ice, which was known to show high ionic conductivity in the direction along the hydrogen bonded chain. In this explanation an ionic defect is represented as the center of a kink soliton, which is extended over many hydrogen bond cites. Ionic conduction along the hydrogen bonded chain could be interpreted as the translational motion of this kink soliton along the chain. This kink soliton is generated by relatively strong coupling between neighboring hydrogen atoms in the chain.

Many theoretical studies have been done to describe properties of such a kink soliton [1–3]. In spite of many efforts, the existence of kink soliton is not clear so far. Most of studies about hydrogen bonded chain are concerned with ice $\cdots$O–H$\cdots$O system. However experimental studies of other hydrogen bonded chain were performed by several researchers. Blanchet *et al.* proposed kink soliton mechanism to explain IR spectra of acetanilide [4]. Moritomo *et al.* suggested the existence of trapped kink soliton in molecular chain of β-diketones from their optical spectra [5].

Acid salt is the salt in which a part of acid hydrogens are substituted by other cations. The remaining acid hydrogens form short hydrogen bonds with negatively charged anions. Many acid salts of dicarboxylic acid form the one-dimensional infinite chain connected by hydrogen bonds in the crystalline state. Double hydrogen bonds connect carboxyl groups in the crystal of dicarboxylic acid On the other hand, a single hydrogen

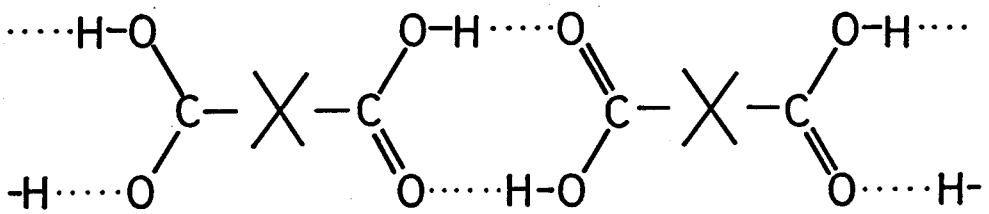

Double hydrogen bond connection in dicarboxylic acid crystal

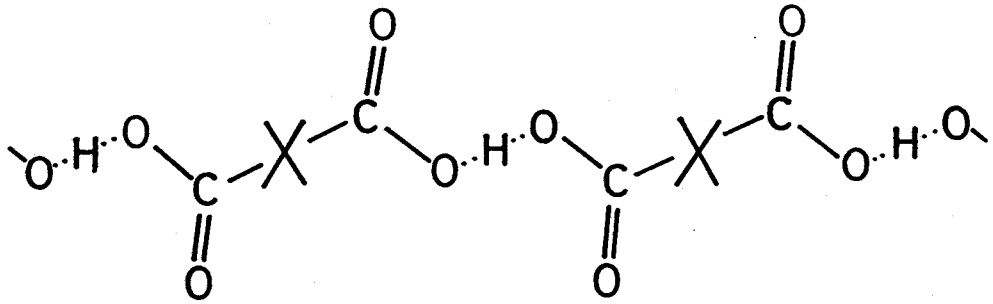

Single hydrogen bond connection in acid salt of dicarboxylic acid

Figure 1.1: Hydrogen bonded network in dicarboxylic acid and it's acid salt

bond connects carboxylate anions in an acid salt crystal. In the double hydrogen bond of dicarboxylic acid it is found that the simultaneous double proton transfer can take place. But the dynamics in one-dimensional hydrogen bonded chain in an acid salt has not yet been investigated. Its one-dimensional chain structure suggests the existence of a cooperative mode, so called "kink soliton". In the present study the dynamics of hydrogen atom in acid salts of dicarboxylic acids are investigated with the view of this cooperative mode.

The static and dynamic properties of the hydrogen bond are dominated by the potential energy function for the hydrogen atom in hydrogen bond. The potential energy function has double-minima in a long hydrogen bond. The potential barrier between two wells becomes smaller as the hydrogen bond length becomes shorter. It is considered that the potential energy function tends to have a single minimum in the very short hydrogen bond being less than 2.47Å (called a critical length which was derived as the criterion for the existence of phase transition). Structural properties of hydrogen bond in acid salts of carboxylic acid have been investigated since 1960s by several researchers, particularly by Speakman and co-workers. Hydrogen bonds connecting dicarboxylate anions belong to short hydrogen bonds and have similar or shorter lengths to the critical length. In these

old studies it is concluded that the hydrogen atom locates at the midpoint of a single-minimum hydrogen bond. Therefore dynamic properties of hydrogen bond in an acid salt of carboxylic acid have not been considered, because of the single-well potential character expected in such a short hydrogen bond. But some recent experimental observations [6–13] pointed out that the problem concerning the potential function in acid salts has not solved yet, and that very close examination of a so-believed single minimum hydrogen bond (see section 3.1) and its dynamical properties are required.

Acetylenedicarboxylic acid and terephthalic acid are typical dicarboxylic acids with rigid linear molecular frame with two carboxyl groups on its both sides. It is expected that the rich π-electrons in the acid anions would be effective influences between neighboring hydrogen bonds. In the present study potassium hydrogen acetylenedicarboxylate (KH(adc)), rubidium hydrogen acetylenedicarboxylate (RbH(adc)), and potassium hydrogen terephthalate (KH(tp)) were chosen as model compounds to study the dynamics of the hydrogen bonded chain of acid salts of dicarboxylic acid. The structures of RbH(adc) and KH(tp) was determined by single crystal X-ray diffraction (Chapter 3). To characterize the hydrogen bonds in these materials, ^{1}H and ^{2}H NMR spectra were measured. Observed spectra are compared with the previous data about NMR spectra of hydrogen bonded system investigated by a number of researchers [14] (Chapter 4). Finally dynamics of hydrogen atoms in these hydrogen bonded materials were investigated by measuring the spin-lattice relaxation rate of ^{1}H (Chapter 5).

Chapter 2

Samples

2.1 Preparation

2.1.1 Potassium Hydrogen terephthalate, KH(tp)

Potassium hydrogen terephthalate (KH(tp)) was prepared by the similar method to the Cobbledick's preparation of ammonium hydrogen terephthalate (NH_4H(tp)) [15]. KOH was dissolved in mixed solvent of H_2O and *N,N*-dimethylformamide (DMF). The solution of KOH was poured slowly into the DMF solution of the stoichiometric amount of terephthalic acid (TPA). The white powders were precipitated immediately. Recrystallization of the precipitates from the 1:1 mixed solvent of H_2O and DMF by slow cooling from *c.a.* 80°C brought about colorless needle like crystals. Chemical analysis found: C,47.17%; and H,2.56%; calculated for $C_8H_5O_4K$: C,47.05%; H,2.47%. An X-ray diffraction study found that it is isomorphous to ammonium hydrogen terephthalate (see section 3.3).

2.1.2 Potassium hydrogen acetylenedicarboxylate, KH(adc)

Potassium hydrogen acetylendicarboxylate (KH(adc)) was purchased from Tokyo-Kasei Inc. and recrystalized by slow cooling of *c.a.* 45°C saturated *aq.* solution. KH(adc) was slightly unstable to heat and light. Especially above 50°C in *aq.* solution decomposition occurred with generation of gas. Therefore specimen was recrystalized very carefully. The specimen was identified by chemical analysis which found: C,31.62%; and H,0.84%; calculated for C_4HO_4K: C,31.5%; H,0.66%. The X-ray powder diffraction pattern coincided with calculated ones (according to lattice constants of Leban *et al.* [16]) within the experimental error.

(Partial) deuteration of KH(adc) was carried out by evapolation of (partially) deuterated aq. solution of KH(adc) in vacuo. In the subsequent chapters the percentage of deuteration means the atomic percentage of deuteron in the source aq. solution. Raman spectrum varied with the extent of deuteration (see section 2.2). This observation indicated that the specimen is homogeneously deuterated.

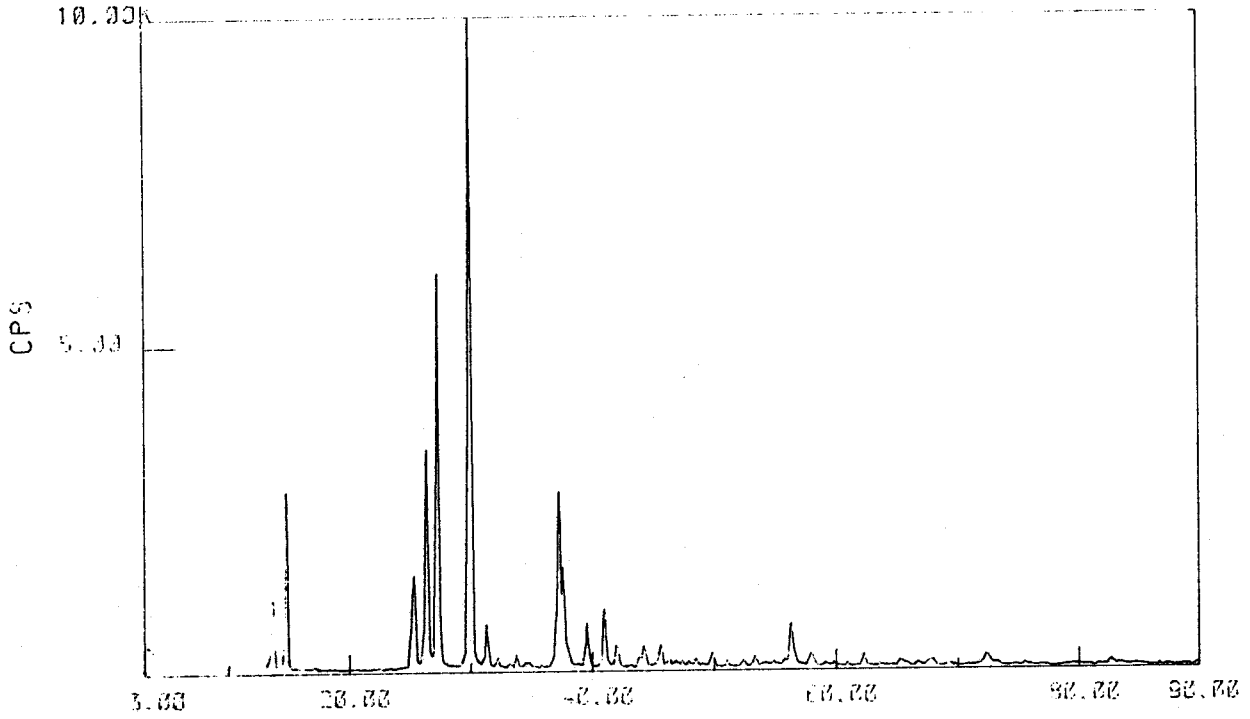

Figure 2.1: X-ray powder diffraction patterns for KH(adc), using Cu-K_α radiation.

2.1.3 Rubidium Hydrogen acetylenedicarboxylate, RbH(adc)

Anhydrous acetylenedicarboxylic acid (ADCA) was purchased from Aldrich Inc. and purified by vacuum sublimation. RbH(adc) *aq.* solution was prepared by adding the stoichiometric amount of ADCA powder to Rb_2CO_3 *aq.* solution. After filtering the solution to remove a trace of insoluble impurities, RbH(adc) was crystallized by slow cooling of concentrated solution. Chemical analysis found: C,24.19%; and H,0.55%; calculated for C_4HO_4Rb: C,24.20%; H,0.51%. For RbH(adc) two modifications were reported at room temperature, *i.e.,* monoclinic α-form and triclinic β-form [17]. Structural analysis revealed that the latter has an asymmetric (type B_2) hydrogen bond [17]. The complete structure of the former has not been solved yet, but the powder diffraction pattern indicates that the α-form is isomorphous with KH(adc) [17]. X-ray powder diffraction of the present specimen resembles KH(adc)'s and peak positions coincide with those of α-form [17] within the experimental error. It was therefore concluded that the specimen of RbH(adc) in this work is the α-form. In this work it was also found that the α-form RbH(adc) is isomorphous to KH(adc) crystal by a single crystal X-ray diffraction experiment (see section 3.4). Deuteration of RbH(adc) was also done by the same way as in KH(adc). Chemical analysis for full(99%) deuterated sample (RbD(adc)) found: C,24.08%; and D(H),1.04%; calculated for $C_4D_{0.99}H_{0.01}O_4Rb$: C,24.08%; D(H),1.00%. The powder X-ray diffraction

pattern of RbD(adc) was not changed significantly by deuterarion (Fig. 2.2). Deuterated compound was also confirmed to be the α-modification.

2.2 Raman spectra of KH(adc) and RbH(adc)

Raman spectra of (adc) acid salts and their deuterated crystals were observed. Fig. 2.3 and Fig. 2.4 show the results for (deuterated) KH(adc) and RbH(adc), respectively. Spectra of KH(adc) and RbH(adc) resemble each other. The bands in the region 900-500 cm^{-1} varied with the extent of deuteration. For KH(adc) the enlarged spectra in this region are shown in Fig. 2.5. As the deuteration proceeded, the intensity of the peak at 829cm^{-1} was reduced and a new peak appeared at 802cm^{-1} and its intensity increased. This seems to show the successful deuteration over the specimen. In the 500-800cm^{-1} region a complex change in the spectra was also observed. Delarbre *et al.* observed the Raman spectra of *aq.* solution of KH(adc) and KD(adc) [18]. According to their assignment, the bands at 829 and 802cm^{-1} are ν(C-COOH) and ν(C-COOD) [1] respectively. In addition several significant differences were seen between spectra in crystal and solution. These are considered to be due to the difference of the molecular symmetry. In solution the $HC_4O_4^-$ anion has planar C_s symmetry [18].

2.3 IR spectra of KH(adc) and RbH(adc)

IR spectra of MH(adc) were measured in collaboration with T. Sekikawa and T. Mitani of the Institute of Molecular Science. Measured spectra by FT-IR using KBr disks are shown in Figs. 2.6-2.8. These spectra have typical characteristics of the short type *A* hydrogen bonds [19,14].

1. ν_{O-H} appears in very low frequency region between 500–1000cm^{-1} where $\nu_{a(OHO)}$ appears.

2. ν_{O-H} forms an extremely broad band.

3. Transmission windows can be observed.

Significant temperature dependence in C=O and C–O vibration regions (near 1700cm^{-1} and 1300cm^{-1} respectively) was observed in KH(adc) and RbH(adc).

[1] They appeared at 825 and 820cm^{-1} in *aq.* solution.

(a) Normal RbH(adc)

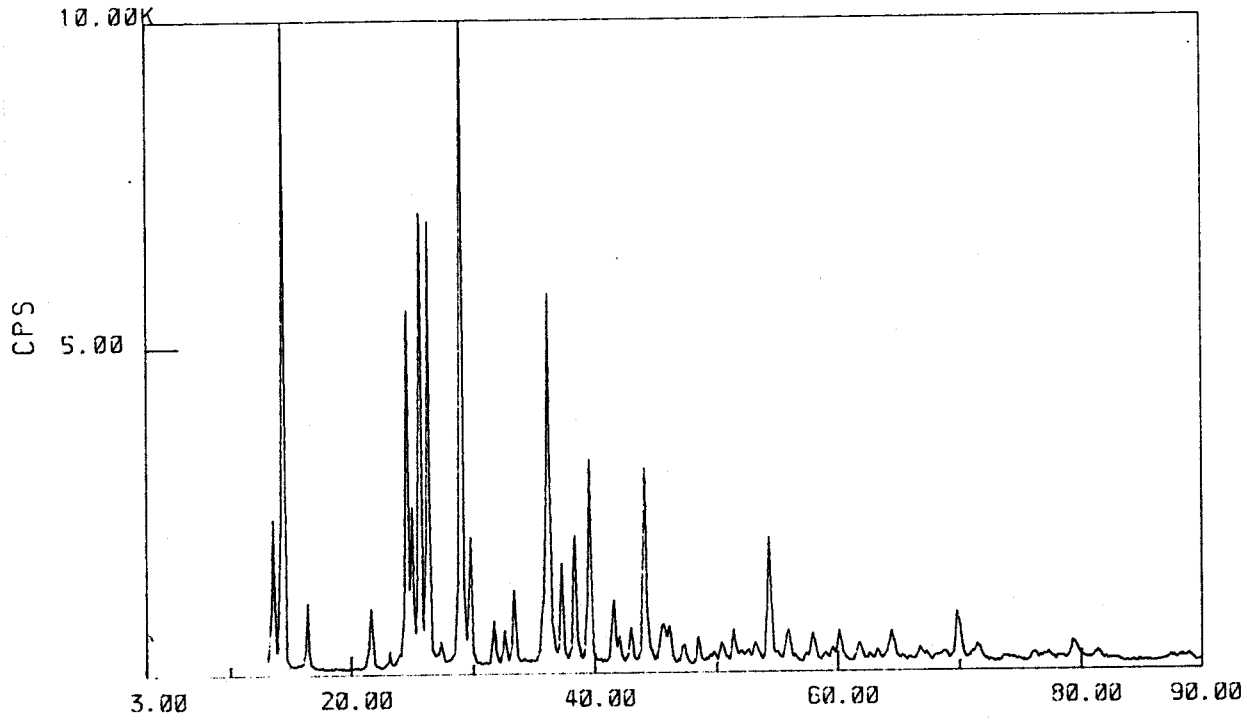

(b) Deuterated RbH(adc)

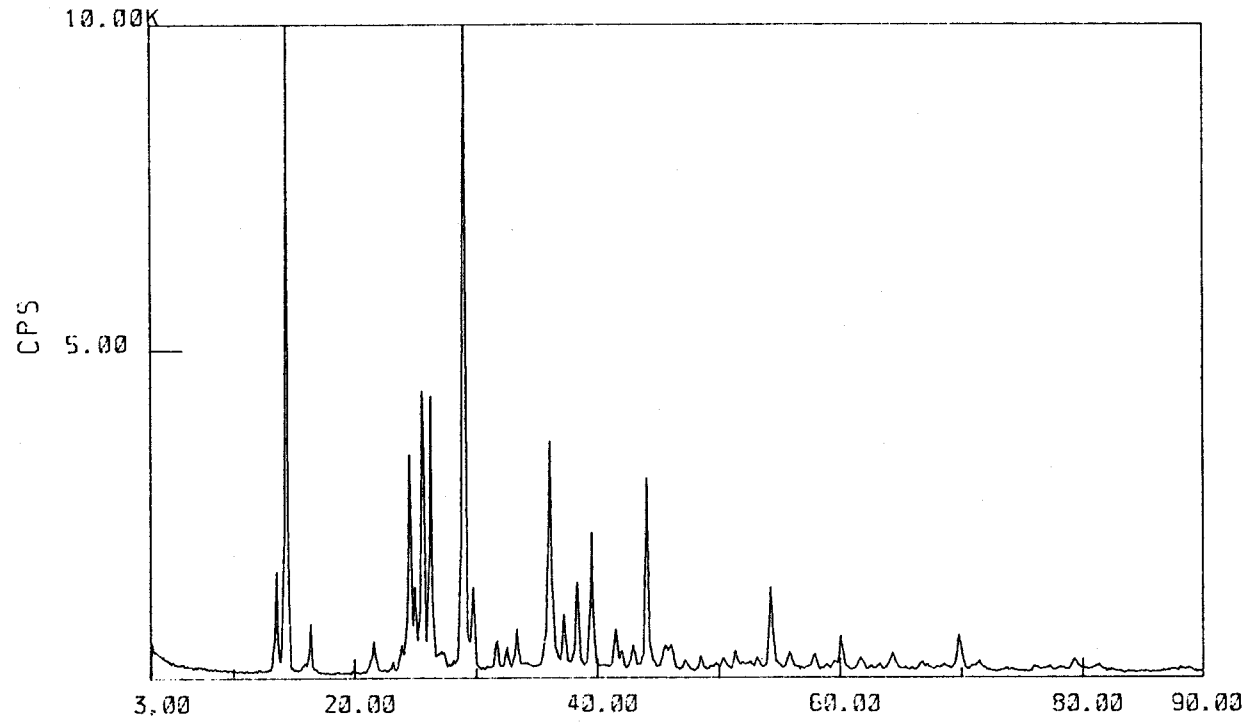

Figure 2.2: X-ray powder diffraction patterns for (a) RbH(adc), (b) RbH(adc)-99%d, using Cu-K_α radiation.

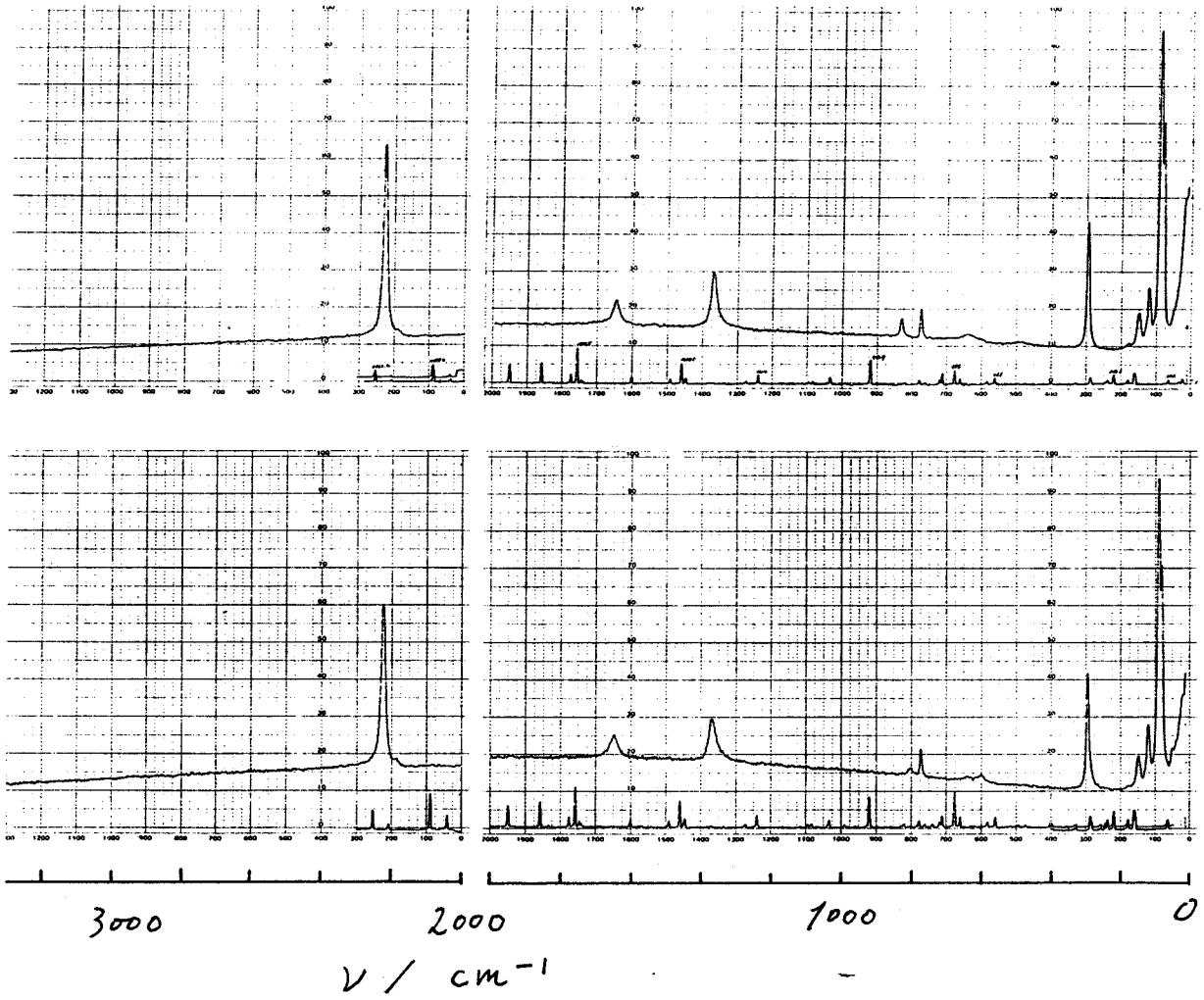

Figure 2.3: Raman spectra of KH(adc):top and KH(adc)-99%*d*:bottom.

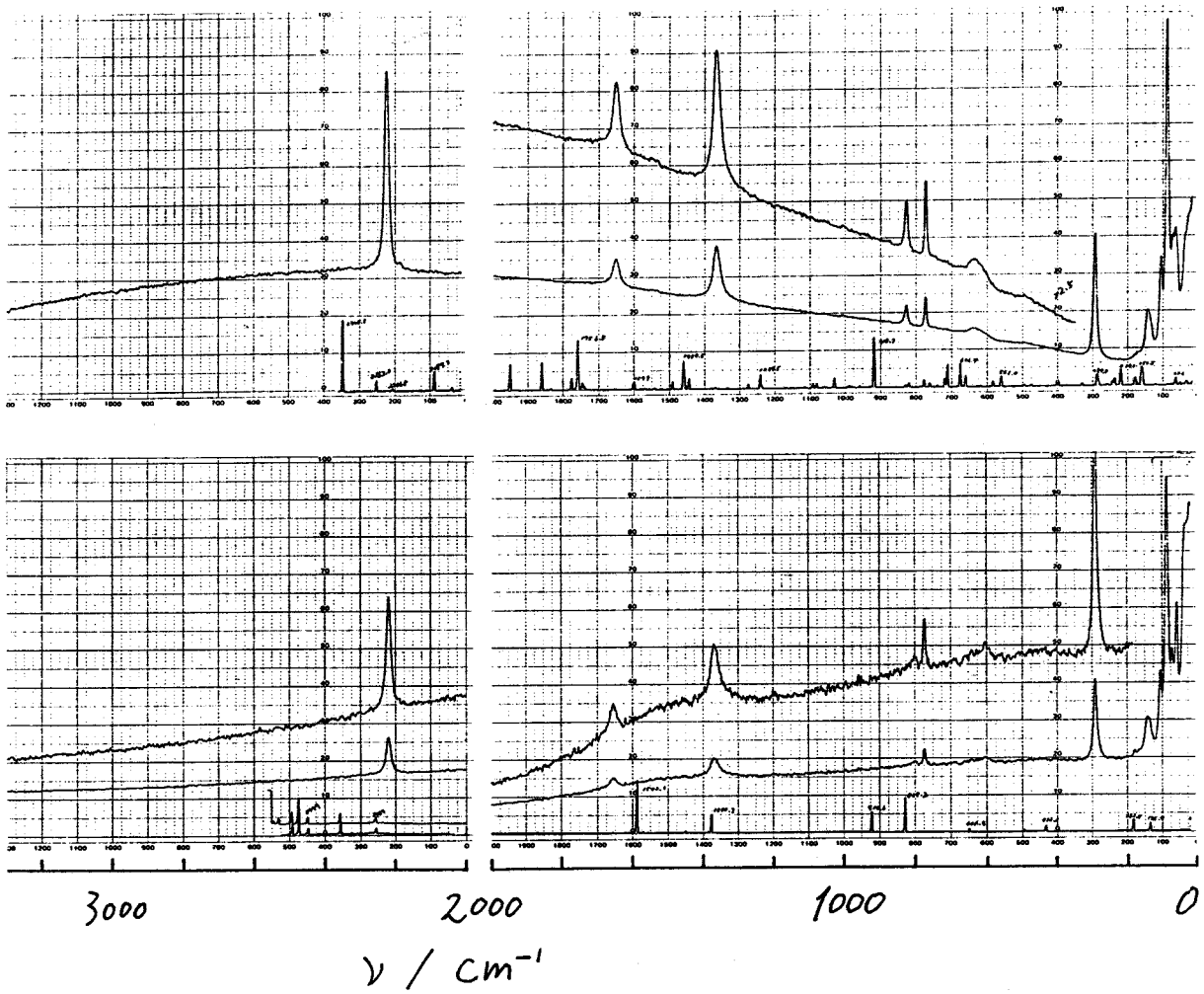

Figure 2.4: Raman spectra of RbH(adc):top and RbH(adc)-99%*d*:bottom.

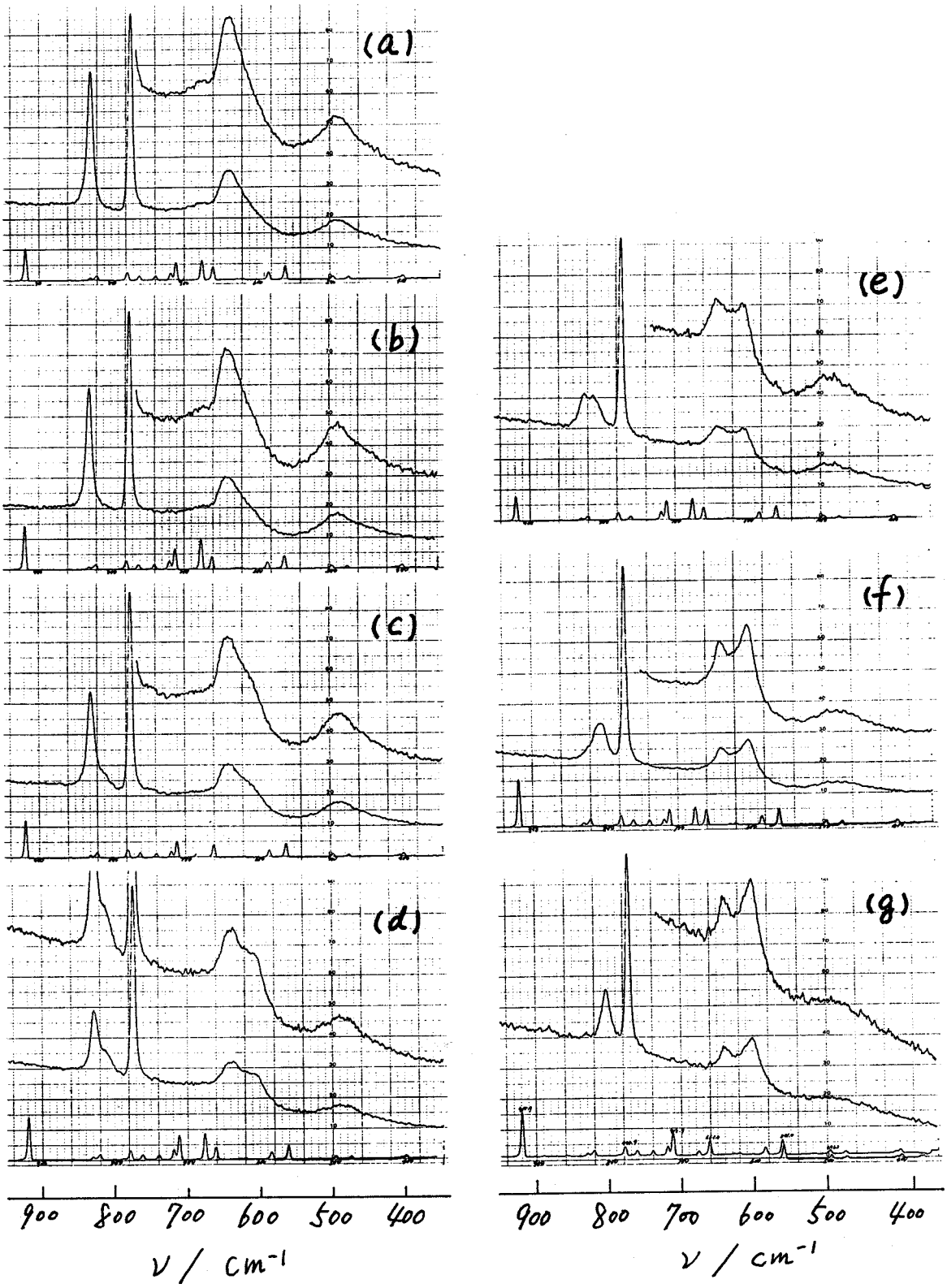

Figure 2.5: Variation of Raman spectra of KH(adc) for various deuteration ratio, (a) Normal, (b) -10%d, (c) -30%d, (d) -50%d, (e) -70%d (f) -90%d, (g) -99%d.

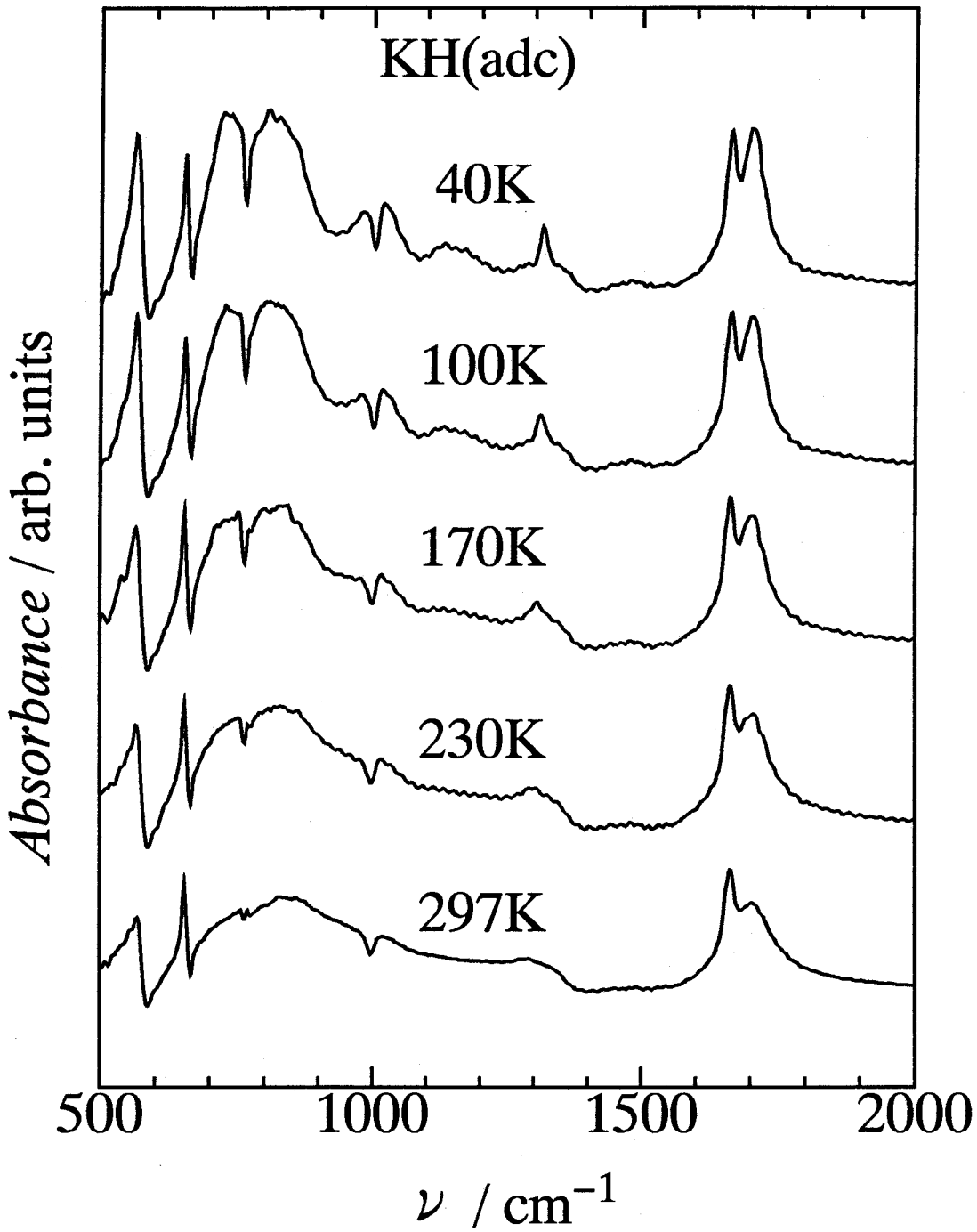

Figure 2.6: IR spectra of KH(adc).

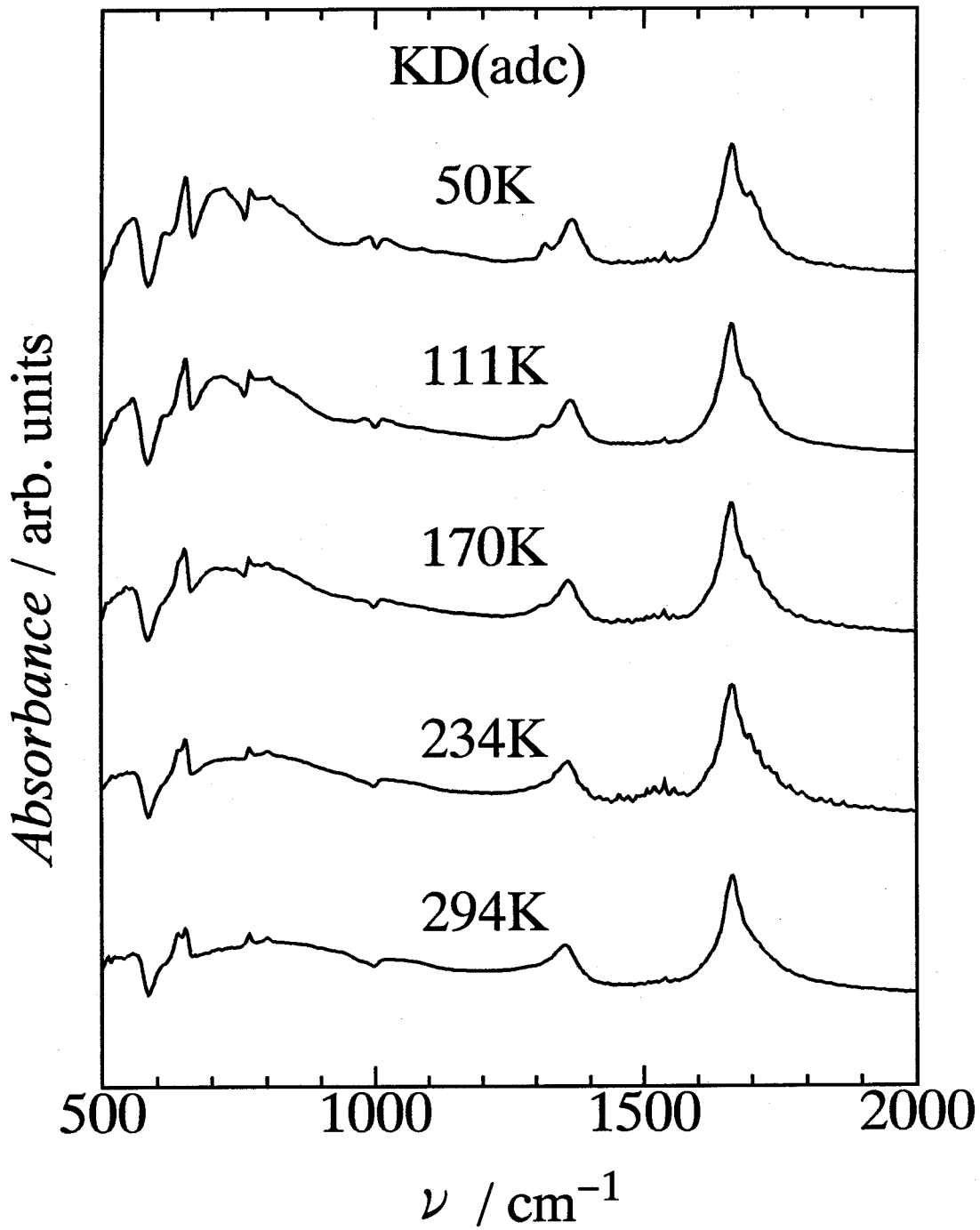

Figure 2.7: IR spectra of KD(adc).

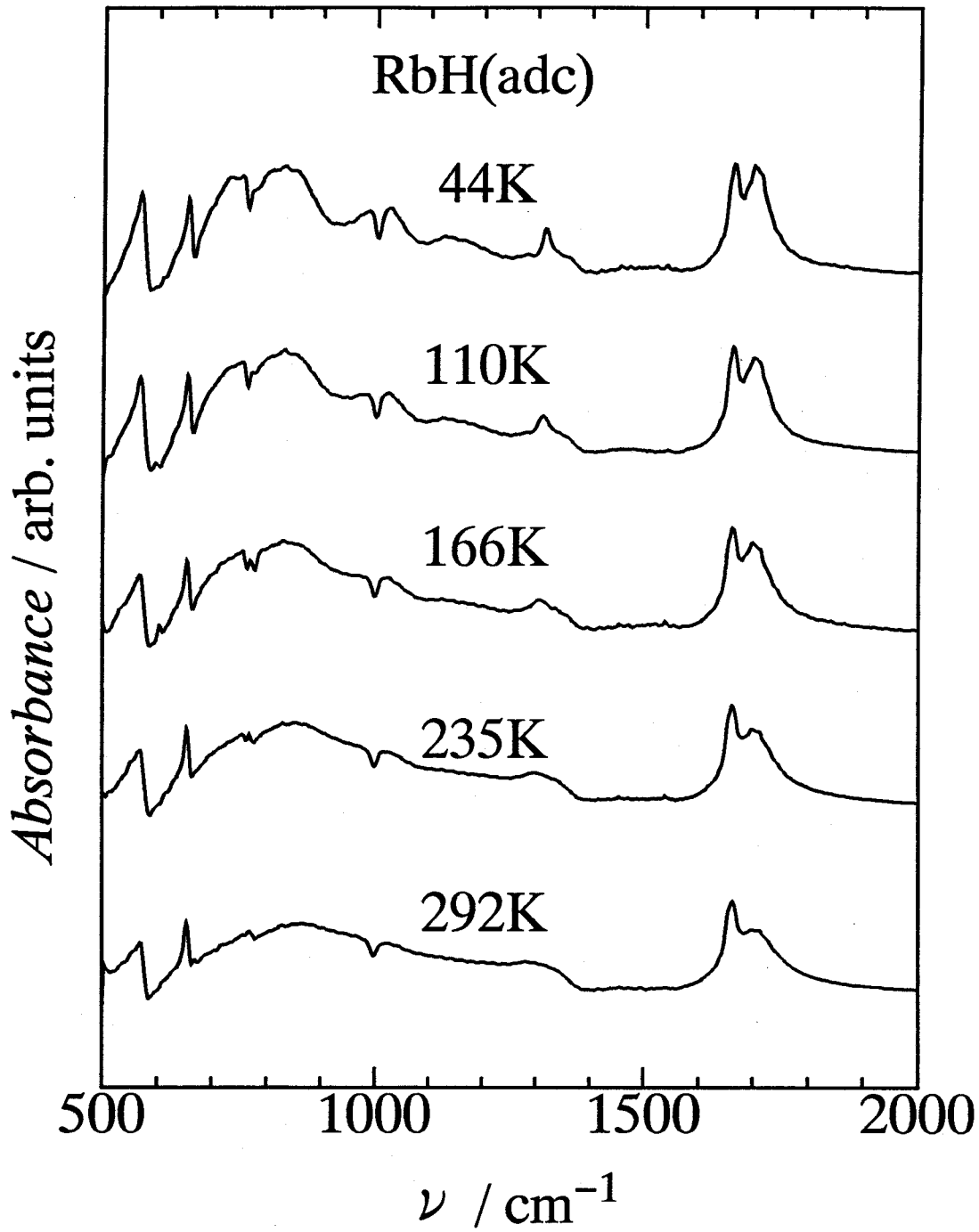

Figure 2.8: IR spectra of RbH(adc).

2.4 Other specification of samples

To examine the existence of the phase transition, DTA (Differential Thermal Analysis) and X-ray powder diffraction experiments at several temperatures were conducted.

No thermal anomaly was detected on DTA(Differential Thermal Analysis) of KH(adc) from room temperature to 100K. Temperature dependence of the powder X-ray diffraction of KH(tp) did not show any significant change from room temperature down to 98K. These results indicate that KH(adc) and KH(tp) do not undergo any phase transition between 100K and room temperature.

Chapter 3
Crystal structure determination

3.1 Introduction

Speakman classified hydrogen bonds in acid salts of carboxylic acid into Types A and B (and Types A_2 and B_2 as special cases for acid salts of dicarboxylic acid) by the presence of symmetry element (for example, i, m, 2) at the mid point between two oxygen atoms (see ref. [20] and references therein). It was found that Type $A(A_2)$ hydrogen bond is shorter than Type $B(B_2)$. The hydrogen atom in many Type $A(A_2)$ hydrogen bonds was found at the center of the hydrogen bond. But in some cases the structure was solved assuming that the hydrogen atom locates at the midpoint in the hydrogen bond and so the possibility that the hydrogen locates at some displaced point from the center was not taken into account.

But some exceptions were also known. Potassium hydrogen *meso*-tartrate [21,22] and potassium hydrogen succinate [23] were typical examples. In these salts X-ray differential Fourier map without acid hydrogen atom showed distinct double peaks located at the equally displaced points from the center of hydrogen bond [24,25]. On the contrary neutron diffraction study revealed that the hydrogen atom position in these crystals is the center of hydrogen bond [22,23]. Speakman and co-workers considered that this inconsistency was due to anisotropic anharmonic vibration of hydrogen atom, and the apparent double minimum character in differential map was fictitious [25]. And this phenomenon has been called 'KKM'(Kroon-Kanters-McAdam) effect [22,25,26]. After all it was concluded that hydrogen atom locates at the center of the symmetric Type $A(A_2)$ hydrogen bond (means a single minimum potential).

However some new views were proposed in recent years. Fillaux *et al.* studied vibrational spectra of some acid salts by infrared, Raman, and INS (inelastic neutron scattering) [6,7]. They estimated the hydrogen bond potential energy function using their vibrational spectral data [6,7]. They observed an intense sharp band in the region of a few hundred cm^{-1} and assigned it to "*tunneling*" band in "*quasi-symmetric*" double minimum potential. Their assignment is based on two interesting assumptions. First, double minimum potential was assumed in the salts which have strong Type A hydrogen bonds. Secondly, Fillaux *et al.* stated that a hydrogen bond which looks like symmetric by macroscopic measurements (like diffraction technique) could be asymmetric by microscopic study. They called this '*quasi-symmetric*' hydrogen bond. Their statement is based on the fact that the diffraction measurement can only determine the averaged structures.

Kalsbeek *et al.* determined the crystal structures of acid salts of succinic acid by X-ray diffraction and found that the crystal structures are best described by putting the acid hydrogen atom at two equally populated equivalent sites on both sides of the center of the Type A_2 hydrogen bond ($R_{O...O}$ is 2.4448(5)Å for methylammonium salt, 2.4395(7)Å for dimethylammonium salt, 2.4370(7)Å for diethylammonium salt, 2.4272(9)Å for partially deuterated sodium salt and 2.4406(15)Å for rubidium salt) [8–10]. Mallinson *et al.* also reached the same result as that of Kalsbeek *et al.* for sodium hydrogen succinate ($R_{O...O}$ is 2.4277(5)Å) [11]. In their structure analysis it was noticed that the temperature factor of the hydrogen atom is too large when the hydrogen bond is considered as a single minimum. Noda *et al.* observed an interesting phenomenon in the X-ray diffraction of $K_3H(SO_4)_2$ [12]. $K_3H(SO_4)_2$ also has a symmetric hydrogen bond and its $R_{O...O}$ is 2.493Å at room temperature. With lowering temperature $R_{O...O}$ becomes short and the differential Fourier synthesis contour map for the hydrogen bond varies from double peaks to a single peak. This suggests that there is no clear distinction between the single minimum hydrogen bond and the double minimum hydrogen bond. The judgement based on the existence of the phase transition is not always valid, because a double minimum hydrogen bond could transform to a single minimum hydrogen bond without the change of crystal symmetry. Therefore the value of the critical length has to be redetermined.

Perrin *et al.* found that mono anions of dicarboxylic acid in *aq.* solution were in equilibrium between tautomers by a precise NMR study [13]. Those anions form symmetric single minimum hydrogen bonds in the crystalline state. Perrin *et al.* considered that this inconsistency was due to the interaction between the solvents and the anion. Interactions in the hydrogen bonds in the hydrogen bond network could vary the potential energy largely. We should not have been prejudiced about the hydrogen atom position in short and symmetric Type $A(A_2)$ hydrogen bond.

Crystal structures of KH(tp) and RbH(adc) are expected to be isomorphous with other acid salts with different cations. But detailed structures have not been determined yet. In this work it is necessary to know the detailed geometry of the hydrogen bond, and so the crystal structure determination by single crystal X-ray diffraction was carried out. The used apparatus and the experimental procedures are briefly described in section 3.2. The solutions of the structures for KH(tp) and RbH(adc) are described in section 3.3 and 3.4, respectively.

3.2 Experimental

In this work two crystal structures of two materials were newly determined. In this section the common procedure to both measurements and structure resolution procedure

Table 3.1: Experimental details of X-ray diffraction

Diffractometer	
Number of reflections for unit cell determination	25
Diffractometer	Rigaku AFC5R
Radiation	Mo K_α ($\lambda = 0.71069$Å)
Attenuators	Ni foil (factors: 3.6, 12.2, 44.1)
Take-off angle	6.0°
Detector Aperture	6.0 mm horizontal, 6.0 mm vertical
Crystal to detector distance	40 cm
Scan type	ω–2θ
Scan rate	8.0°/ min (in ω) (2 rescans)
$2\theta_{max}$	60.1°
Structure Solution	
Program for calculation	TEXSAN [27]
Structure solution method	Direct method by MITHRIL [28] and DIRDIF [29]
Function minimized	$\sum w(\|F_o\| - \|F_c\|)^2$
Weighting scheme	$w = (\sigma_{cs}^2(F_o) + 0.0009\sigma^2(F_o))^{-1}$
Criterion for ignoring peaks	$I < 3.00\sigma(I)$

are described.

X-ray diffraction measurement was made on a full-automated four-circle diffractometer (Rigaku Co. Ltd. model AFC5R) with graphite-monochromated Mo K_α radiation and 12kW rotating anode X-ray generator at the X-ray Diffraction Service of the Department of Chemistry, Faculty of Science, Osaka University. Specifications of the diffractometer and the measuring conditions are given in Table 3.1.

The data were collected at room temperature using the ω–2θ scan technique up to the maximum 2θ value of 60.1°. The weak reflections ($I < 10.0s(I)$) were rescanned (maximum of 2 rescans) and the counts were accumulated to assure good counting statistics. Stationary background counts were recorded on each side of the reflections. The ratio of peak counting time to background counting time was 2:1. The diameter of the incident beam collimator was 0.5mm and the crystal to detector distance was 40cm.

All calculations were performed using TEXSAN [27] crystallographic software package. The structure was solved by direct methods using MITHRIL [28] and DIRDIF [29]. Neutral atom scattering factors were taken from Cromer and Waber [30]. Anomalous dispersion effects were included in F_c; the values for anomalous dispersion term $\Delta f'$ and $\Delta f''$ were those presented by Cromer [30]. The function $\sum w(|F_o| - |F_c|)^2$ was minimized for refinement. The weighting scheme was based on counting statistics and included a factor ($p = 0.03$) to downweight the intense reflections.

After all calculations, plots of $\sum w(|F_o| - |F_c|)^2$ versus $|F_o|$, the reflection order

in data collection, $\sin\theta/l$, and other various classes of indices were checked to show no unusual trends.

3.3 Potassium hydrogen terephthalate

3.3.1 Data collection

A needle like colorless crystal with dimension of $0.7 \times 0.3 \times 0.05\,\mathrm{mm}^3$ was used for measurement. The unit cell and crystal orientation were determined by least squares refinement using 25 reflections in the range $3.00 < 2\theta < 60.00^\circ$. The monoclinic unit cell with the lattice constants: $a = 18.776(6)$Å, $b = 3.761(3)$Å, $c = 11.150(4)$Å, $\beta = 94.72(3)^\circ$, $V = 784.6(8)$Å^3 was obtained. A unit cell contains 4 formula units ($C_8H_5O_4K$), and the calculated density is $1.729\mathrm{g/cm}^3$.

ω scans of several intense reflections, made prior to data collection, had an average width at half-height of $0.39^\circ$with a take-off angle of 6.0°. The intensity data were collected as described in section 3.2, The scan rate was 8.0°/min in ω axis and the scan width $\Delta\omega$ was $1.37^\circ + 0.35^\circ \tan\theta$. 1320 reflections among the 1359 observed reflections were independent ($R_{\mathrm{int}} = 0.016$).

During the data collection, the intensities of three representative reflections were monitored after every 100 reflections. The intensities of these reflections decreased only slightly (0.20%) and all intensities were corrected linearly toward this decrease. The linear absorption coefficient for Mo-K_α was $6.4\mathrm{cm}^{-1}$. An empirical absorption correction based on the azimuthal scans of several reflections was applied. The transmission factors were between 0.86 and 1.00. The data were also corrected for Lorentz and polarization effects. 957 independent reflections chosen by the criterion ($I < 3.0\sigma(I)$) for ignoring data, were used in the structure refinement.

3.3.2 Structure solution

Based on the systematic absence of $hkl : h+k \neq 2n$, $h0l : l \neq 2n$, the space group is either Cc(No.9) or $C2/c$(No.15) as in the case of RbH(adc). A statistical analysis of the intensity distribution indicated centric space group, *i.e.* the $C2/c$ space group. This is the same space group as that in the ammonium salt $(NH_4)H(tp)$ [15]. The $C2/c$ space group was concluded. This was confirmed by a successful structure solution and a least-squares refinement.

In the first step of the structure refinement all hydrogen atoms were excluded and the positional parameters of non-hydrogen atoms and their anisotropic temperature factors were refined. In the second step the hydrogen atoms bonded to the phenyl group were

Table 3.2: Experimental details of X-ray diffraction of KH(tp)

2θ range of 25 reflections used for unit cell determination	27.0–30.0°
a	18.776(6)Å
b	3.761(3)Å
c	11.150(4)Å
β	94.72(3)°
V	784.6(8)Å^3
Z	4
D_{calc}	1.729g/cm^3
ω scan peak width at half height	0.39
F_{000}	416
$\mu_{MoK\alpha}$	6.43cm^{-1}
Scan width	$(1.37 + 0.35 \tan\theta)°$
Number of reflection measured	Total:1359, Unique:1320 ($R_{int} = 0.016$)
corrections	Lorentz-polarization absorption (transmission factors: 0.86–1.00) Decay(−0.20% decline)

generated at the peak positions of the differential Fourier map. The structure without the acidic hydrogen atom was refined by the block diagonal least squares method including the phenyl hydrogen atoms.

Finally the position of the acid hydrogen atom in the hydrogen bond was refined as follows. The differential Fourier map obtained in this step gave two clearly separated maxima for the acidic hydrogen atom which are related to each other by the center of inversion at the center of the hydrogen bond (O(2)···O(2')). The maximum intensity of these peaks was 0.47 e/Å^3. Another remarkable peak (0.37 e/Å^3) of the Fourier map was observed between the the carboxyl carbon C(1) and the carbon C(2) of the phenyl group. Thus the half-hydrogen model for the hydrogen bond was used. The final cycle of the full-matrix least-squares refinement was based on 957 observed reflections (selected by criterion $I > 3.00\sigma(I)$) and 79 variable parameters and converged (largest parameter shift was 0.23 times its esd) with $R = 0.034$ and $R_w = 0.053$. The final positional parameters and the temperature factors are listed in Tables 3.4 and 3.5; the numbering scheme is given in Fig. 3.1 which represents the crystal structure viewed along the $\boldsymbol{b}$-axis. The complete list of the structure factors is given in Appendix.

In Fig. 3.1 the unit cell is projected from the $\boldsymbol{b}$-axis direction. There is the center of symmetry at the center of benzene ring. Therefore asymmetric unit includes only a half of the (tp) anion. Potassium atom is on the 2-fold axis. Anion chains run along the $\boldsymbol{a}$-axis.

Table 3.3: Final least squares parameters of KH(tp)

R	0.034
R_w	0.053
N_v	79
S	2.40
$(\Delta/\sigma)_{max}$	0.23
Max. peak in D-map	0.36 e/Å^3
Min. peak in D-map	-0.37 e/Å^3

Table 3.4: Final converged fractional coordinates and equivalent isotropic temperature factors for KH(tp).

Atom	x	y	z	B_{eq}/Å^2
K	0	0.1555(2)	0.75	3.21(2)
O(1)	0.08697(6)	0.6794(4)	0.6573(1)	2.59(5)
O(2)	0.05996(6)	0.5411(5)	0.4654(1)	3.34(6)
C(1)	0.10415(8)	0.6396(5)	0.5536(1)	1.96(6)
C(2)	0.17939(7)	0.6982(4)	0.5244(1)	1.60(5)
C(3)	0.22829(8)	0.8414(5)	0.6114(1)	1.83(5)
C(4)	0.20142(8)	0.6069(5)	0.4121(1)	1.88(5)
H(1)	0.170(1)	0.497(7)	0.353(2)	2.7
H(2)	0.214(1)	0.900(6)	0.687(2)	2.7
H(3)	0.023(2)	0.50(1)	0.492(4)	2.7(9)

$$B_{eq} = \frac{8\pi^2}{3} \sum_{i=1}^{3} \sum_{j=1}^{3} U_{ij} a_i^* a_j^* \vec{a}_i \vec{a}_j$$

Table 3.5: Final anisotropic temperature factors(Å^2) for KH(tp).

Atom	U_{11}	U_{22}	U_{33}	U_{12}	U_{13}	U_{23}
K	0.0432(3)	0.0405(3)	0.0413(3)	0	0.0217(3)	0
O(1)	0.0187(5)	0.0529(8)	0.0277(6)	-0.0049(6)	0.0086(4)	-0.0045(6)
O(2)	0.0134(5)	0.085(1)	0.0285(6)	-0.0137(6)	0.0029(4)	-0.0044(7)
C(1)	0.0137(6)	0.0352(9)	0.0258(7)	-0.0022(6)	0.0031(5)	0.0019(7)
C(2)	0.0110(6)	0.0276(8)	0.0226(6)	-0.0018(6)	0.0026(5)	0.0014(6)
C(3)	0.0155(6)	0.0343(9)	0.0203(6)	-0.0023(6)	0.0041(5)	-0.0019(6)
C(4)	0.0141(6)	0.0352(9)	0.0221(7)	-0.0048(6)	0.0007(5)	-0.0025(6)

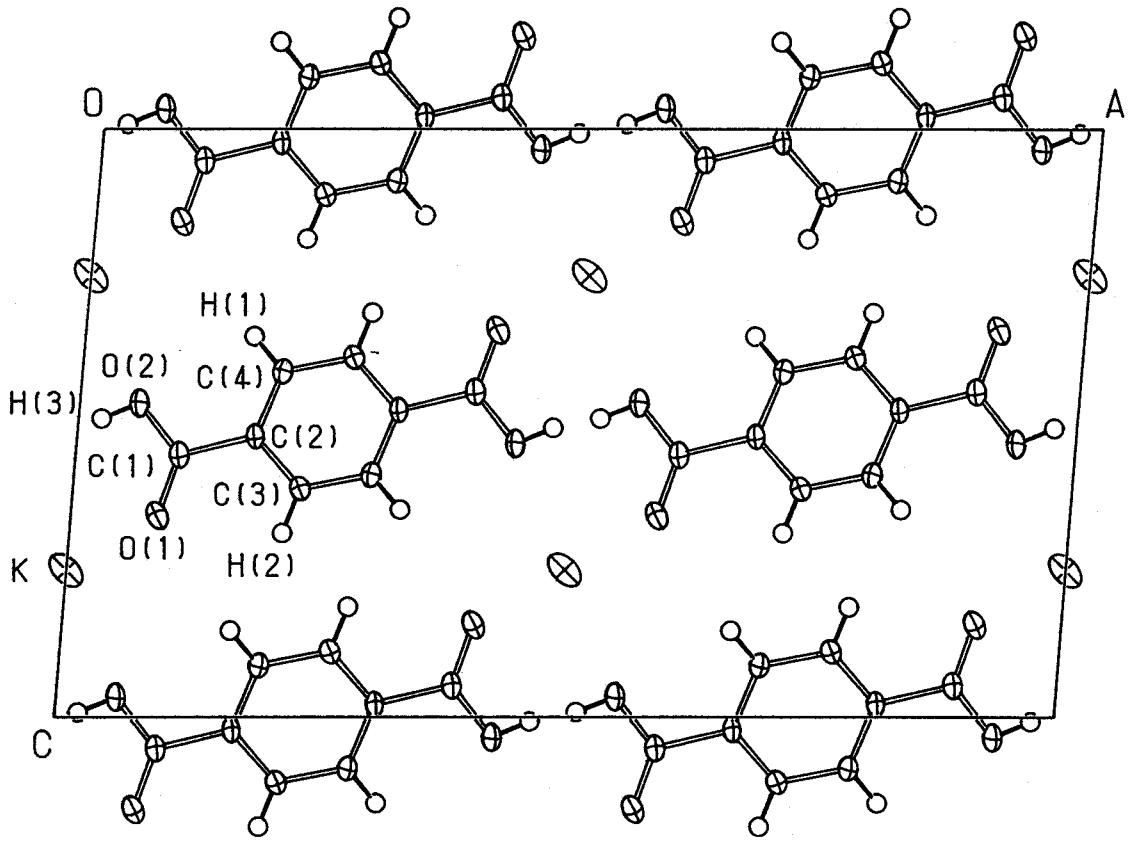

Figure 3.1: ORTEP [31]-plot of ***b***-axis projection of KH(tp).

Table 3.6: Bond distances (Å) and bond angles (deg.) in terephthalic acid anion

C(1)–O(1)	1.235(2)	O(1)–C(1)–O(2)	123.3(1)
C(1)–O(2)	1.288(2)	O(1)–C(1)–C(2)	120.8(1)
C(1)–C(2)	1.492(2)	O(2)–C(1)–C(2)	116.0(1)
C(2)–C(3)	1.389(2)	C(1)–C(2)–C(3)	119.2(1)
C(2)–C(4)	1.394(2)	C(1)–C(2)–O(4)	121.1(1)
C(3)–C(4')	1.380(2)	C(3)–C(2)–C(4)	119.7(1)
C(4)–H(1)	0.943(2)	C(2)–C(3)–C(4')	120.6(1)
C(3)–H(2)	0.932(2)	C(2)–C(4)–C(3')	119.7(1)
K–O(1)	2.687(2)		
K–O(1')	2.810(2)		
K–O(2)	2.809(2)		

Table 3.7: Hydrogen bond geometry in KH(tp)

O(2)–O(2)	2.459(3)Å
O(2)–H	0.79(4)Å
O(2)···H(3)'	1.68(4)Å
H(3)···H(3)	0.91(8)Å
O(2)–H(3)···O(2)'	170(5)°
H(3)–O–C(1)	107(3)°

3.3.3 Bond lengths and bond angles

Bond distances and bond angles are listed in Table 3.6. For a carboxyl group the bond lengths (C=O = 1.235Å and C–O = 1.288Å) and bond angles (CC=O = 116.0° and CC–O = 120.8°) differ significantly from each other as can be seen in the mono-hydrogen salts of other types of dicarboxylic acids. The carboxyl groups are tilted by 9° from the plane of the benzene ring. This value is almost the same as that of $NH_4H(tp)$

The potassium ion lies on the two fold symmetry axis and is surrounded by six oxygen atoms of nearby six carboxyl groups. Three inequivalent distances between the potassium ion and oxygen atoms are also listed in Table 3.6.

3.3.4 Hydrogen bond geometry

The geometry around hydrogen bond is summarized in Table 3.7. $R_{O\cdots O}$ in KH(tp) is 2.459Å which is the typical value for the hydrogen bond of the Type A_2. The double minimum character of the hydrogen bond was observed. Cobbledick *et al.* carried out their structure analysis of $NH_4(tp)$ by assuming that the hydrogen is located at the center of the (single minimum) hydrogen bond, but did not rule out the possibility of the double minimum hydrogen bond [15]. Cobbledick's analysis has slightly poor accuracy ($R = 0.0759$). $R_{O\cdots O} = 2.51$Å in $NH_4(tp)$ is longer than that in KH(tp). Longer $R_{O\cdots O}$

than that of other isomorphous acid salt is also seen in (adc) salt (subsection 3.4.4). This is considered to be the effect of the hydrogen bonds between $(NH_4)^+$ cation and the oxygens in carboxyl groups.

3.4 Rubidium hydrogen acetylenedicarboxylate

3.4.1 Data collection

A colorless crystal with dimension of $0.8 \times 0.2 \times 0.2\,mm^3$ was used for measurement. The unit cell and crystal orientation were determined by the least squares refinement using 25 reflections in the range $27.03 < 2\theta < 30.00°$. The monoclinic unit cell with the lattice constants: $a = 8.666(2)$Å, $b = 12.278(4)$Å, $c = 6.209(2)$Å, $\beta = 118.01(2)°$, $V = 583.2(4)$Å^3 was obtained. The unit cell contains 4 formula units (C_4HO_4Rb), and the calculated density is $2.261 g/cm^3$.

ω scans of several intense reflections, made prior to data collection, had an average width at half-height of 0.35°with a take-off angle of 6.0°. The intensity data were collected as described in section 3.2, The scan rate was 8.0°/min in ω axis and the scan width $\Delta\omega$ was $1.10° + 0.35° \tan\theta$. 902 reflections among the 953 observed reflections were independent ($R_{int} = 0.055$).

During the data collection, the intensities of three representative reflections were measured after every 100 reflections. The drift in intensity was 1.94% increase and all intensities were corrected linearly toward this drift [1]. The linear absorption coefficient for Mo-K_α was $81.9 cm^{-1}$. An empirical absorption correction based on azimuthal scans of several reflections was applied. The transmission factors were between 0.86 and 1.00. The data were also corrected for Lorentz and polarization effects. 768 independent reflections, chosen by the criterion ($I < 3.0\sigma(I)$) for ignoring data, were used in the structure refinement.

3.4.2 Structure solution

Based on systematic absence of $hkl : h + k \neq 2n$, $h0l : l \neq 2n$, the space group is either Cc(No.9) or $C2/c$(No.15). A statistical analysis of the intensity distribution suggested acentric space group, *i.e.*, the Cc space group. But the space group of KH(adc) [16] and NH_4H(adc) [32] was known as $C2/c$[2] Therefore crystal structure was resolved for both Cc and $C2/c$ space groups. Three model structures were tried for the final solution. In the first model the Cc space group was assumed. In the other two models the $C2/c$

[1] After the measurement, the crystal surface was slightly colored.

[2] In the original papers of Leban *et al.* $I2/a$ was used [16, 32]. It is identical with $C2/c$ except axis setting of the unit cell.

Table 3.8: Experimental details of X-ray diffraction of RbH(adc)

2θ range of 25 reflections used for unit cell determination	27.0–30.0°
a	8.666(2)Å
b	12.278(4)Å
c	6.209(2)Å
β	118.01(2)°
V	583.2(4)Å^3
Z	4
D_{calc}	2.261g/cm^3
ω scan peak width at half height	0.35
F_{000}	376
$\mu_{\mathrm{Mo}K\alpha}$	81.92cm^{-1}
Scan width	$(1.10 + 0.35 \tan\theta)°$
Number of reflection measured	Total:953, Unique:902 ($R_{\mathrm{int}} = 0.055$)
Corrections	Lorentz-polarization absorption (transmission factors: 0.63–1.00) Decay(1.94% decline) Secondary extinction (coefficient: 0.61678E-05)

space group was assumed. Firstly, each structure without hydrogen atom was resolved for each space group and refined by the least squares calculation with the anisotropic temperature factors. Secondly, each structure including acid hydrogen atom was refined. In the Cc space group no restriction is imposed on the position of the hydrogen atom, because the hydrogen bond is not symmetric. Then in the first model the hydrogen position was set on the maximum peak (+0.59 eÅ^3) position of differential Fourier map, and parameters were refined by the least squares calculation. In the $C2/c$ space group the hydrogen bond must be symmetric; the center of hydrogen bond is on the 2–fold axis. The position of the hydrogen atom is restricted to satisfy this symmetry. Two model structures are possible; the hydrogen locates on the 2–fold axis or hydrogen is divided equivalently into two symmetry-related positions. The former means a single-minimum hydrogen bond and the latter means a symmetric double-minimum hydrogen bond. In previous structure solutions of KH(adc) and NH_4(adc) the centered hydrogen model was assumed [16, 32]. In this model the position of hydrogen atom was constrained on the 2–fold axis. However the maximum peak (+0.67 eÅ^3)in the differential Fourier map for the $C2/c$ structure without the hydrogen atom appeared at a displaced point from the center of hydrogen bond. Therefore the double minimum model was the most natural selection. In the double minimum model the hydrogen positions are not restricted to the center of hydrogen bond, but the population should be divided into two equal parts to

Table 3.9: Final least squares parameters of RbH(adc)

Space group	Cc	$C2/c$	$C2/c$
Hydrogen position	asymmetric	centered	double minimum
R	0.028	0.024	0.024
R_w	0.034	0.033	0.032
N_v	84	45	47
S	1.72	1.61	1.58
$(\Delta/\sigma)_{\max}$	0.90	0.01	0.19
Max. peak in D-map	0.44	0.47	0.46
Min. peak in D-map	-1.04	-0.54	-0.52

$$S = \left\{ \frac{\sum w(|F_0| - |F_c|)^2}{N_o - N_v} \right\}$$

generate the hydrogen atom at symmetry-related positions.

Successful result was obtained for each of three models (see Table 3.9). The final cycle of the full-matrix least-squares refinement was based on 768 observed reflections ($I > 3.00\sigma(I)$). Table 3.9 indicates that the $C2/c$ (No.15) is favorable, because it gives better R or R_w than Cc models which have almost twice number of variables (N_v) and equivalent isotropic temperature factor, $B_{\rm eq}$, of the hydrogen atom is unusually large in the case of Cc as shown in Table 3.10. It is difficult to determine the hydrogen atom positions definitely, because RbH(adc) contains a heavy Rb atom in the vicinity of the hydrogen bond (see Fig. 3.4). Finally the double minimum model was chosen in the bases of the difference Fourier map. The final converged atomic coordinates are listed in Table 3.10 for three models. The anisotropic temperature factors of non-hydrogen atoms are listed in Table 3.11. The complete lists of the structure factors for half hydrogen structure in $C2/c$ space group are given in Appendix.

In the $C2/c$ space group, there is a 2-fold axis through the mid point of C≡C triple bond. Therefore the asymmetric unit contains only a half of the (adc) anion. Fig. 3.2 is the ORTEP plot projected in the **c** direction. The anion chains viewed along the ***b***-axis are shown in Fig. 3.3 in which atoms in a half unit cell are projected in the ***b*** direction for simplicity.

3.4.3 Bond lengths and bond angles

In Table 3.12 intramolecular bond distances and bond angles in the α-RbH(adc) are listed. These values resemble those in the β-form RbH(adc) and KH(adc) [17]. The clear distinction of the bond lengths (C=O = 1.220Å and C–O = 1.285Å) and bond angles (CC=O = 119.5° and CC–O = 114.3°) in a carboxyl group is similar to those in KH(tp)

Table 3.10: Final fractional coordinates and equivalent isotropic temperature factors for three model structures(see text) of RbH(adc) and fractional coordinates of KH(adc) [16].

Cc. lower symmetry (asymmetric hydrogen bond) model

Atom	x	y	z	B_{eq}/Å^2
Rb	1	0.16974(3)	0.25	2.36(2)
O(1)	0.739(2)	0.1727(7)	0.735(2)	3.5(4)
O(2)	0.856(1)	0.0609(6)	0.562(1)	1.8(2)
O(3)	0.263(1)	0.1667(6)	-0.238(2)	2.7(3)
O(4)	0.134(1)	0.0735(7)	-0.061(2)	2.4(2)
C(1)	0.735(1)	0.119(1)	0.568(2)	2.3(4)
C(2)	0.562(2)	0.106(1)	0.336(3)	2.6(3)
C(3)	0.271(1)	0.1149(7)	-0.067(2)	1.8(3)
C(4)	0.428(1)	0.110(1)	0.152(2)	1.9(3)
H	-0.01(2)	0.07(1)	-0.21(3)	9(4)

*C*2/*c*. Hydrogen special position (single minimum) model

Atom	x	y	z	B_{eq}/Å^2
Rb	1	0.16969(3)	0.25	2.48(2)
O(1)	0.7387(3)	0.1703(2)	0.7368(4)	3.13(7)
O(2)	0.8608(2)	0.0668(2)	0.5620(3)	2.48(2)
C(1)	0.7321(3)	0.1168(2)	0.5669(4)	2.07(7)
C(2)	0.5675(3)	0.1089(2)	0.3414(5)	2.41(8)
H	1	0.056(5)	0.75	6(1)

*C*2/*c*, half hydrogen (symmetric double minimum) model

Atom	x	y	z	B_{eq}/Å^2
Rb	1	0.16969(3)	0.25	2.48(2)
O(1)	0.7387(3)	0.1703(1)	0.7367(4)	3.13(7)
O(2)	0.8607(2)	0.0668(2)	0.5617(3)	2.50(6)
C(1)	0.7321(3)	0.1167(2)	0.5669(4)	2.08(7)
C(2)	0.5675(3)	0.1089(2)	0.3412(5)	2.41(8)
H	0.943(6)	0.058(4)	0.685(9)	1(1)

*C*2/*c* converted coordinate (original *I*2/*a* unit cell [16]) of KH(adc)

Atom	x	y	z
Rb	1	0.17167	0.25
O(1)	0.73924	0.17080	0.75243
O(2)	0.86196	0.06870	0.55781
C(1)	0.73315	0.11796	0.57198
C(2)	0.56773	0.10853	0.34282
H	1	0.09139	0.75

$$B_{eq} = \frac{8\pi^2}{3} \sum_{i=1}^{3} \sum_{j=1}^{3} U_{ij} a_i^* a_j^* \vec{a}_i \vec{a}_j$$

Table 3.11: Final temperature factors (Å^2) for three model structures of RbH(adc).

Cc and lower symmetry (asymmetric hydrogen bond) model

Atom	U_{11}	U_{22}	U_{33}	U_{12}	U_{13}	U_{23}
Rb	0.0265(2)	0.0358(2)	0.0231(2)	-0.0001(6)	0.0081(2)	-0.0003(7)
O(1)	0.048(6)	0.046(5)	0.025(5)	0.014(4)	0.004(5)	-0.013(3)
O(2)	0.008(3)	0.031(3)	0.019(3)	-0.002(2)	-0.003(2)	-0.002(2)
O(3)	0.018(4)	0.045(5)	0.028(5)	-0.007(3)	0.002(3)	0.003(3)
O(4)	0.017(3)	0.036(3)	0.031(3)	0.006(2)	0.008(3)	0.007(2)
C(1)	0.007(4)	0.039(6)	0.029(6)	-0.003(4)	-0.002(4)	0.007(5)
C(2)	0.014(4)	0.043(6)	0.025(4)	0.003(4)	-0.006(3)	0.008(4)
C(3)	0.028(6)	0.017(4)	0.016(4)	-0.002(4)	0.005(4)	0.004(3)
C(4)	0.015(4)	0.029(4)	0.027(5)	0.004(3)	0.008(3)	0.009(3)

*C*2/*c* and hydrogen special position (single minimum) model

Atom	U_{11}	U_{22}	U_{33}	U_{12}	U_{13}	U_{23}
Rb	0.0279(2)	0.0371(2)	0.0247(2)	0	0.0086(1)	0
O(1)	0.031(1)	0.048(1)	0.028(1)	0.0085(8)	0.0042(8)	-0.0081(8)
O(2)	0.0169(8)	0.042(1)	0.0259(8)	0.0019(7)	0.0023(6)	-0.0049(7)
C(1)	0.018(1)	0.030(1)	0.022(1)	-0.0018(8)	0.0012(8)	0.0001(8)
C(2)	0.020(1)	0.035(1)	0.028(1)	0.0010(9)	0.005(1)	-0.001(1)

*C*2/*c* and half hydrogen (symmetric double minimum) model

Atom	U_{11}	U_{22}	U_{33}	U_{12}	U_{13}	U_{23}
Rb	0.0279(2)	0.0371(2)	0.0247(2)	0	0.0086(1)	0
O(1)	0.031(1)	0.049(1)	0.028(1)	0.0085(8)	0.0042(8)	-0.0080(8)
O(2)	0.0169(8)	0.043(1)	0.0254(8)	0.0021(7)	0.0018(6)	-0.0046(7)
C(1)	0.018(1)	0.029(1)	0.022(1)	-0.0019(8)	0.0013(8)	0.0000(8)
C(2)	0.020(1)	0.035(1)	0.028(1)	0.0010(9)	0.005(1)	-0.001(1)

Table 3.12: Bond distances(Å) and bond angles (degree) of rubidium acetylenedicarboxylate.

C(1)–O(1)	1.220(3)	O(1)–C(1)–O(2)	126.1(2)
C(1)–O(2)	1.285(3)	O(1)–C(1)–C(2)	119.5(2)
C(1)–C(2)	1.460(3)	O(2)–C(1)–C(2)	114.3(2)
C(2)–C(2)'	1.186(3)	C(1)–C(2)–C(2)'	176.2(1)
Rb–O(1)	2.882(2)		
Rb–O(1)'	2.917(3)		
Rb–O(2)	2.999(2)		

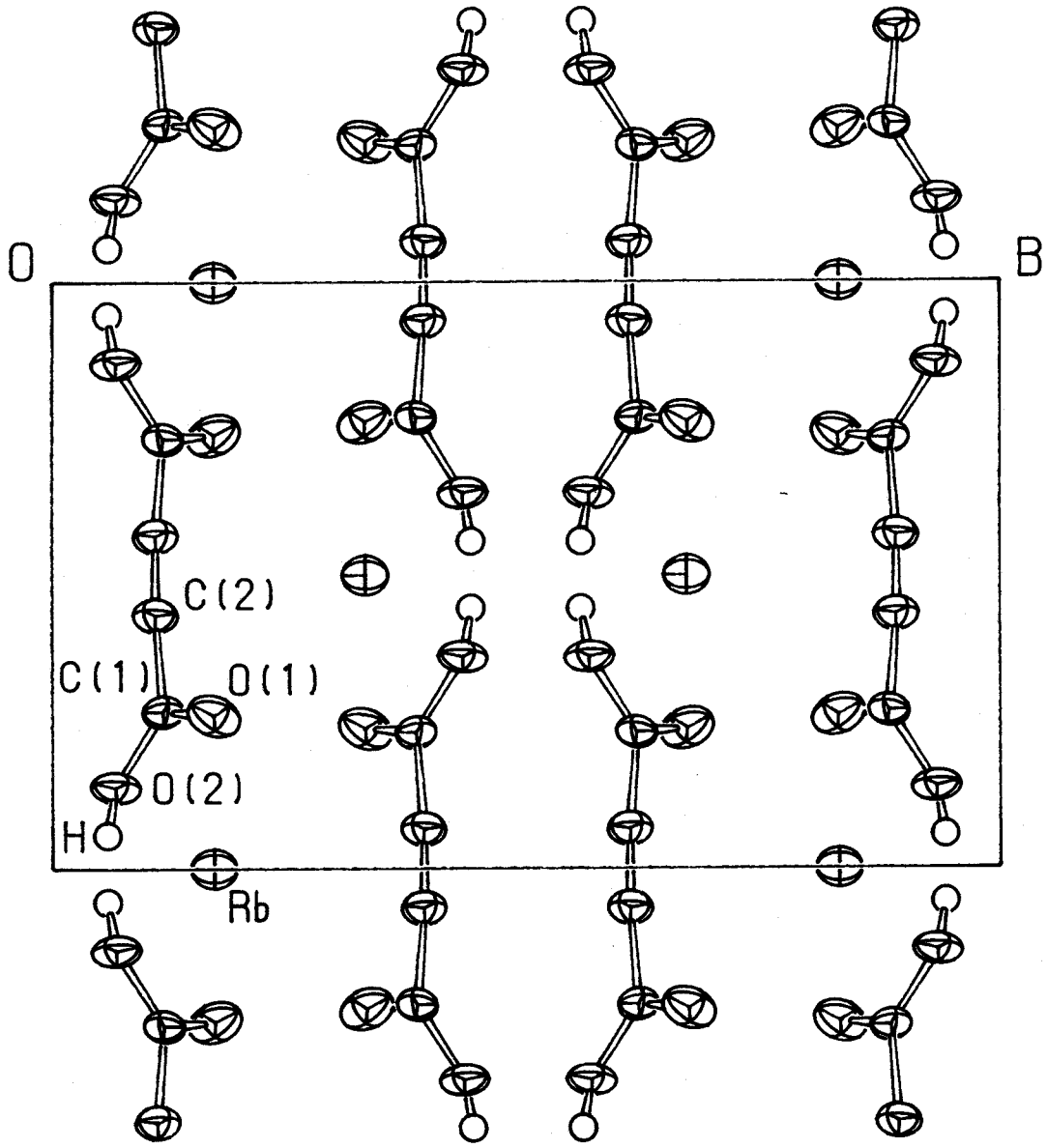

Figure 3.2: ORTEP [31]-plot of c-axis projection of RbH(adc).

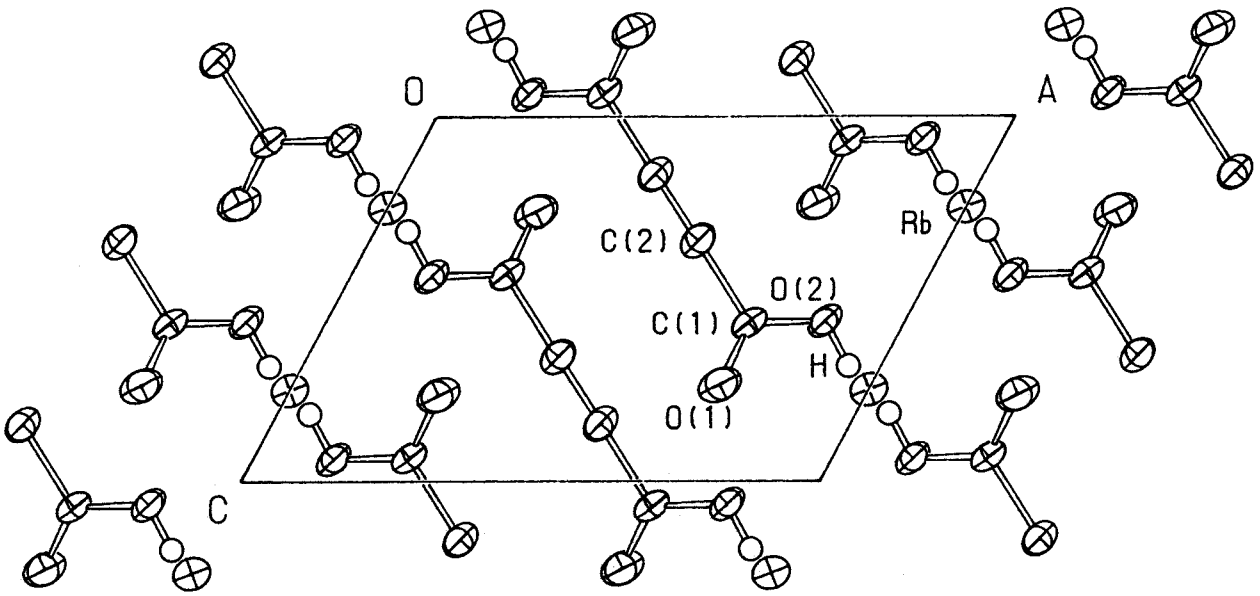

Figure 3.3: ORTEP [31]-plot of $\boldsymbol{b}$-axis projection of RbH(adc). Atoms ($-0.25 < y < 0.25$ in fractional coordinate) are projected

and those which can be seen in other acid salts of dicarboxylic acids. Other bond lengths in the (adc) anion are fairly close to those in KH(adc) or β-RbH(adc). Dihedral angle between two carboxyl groups of this α-form RbH(adc) is 70° is similar to that in KH(adc) (66°) [16] and NH_4H(adc) (74°) [32] but differ considerably from that in β-form RbH(adc) (61°) [17].

Coordination scheme around the Rb^+ cation is alike to KH(adc) and β-RbH(adc). Six oxygen atoms which belong to six different carboxyl groups of six different (adc) anions surround Rb^+ (Fig. 3.4).

3.4.4 Hydrogen bond geometry

The geometry around hydrogen bond is summarized in Table 3.13 $R_{O\cdots O} = 2.449$Å in the α-form RbH(adc) is almost the same as 2.446(3)Å in KH(adc) (centered hydrogen atom). These values are typical for the Type-A_2 acid salts. Speakman's statement that symmetric hydrogen bond is generally shorter than asymmetric hydrogen bond is confirmed to be valid for RbH(adc). It is noted that $R_{O\cdots O}$ in NH_4(adc) is 2.472(3)Å. This value is longer than $R_{O\cdots O}$ in α-RbH(adc) and KH(adc). But NH_4(adc) belongs also to the Type A_2 acid salt. As predicted previously in subsection 3.3.4, $R_{O\cdots O}$ in ammonium

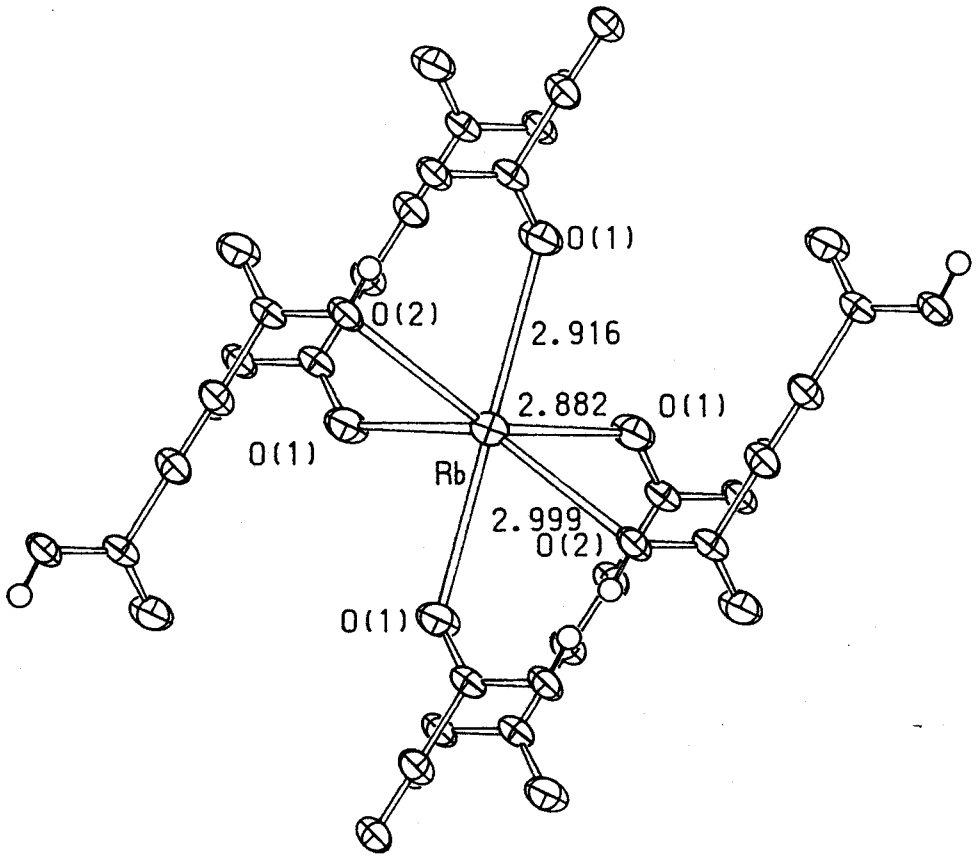

Figure 3.4: Coordination scheme around Rb^+ of RbH(adc), 6 molecules coordinating to one Rb^+ cation were viewed from $(0, -1, 0)$ direction

Table 3.13: Geometry around hydrogen bond of RbH(adc). Bond lengths (Å) and angles (degree) are listed

	half hydrogen	centered	β-form [17]
O···O'	2.449(4)	2.445(4)	2.461(8)†
O–H···O'	0.77(4)	1.230(7)	1.14(15)
O···H	1.69(4)	—	1.32(14)
H···H'	0.94(9)	—	—
O–H···O'	167(5)	167(6)	172(13)
C–O–H	117(4)	120(1)	—
C–O···H	120(2)	—	—

†2.464(8)Å for the structure refined without hydrogen atom was noted in the abstract of ref. [16].

salt is longer than that of other isomorphous (adc) salt. This is considered to be the effect of the structure forming by the hydrogen bonds between $(NH_4)^+$ and oxygens of carboxyl groups.

Chapter 4
NMR line shape

This chapter describes the line shape studies of ^{1}H, ^{2}H, and ^{87}Rb NMR. These NMR spectra gives various information about microscopic structure of the samples, particularly the nature of the hydrogen bond.

4.1 ^{2}H NMR

4.1.1 Introduction

A nucleus with $I > 1/2$ spin has a finite electric quadrupole moment (eQ). An electric quadrupole moment interacts with the electric field gradient (EFG) tensor and gives the electric quadrupole coupling term to the nuclear Hamiltonian [33,34]. The EFG tensor is defined by the second derivative of the static electric potential V:

$$V_{pq} = \frac{\partial^2 V}{\partial p \partial q}, \qquad (p, q = x, y, z). \tag{4.1}$$

The Laplace equation for V requires that the trace of EFG tensor is zero,

$$V_{xx} + V_{yy} + V_{zz} \equiv 0, \tag{4.2}$$

for any choice of the cartesian coordinates. Because the EFG tensor is a symmetric tensor, it is diagonalized by the orthogonal transformation. In the transformed principal axes frame (X, Y, Z), only V_{XX}, V_{YY}, and V_{ZZ} have finite values among the elements of EFG tensor, and called the principal values

$$|eq \equiv V_{ZZ}| \geq |V_{YY}| \geq |V_{XX}|. \tag{4.3}$$

The EFG tensor reflects the charge distribution around the nucleus, therefore it is a very sensitive probe to investigate the microscopic environment of an atom. For the description of the principal values it is convenient to introduce the asymmetry parameter η,

$$\eta = \frac{V_{XX} - V_{YY}}{V_{ZZ}}. \tag{4.4}$$

According to the relation (4.3) η takes the value in the range of $0 \leq \eta \leq 1$. And the principal values are given by

$$V_{ZZ} = eq, \; V_{YY} = -\frac{1}{2}eq(1+\eta), \; V_{ZZ} = -\frac{1}{2}eq(1-\eta). \tag{4.5}$$

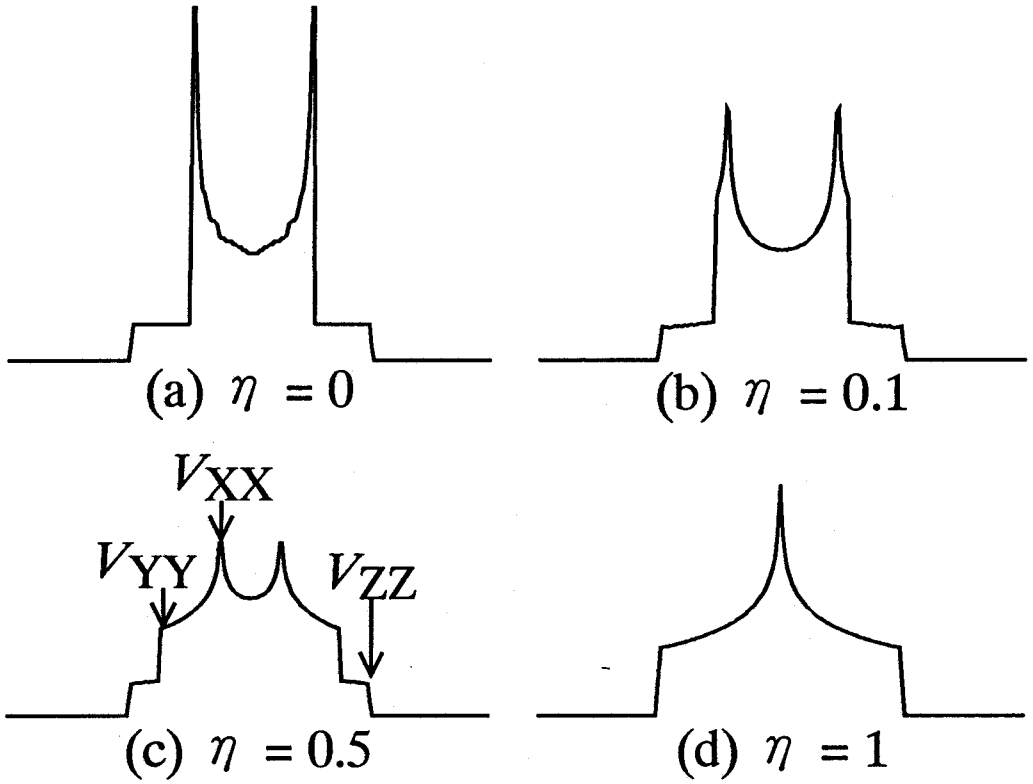

Figure 4.1: Some typical ^{2}H-NMR line shapes of powder sample; (a) $\eta = 0$, axial symmetric; (b) $\eta = 0.1$, near axial symmetric; (c) $\eta = 0.5$; (d) $\eta = 1$.

Then the nuclear electric quadrupole Hamiltonian is given by

$$H_Q = \frac{e^2Qq}{4I(2I-1)}[3I_Z^2 - I(I+1) + \frac{1}{2}\eta(I_+^2 + I_-^2)]. \tag{4.6}$$

In the high external magnetic field H_0, the perturbation theory gives the first and the second order shift through the quadrupole coupling.

^{2}H is a nucleus with $I = 1$ spin. The powder line shape of ^{2}H is determined by the first order perturbation of the nuclear electric quadrupole coupling. Some typical powder line shapes for various η are pictured in Fig. 4.1. A powder spectrum gives $|e^2Qq/h|$ and η of measuring ^{2}H. The characteristic line shape of ^{2}H resonance spectrum of the O–H$\cdots$O hydrogen bond is originated from the nuclear quadrupole interaction between the nuclear quadrupole moment of ^{2}H nucleus and the electric field gradient which is produced at the nuclear position by the surrounding charge distribution, mainly the charges of electrons in the O–H bond.

Table 4.1: Quadrupole coupling constant e^2Qq/h and η of ^{2}H in KH(adc)-99%d.

$\frac{T}{K}$	$\frac{e^2Qqh^{-1}}{kHz}$	η
132	48.8	0.098
179	52.7	0.088
242	57.3	0.082
290	61.4	0.078
324	64.0	0.076
353	66.2	0.072

4.1.2 Experimental

Acid salt of acetylenedicarboxylic acid is soluble in (heavy) water and easily deuterated as described in section 2.1. ^{2}H NMR spectra were measured for (partially) deuterated acid salts of acetylenedicarboxylic acid. All ^{2}H NMR measurements were performed using a Bruker MSL-200 spectrometer at ν_L = 30.288MHz. Data above 120K were measured using Bruker variable temperature probe cooled by N_2 gas. Other ^{2}H spectra below 120K were measured by a home-build cryostat and a Oxford superconducting magnet at almost the same ν_L as in the Bruker magnet. ^{2}H line shape is determined by the first order perturbation due to the nuclear quadrupole coupling, therefore such a only difference between the two magnet is negligible. FIDs were taken by the quadrupole-echo method with the pulse separation of 20μs to avoid the undesirable effect of the dead time of the spectrometer. Typically 80 FIDs were accumulated to obtain higher (S/N) ratio. ^{2}H-T_1 was 470s at room temperature (286K) for KD(adc). This was too long to wait recovering to thermal equilibrium, a several dummy scan was taken for ignoring initial unbalance of FID for the phase cycling technique. At lower temperatures below 80 K, a single FID brings about only distorted spectra. But it was impossible to accumulate FIDs because of the extremely long T1.

4.1.3 Results and Discussion

Measured line shapes are shown in Figs. 4.2–4.4. Asymmetry parameter η at each temperature was calculated from the position of the edges of absorption line for KH(adc), which had relatively good (S/N) ratio. The result is plotted in Fig. 4.5 as a function of temperature. η is nearly equal to 0.1 at all temperatures. For KH(adc)-50%d and RbH(adc) the (S/N) ratio of the spectral lines was too poor to calculate the η values from the edge positions. But the observed line shapes were similar to that in KD(adc), and can be considered to give similar value of η. In Fig. 4.6 temperature dependencies of the frequency difference $\Delta\nu$ between two peaks of acid salts of acetylenedicarboxylic acid are shown. Clear increase of $\Delta\nu$ is observed with increasing temperature for each sample.

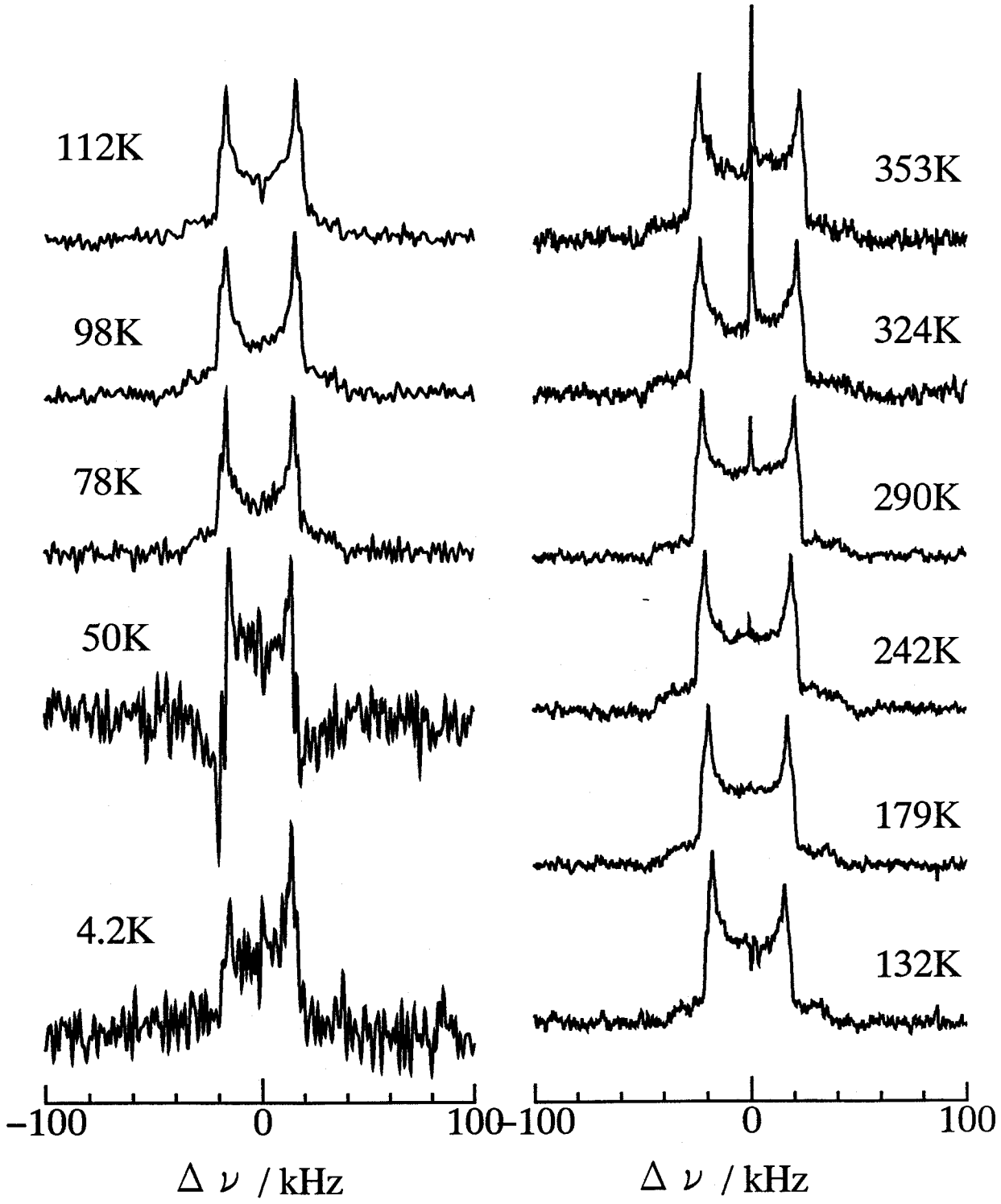

Figure 4.2: ^{2}H line shapes of KH(adc)-99%d,

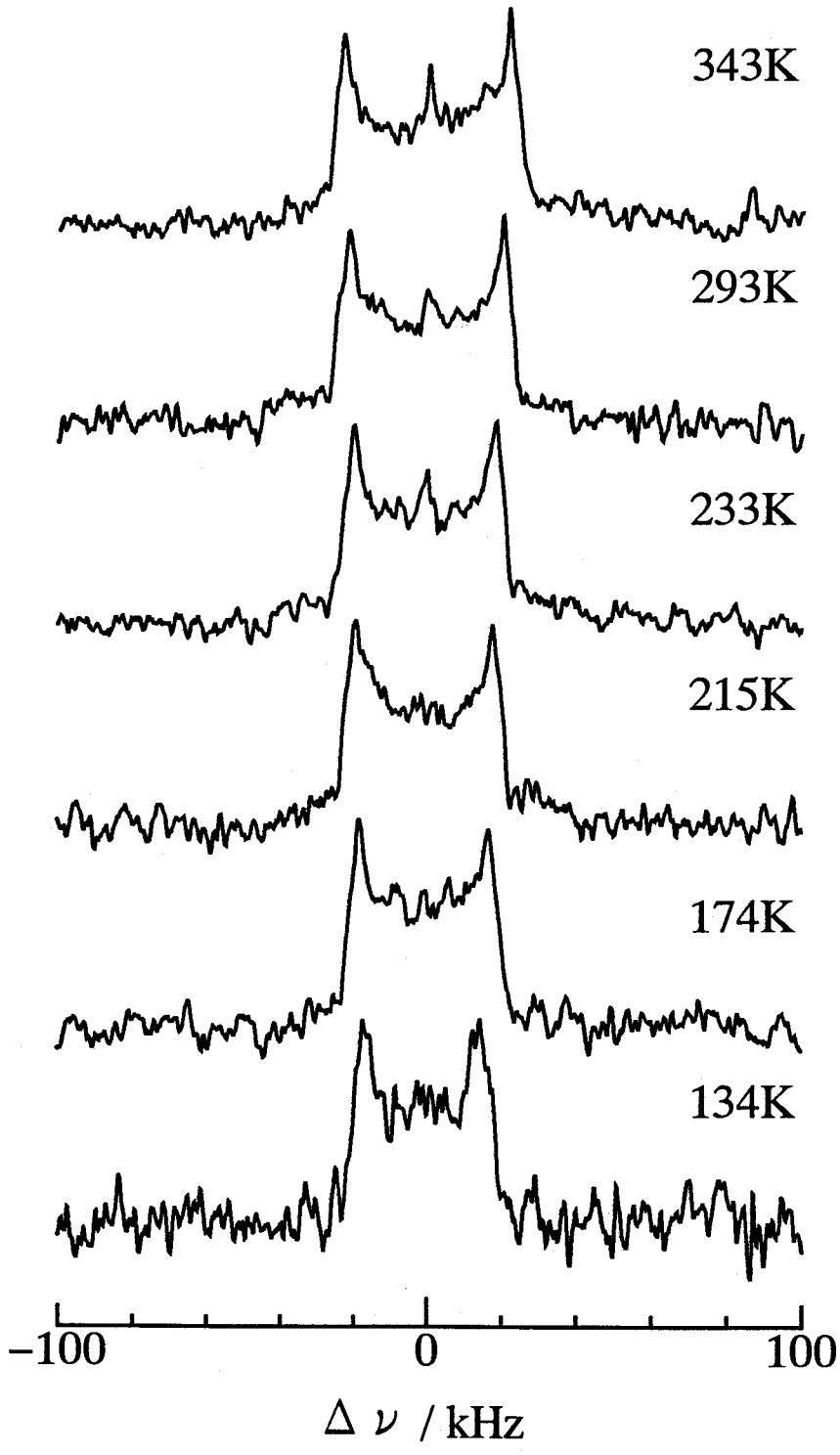

Figure 4.3: ^{2}H line shapes of KH(adc)-50%d.

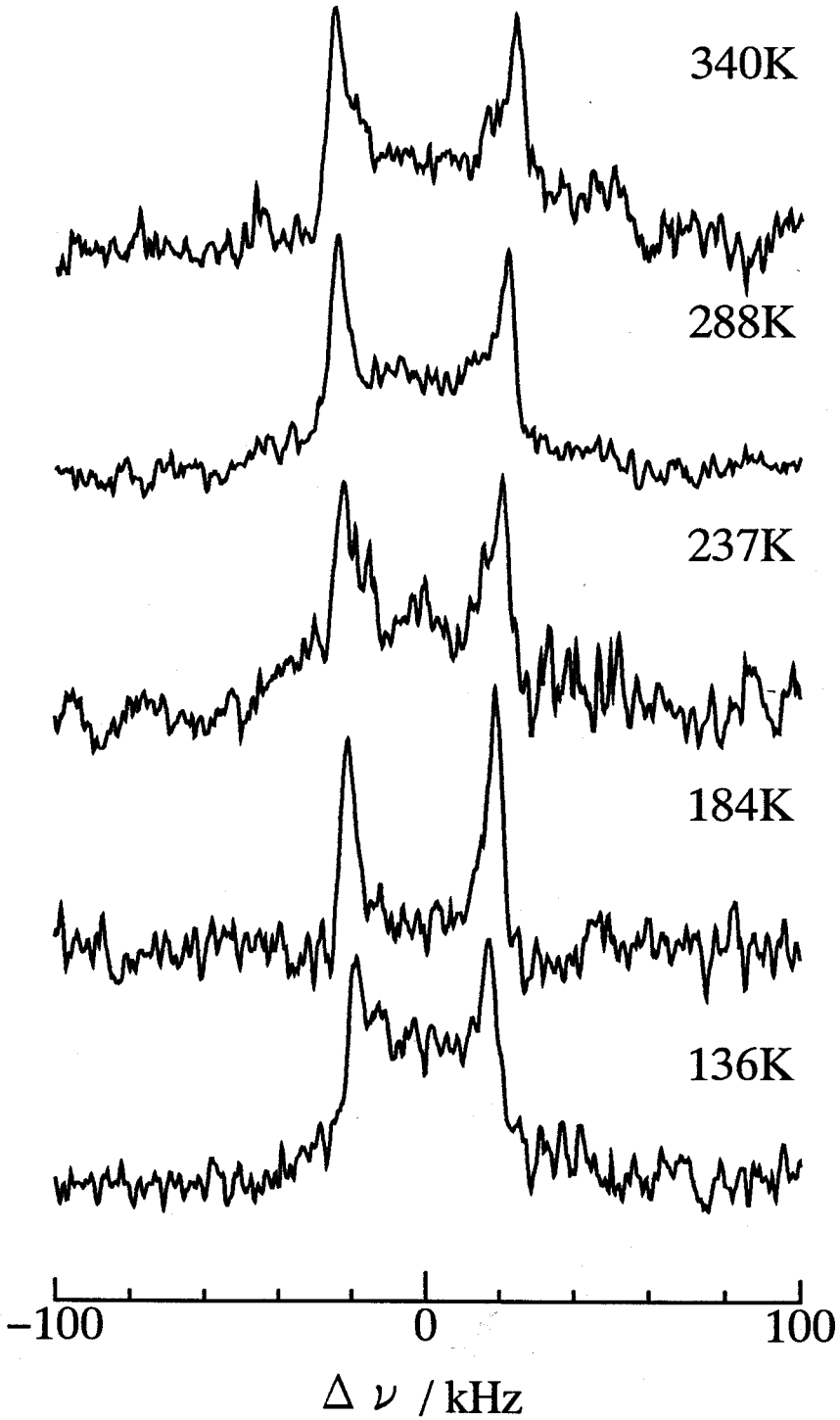

Figure 4.4: ^{2}H line shapes of RbH(adc)-99%d.

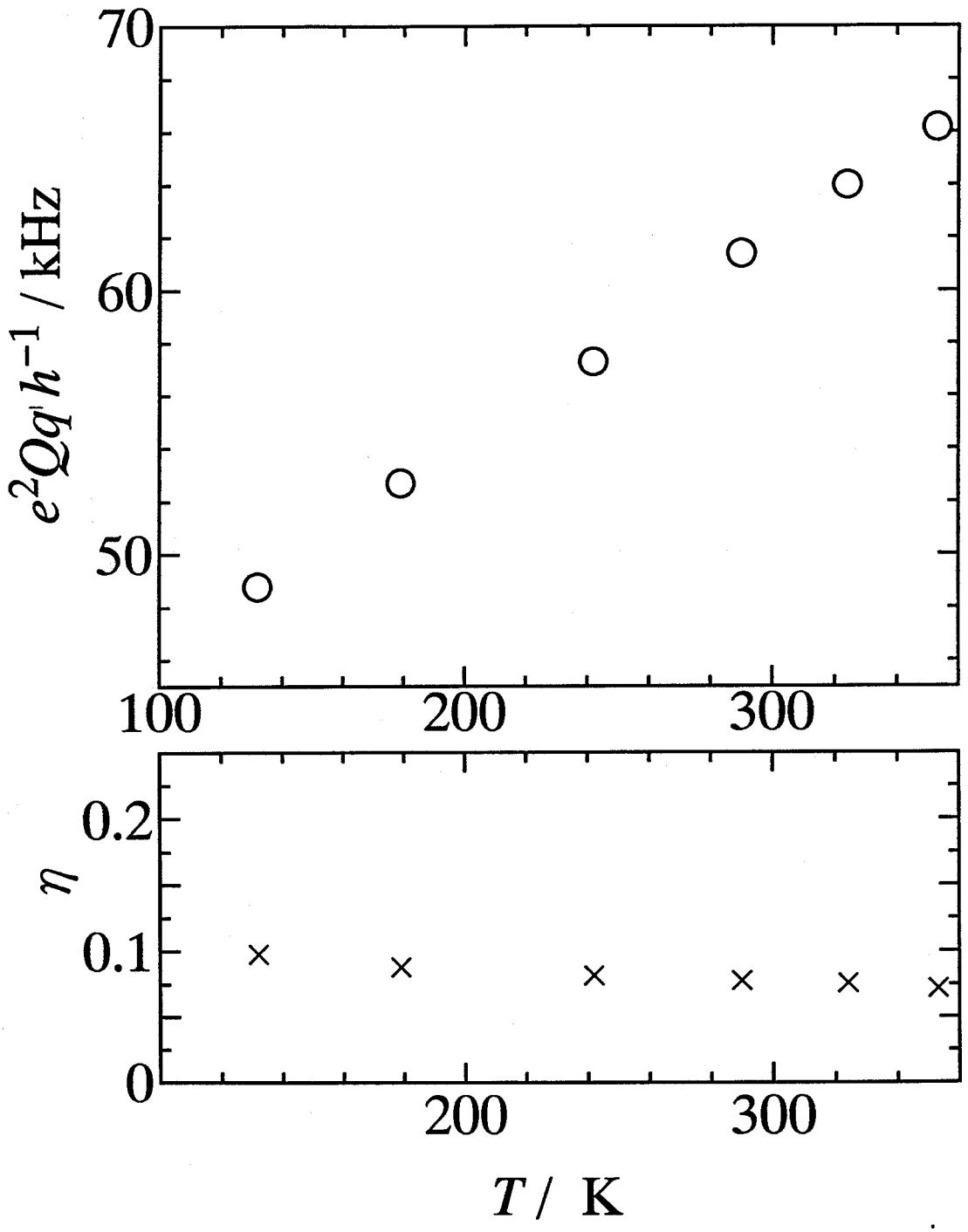

Figure 4.5: Temperature dependencies of e^2Qq/h:open circle and η:$\times$ of KH(adc)-99%d.

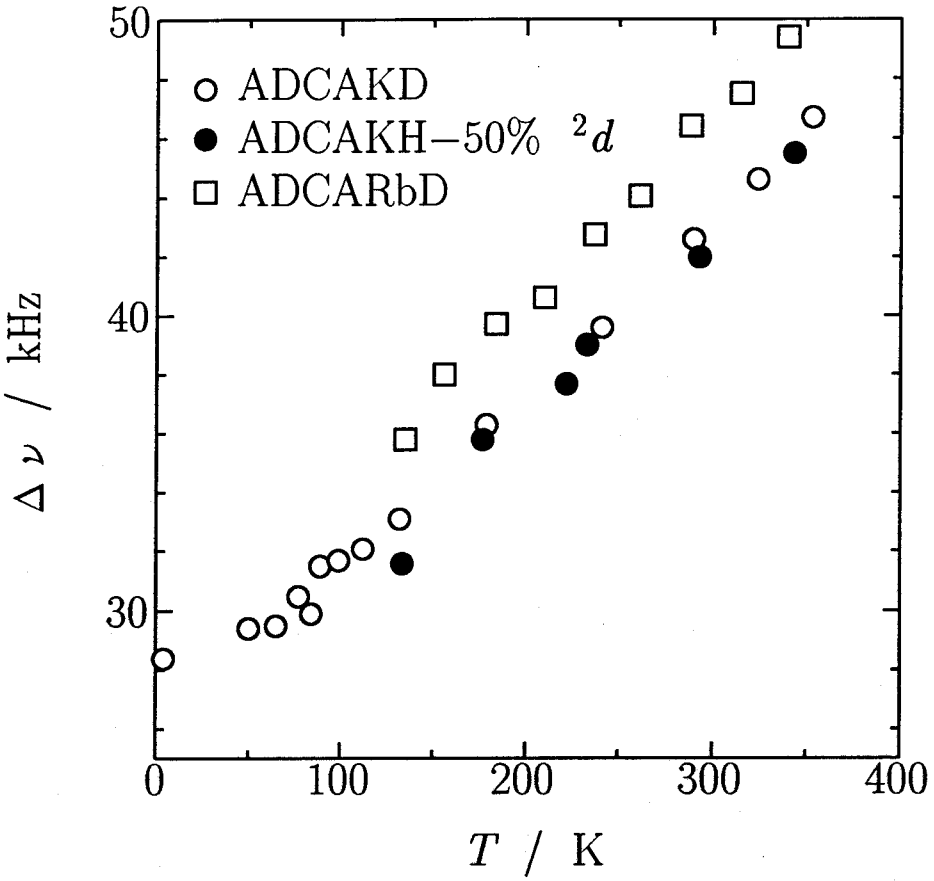

Figure 4.6: Peak to peak splittings of ^{2}H line shapes of KH(adc)-99%d:open circle, KH(adc)-50%d:closed circle, and RbH(adc)-99%d:open square.

$\Delta\nu$ of KH(adc) is not changed by partial deuteration of acid hydrogens. $\Delta\nu$ is related to e^2Qq/h and η by $(3/4)|e^2Qq/h|(1-\eta)$. Since η is nearly temperature independent, the temperature dependence of $\Delta\nu$ reflects the variation of e^2Qq/h with temperature.

The correlation between e^2Qq/h and $R_{O\cdots O}$ or $R_{O\cdots H}$ bond length was reported by several researchers [35–40]. In most O-H$\cdots$O hydrogen bonds ($R_{O\cdots O} > 2.6$Å) stronger hydrogen bond results in shorter $R_{O\cdots O}$ longer R_{O-H}, and lower e^2Qq/h (and *vice versa*). Empirical relationship such as

$$\frac{e^2Qq}{h} = 311.0 - \frac{560.4}{R_{O\cdots H}{}^3}(\text{kHz}) \tag{4.7}$$

by Soda and Chiba is derived [38,39]. An empirical relation (4.7) was converted to the equation between e^2Qq/h and $R_{O\cdots O}$,

$$\frac{e^2Qq}{h} = 311.0 - \frac{223.8}{(R_{O\cdots O} - 1.433)^3}(\text{kHz}), \tag{4.8}$$

which was obtained for $R_{O\cdots O} > 2.48$Å. But there happens a more complex situation in the short hydrogen bond region. In this region the above correlation of $R_{O\cdots O}$ and e^2Qq/h does not apply to single-minimum hydrogen bonds. Poplett *et al.* summarized various

experimental data of e^2Qq/h and η in the short hydrogen bonds [40]. They recognized two features in the short hydrogen bond region. Firstly $(R_{O...O} - 1.433\mathring{A})^{-3}$ correlation breaks and e^2Qq/h becomes insensitive to $R_{O...O}$ and assumes a mean value of *ca.* 56kHz. Secondly high $\eta \sim 0.5$ groups appear in $R_{O...O} < 2.44$Å region. In usual hydrogen bonds the values of η of acid hydrogen are small ($\eta \sim 0.1$). However there have been found very short hydrogen bond with ($R_{O...O} < 2.4$Å) in which the value of η is as large as 0.5. According to Poplett's investigation, present data in Figs. 4.5 through 4.6 lies in the region where e^2Qq/h looks like insensitive to the sample and $R_{O...O}$. But present data showed that e^2Qq/h does not seem to be insensitive to $R_{O...O}$ in these short hydrogen bonds.

It is noted that $R_{O...O}$ decreases with decreasing in temperature in $K_3H(SO_4)_2$ [12]. Figs. 4.5 and 4.6 show that $|e^2Qq/h|$'s decreases with decrease in temperature in KD(adc) and RbD(adc). Since e^2Qq/h varies with $R_{O...O}$ as $e^2Qq/h \propto (R_{O...O} - 1.433)^{-3}$ for relatively long hydrogen bond as mentioned above, Figs. 4.5 and 4.6 suggest that $R_{O...O}$ in KD(adc) and KH(adc) decreases with decrease in temperature (thermal contraction), supporting the result of the present X-ray diffraction experiment for RbH(adc). X-ray diffraction of KH(adc) states that the hydrogen bond in this compound is a single minimum one [16], but ^{2}H NMR study for KD(adc) suggests that the hydrogen bond in each of KH(adc) and RbH(adc) has a double minimum character. Let us estimate the magnitude of the thermal contraction of the hydrogen bond length, $R_{O...O}$ in KD(adc) crystal by assuming Eq. (4.8). The differential form of Eq. (4.8) can be given as

$$\frac{\Delta e^2Qq}{h} = \frac{671.4\Delta R_{O...O}}{(R_{O...O} - 1.433)^4}. \tag{4.9}$$

Here the change of the hydrogen bond length $\Delta R_{O...O}$ may be estimated by putting $\Delta(e^2Qq/h) = -17.4$kHz for the temperature difference ΔT between 132 and 353K as shown in Table 4.1 and $R_{O...O} = 2.446$Å determined at room temperature [16]. Then we obtain $\Delta R_{O...O}/\Delta T = 1.2 \times 10^{-4}$Å/K for KD(adc). The estimation for the thermal contraction coefficient of the hydrogen bond of KD(adc) is similar to 9.4×10^5Å/K observed by X-ray diffraction for $K_3H(SO_4)_2$ which has short hydrogen bond ($R_{O...O} =$ 2.493Åatroomtemperature) [12]. In the case of $K_3H(SO_4)_2$ the contraction of the hydrogen bond length is parallel to the thermal contraction of the lattice parameters. Fig. 4.6 suggests that for $KH_{0.5}D_{0.5}$(adc) and α-RbD(adc) the same mechanism operates to the quadrupole coupling constants of deuterium as in the case of KD(adc).

4.2 ^{1}H high-resolution spectra

4.2.1 Introduction

A nucleus with a nuclear spin $I = 1/2$ does not have the quadrupole moment. A line shape is determined by the nuclear magnetic dipole-dipole interaction and/or the anisotropic chemical shift. The former depends on the positions of nuclei, and the latter depends on the electron environment. For abundant spin like ^{1}H in solid samples, however, the strong nuclear magnetic dipole-dipole interaction between nuclei broaden the spectrum and hinder to obtain information about the chemical shift. The coherent averaging technique by multi-pulse NMR enables one to eliminate this strong homonuclear dipolar coupling and observe the fine structure by chemical shift anisotropy [41–44]. However, the resolution of the spectrum is often insufficient for the detailed study of the chemical shift, due to the imperfectness of the pulse sequence and to inhomogeneity of the external field. Especially when there are several protons which are chemically distinguishable, it is hard to analyze the spectrum which consists of the overlapped powder spectra with the fine structure by the chemical shift anisotropy.

The CRAMPS (Combinated Rotation and Multi-Pulse Spectroscopy) is a convenient technique to obtain the chemical shift of ^{1}H in solids [44]. This is the application of the multipulse decoupling of the homonuclear dipolar interaction to the sample which is rotating at a high speed about the axis which is tilted by the magic angle from H_0. Using the MAS (Magic Angle Spinning) technique, the dipolar broadening which remains unremoved by the multi-pulse NMR, the chemical shift anisotropy, and the inhomogeneous broadening are averaged out. The information about the chemical shift anisotropy is lost in MAS, butthe isotropic chemical shift $\bar{\sigma}$ for each of chemically distinguishable protons can be obtained with better resolution.

Chemical shift reflects the behavior of the electrons around the measuring nucleus, especially the character of the chemical bonding. In the hydrogen bond the nature of the bonding such as O–H$\cdots$O varies with the strength of the hydrogen bond. Therefore the chemical shift shielding $\bar{\sigma}$ is considered to be one of the good indicators of the hydrogen bond strength, and many studies have been carried out so far [45–48]. In this section the chemical shift of ^{1}H is investigated by the CRAMPS experiment and the result is discussed with respect to the strength of the hydrogen bond.

4.2.2 Experimental

^{1}H CRAMPS spectra were measured using a Bruker MSL-200 NMR system and a Bruker MAS probe. The coil for ^{1}H nuclei is equipped for the cross-polarization or the

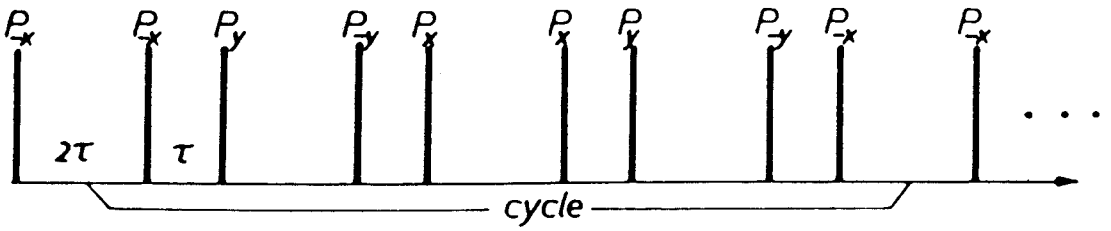

Figure 4.7: MREV-8 pulse sequence consists of the repetition of the eight 90° pulses. The sampling of a point of the time domain signal is done at the timing between the 8 pulse assemblies (from Haeberlen(1976) [43]).

broad-band decoupling for CPMAS. Sample is packed into the rotor for the CRAMPS which has a spacer to keep the powdered sample into the sphere of 4mm diameter to minimize the effect of the the inhomogeneity of H_0. Tuning of the spectrometer and data calibration were carried out using the method presented by Jackson *et al.* [49]. 90°pulse with the length of 2.05μs and the cycle time 35.4μs were used for MREV-8 [50] pulse sequence(Fig. 4.7) at 2.3kHz MAS speed.

By Fourier transformation an observed time domain signal is transformed to a frequency domain signal with scaled frequency axis. The scaling factor of the frequency domain is constant which depends on the used multi-pulse sequence and the 90° pulse length and the cycle time of it. However, due to the experimental mismatch of the spectrometer, the actual scaling factor is different from the theoretical value. Therefore, the scaling factor was obtained experimentally for each sample. After the assigning peaks in the sample a small amount of adamantan powder was mixed to the sample and measured its proton signal which was used as an internal reference (δ = 1.74ppm) for the chemical shift.

4.2.3 Results and Discussion

Observed spectrum of KH(tp) was shown in Fig. 4.8. Observed chemical shifts are listed in Table 4.2 together with some reference data of compounds with shorter $R_{O...O}$(< 2.5)Å.

Correlation between ^{1}H chemical shift and hydrogen bond length was investigated experimentally and theoretically by several authors [45–48]. Such correlation could be summarized briefly as follows.

1. The isotropic chemical shift shielding $\bar{\sigma}$ decreases as $R_{O...O}$ decreases ($\bar{\sigma}_{TMS} = -\delta_{TMS}$).

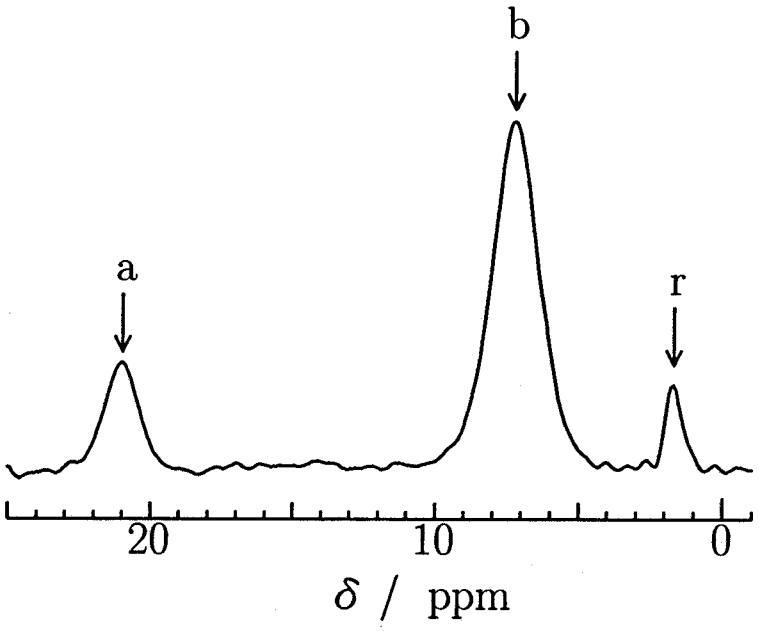

Figure 4.8: ^{1}H-CRAMPS spectrum of KH(tp). Peak (a) : acid proton ($\delta_{\mathrm{TMS}} = 21.2$ppm), and phenyl proton ($\delta_{\mathrm{TMS}} = 7.5$ppm). Peak (r) is the reference signal of adamantan $\delta_{\mathrm{TMS}} = 1.74$ppm. Here $\delta_{\mathrm{TMS}} = -\bar{\sigma}_{\mathrm{TMS}}$.

Table 4.2: ^{1}H chemical shifts of acid proton in some short symmetric hydrogen bonds in solid

Crystal	$R_{\mathrm{O\cdots O}}$	$R_{\mathrm{O\cdots H}}$	δ_{TMS}	ref
KH(tp)	2.459	1.68	21.2	this work
KH(adc)	2.445		20.4	this work
RbH(adc)	2.449	1.69	20.3	this work
KH(malonate)	2.468	1.234	20.5	[45]
KH(oxidiacetate)	2.476	1.328	19.6	[45]
KH(dicrotonate)	2.488	1.348	18.2	[45]
KH(maleate)	2.437		21.0	[45]

2. $\sigma_\perp$ is mainly respomsible for the variation of $\bar{\sigma}$. $\sigma_\perp$ is mainly determined by the lone pair electrons of the oxygen atom of hydrogen accepter,

Data obtained in the present work satisfy the well known correlation between $\bar{\sigma}$ and $R_{O...O}$. Jeffrey *et al.* remarked that $R_{O...H}$ also has a good correlation with $\bar{\sigma}$ [46]. However the data given in Table 4.2 do not obey the Jefferey's correlation. In their correlation diagram sampling of data $R_{O...H}$s' are the values for the hydrogen atoms which are assumed to locate at the center of hydrogen bond in the short hydrogen bonds.

4.3 ^{87}Rb NMR

4.3.1 Introduction

^{87}Rb is a nucleus with the nuclear spin $I = 3/2$ and has a nuclear electric quadrupole moment eQ. As was mentioned in section 4.1.1 the interaction between eQ and the electric field gradient eq which is produced at the nuclear position by the surrounding ionic charges modifies the nuclear spin interaction. The amount of the energy variation by the nuclear quadrupole interaction is specified by the nuclear quadrupole coupling constant e^2Qq/h and the asymmetry parameter η of the electric field gradient which is defined in section 4.1.1. The magnitude of e^2Qq/h of ^{87}Rb in ordinary ionic crystals falls in the MHz region. The energy scheme is determined by the main Zeeman energy and the quadrupole perturbation energy; energy diagram for the $I = 3/2$ nucleus with a quadrupole interaction is schematically depicted in Fig. 4.9. The transitions other than the central transition ($I = -1/2 \leftrightarrow 1/2$) are broaden out when e^2Qq/h is large ($>$ 1MHz) and only the central transition can be detected in powdered sample. The line shape of the central transition is governed by the quadrupole interactions. Therefore, the line shape can be theoretically calculated by the second order perturbation of the quadrupole Hamiltonian. This is also orientation dependent. Some typical examples of powder spectra for $I = 3/2$ case are given in Fig. 4.10.

4.3.2 Experimental

The ^{87}Rb spectra was measured by a Bruker MSL-200 spectrometer. The cryostat and the procedure of temperature control were already described in 4.1.2. Measuring Larmor frequency $\nu_L$is 65.485MHz on a Bruker magnet, while ν_L is 65.75MHz on a Oxford magnet. The length of the 90° pulse for observing the central transition was 1.9μs. The FID (free induction decay) signal given following the 90° pulse was observed in the time domain, and accumulated. Then it was Fourier transformed to the frequency domain signal which corresponds to the frequency spectrum.

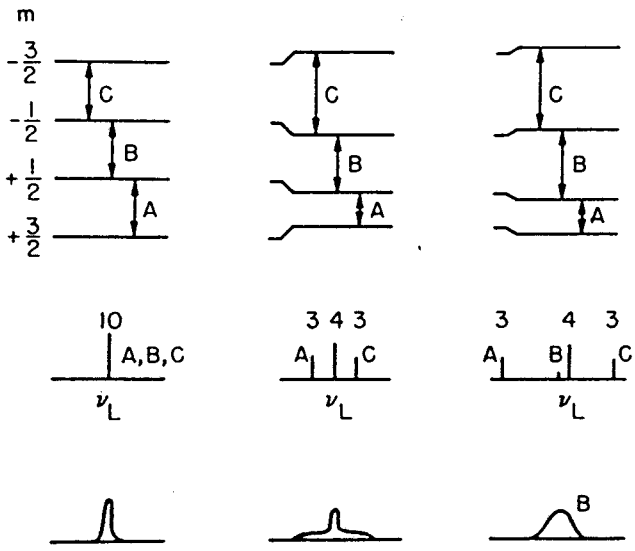

Figure 4.9: Energy level diagram of $I = 3/2$ nucleus under strong H_0 with electric quadrupole interaction (from Cohen and Reif(1957) [33]).

The temperature dependence of the spin-lattice relaxation time T_1 was also measured for the central transition of ^{87}Rb in RbH(adc) and RbD(adc) by the use of the inversion recovery method (180°—τ—90°).

4.3.3 Result and discussion

The temperature dependence of the observed spectrum is presented in Fig. 4.11. The spectrum shows that the electric field gradient (EFG) tensor is nearly axial-symmetric (see Fig. 4.10). e^2Qq/h was estimated to be 5.1MHz using $\Delta\nu_{pp} \sim (25/192)(e^2Qq/h)^2/\nu_L$ assuming $\eta \simeq 0$, where $\Delta\nu_{pp}$ is the magnitude of the splitting between two peaks. Spectrum was unchanged over temperature range of the measurements. Spectrum of RbD(adc) was almost the same as that in RbH(adc). Rb is on the 2-fold axis parallel to the crystallographic ***b***-axis, therefore one of the principal axis of EFG is also parallel to the ***b***-axis. The other two axis are in the *ac*-plane. But the actual directions can not be deduced from a powder spectrum.

Temperature dependence of spin-lattice relaxation rate T_1^{-1} of ^{87}Rb in RbH(adc) and RbD(adc) is plotted against $1/T$ in Fig. 4.12. It is noted that the T_1^{-1} for RbH(adc) and RbD(adc) coincided with each other within the experimental error. This fact suggests strongly that the relaxation of ^{87}Rb is not due to the fluctuation of the dipole coupling of ^{87}Rb with ^{1}H, but is caused by the fluctuation of the electric field gradient. The Rb^+ are surrounded by six oxygens of C=O and C–O–H. The fluctuation of EFG is probably

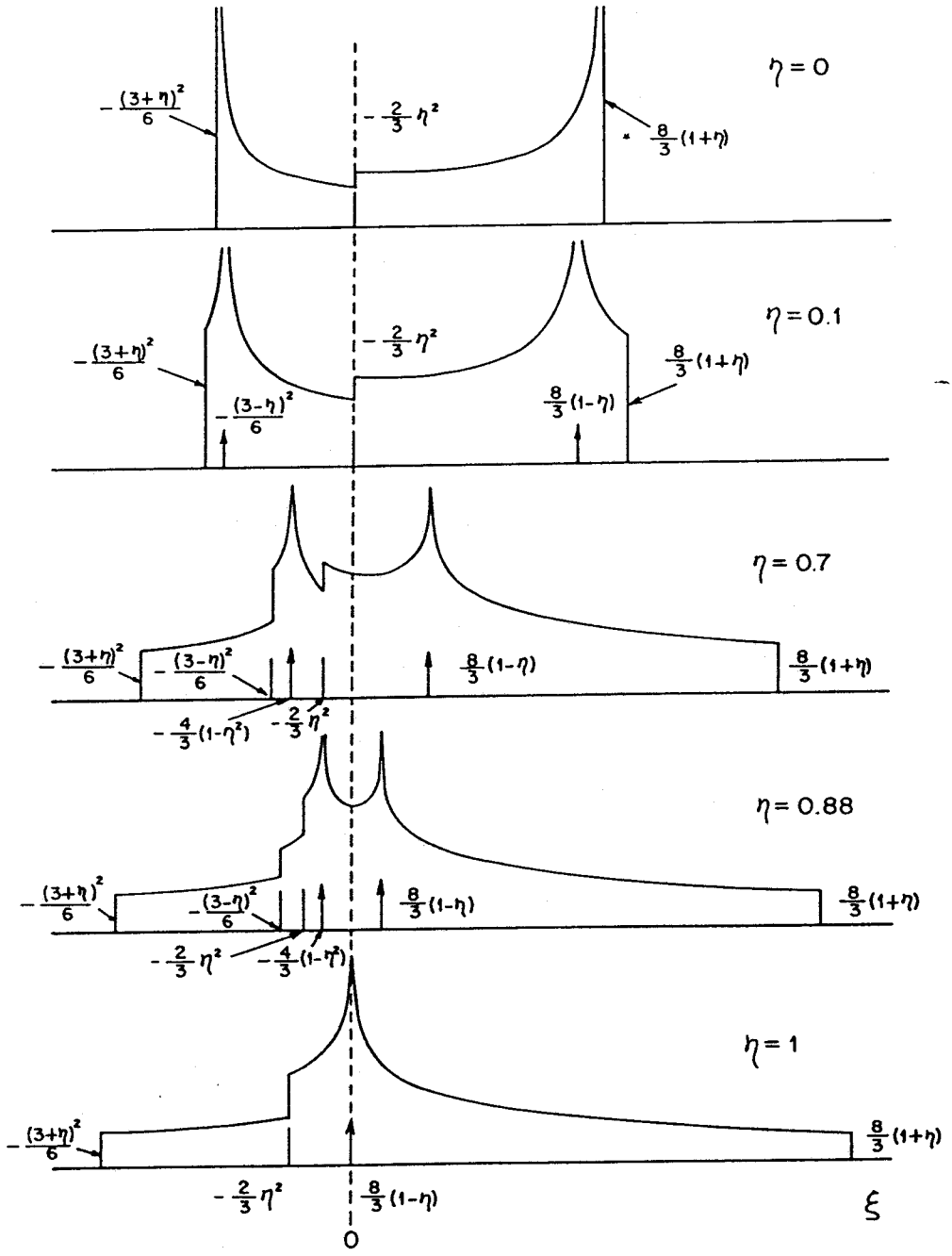

$$\xi = -\frac{96\nu_L(\nu - \nu_L)}{\nu_Q^2[4I(I+1)-3]} \quad \text{and} \quad \nu = \nu_L + \frac{\nu_Q^2[4I(I+1)-3]}{96\nu_L}\xi \quad \text{with} \quad \nu_Q = \frac{3e^2Qq}{2hI(I-1)}$$

Figure 4.10: NMR spectra of the central transition of a nucleus with half odd spin. (from González-Tovany and Beltrán-López(1990) [51])

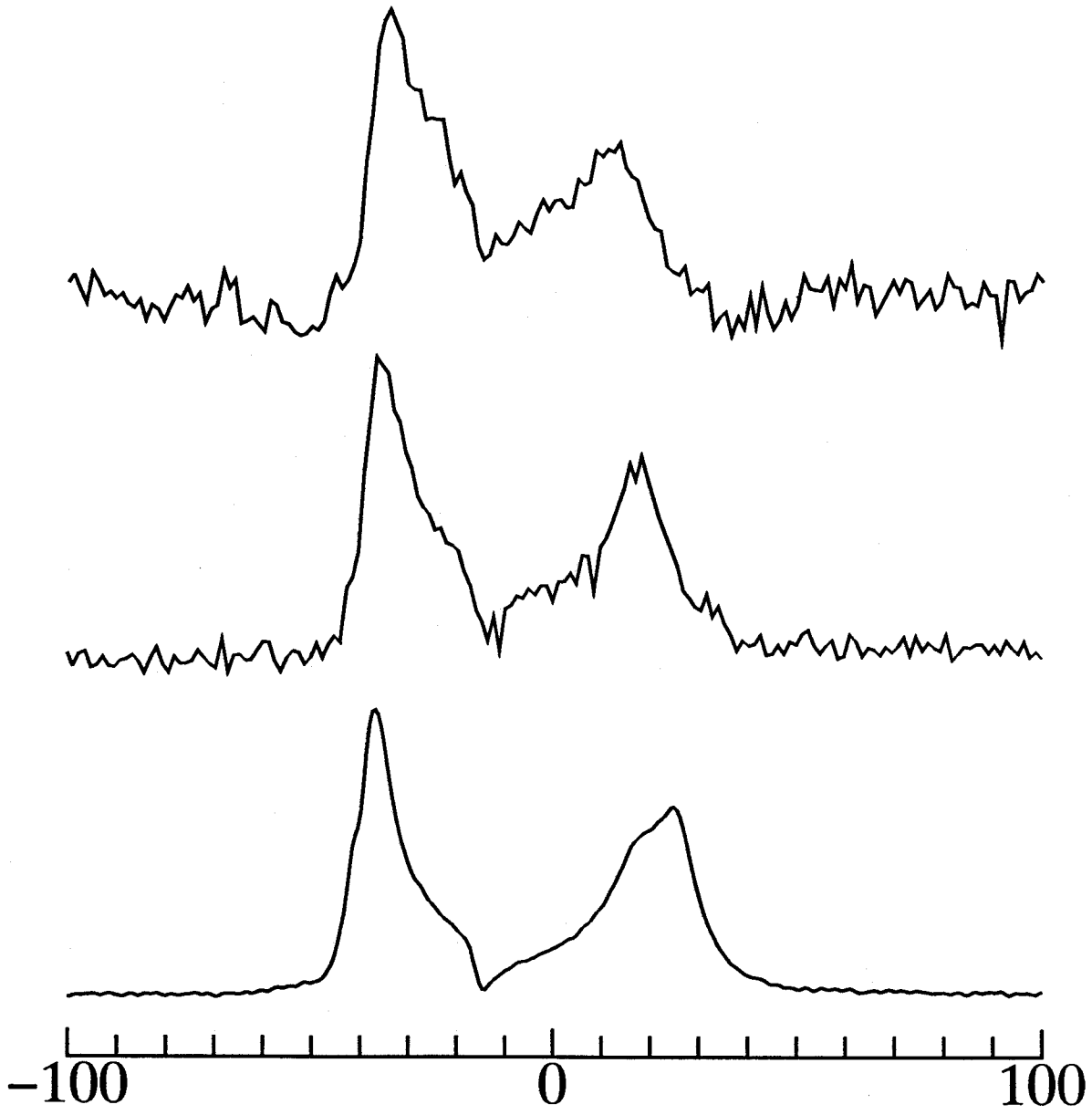

Figure 4.11: ^{87}Rb line shape of RbH(adc). (a) 4096 scans at room temperature, (b) 512 scans at *liq.* N_2 temperature, and (c) 32 scans at *liq.* He temperature.

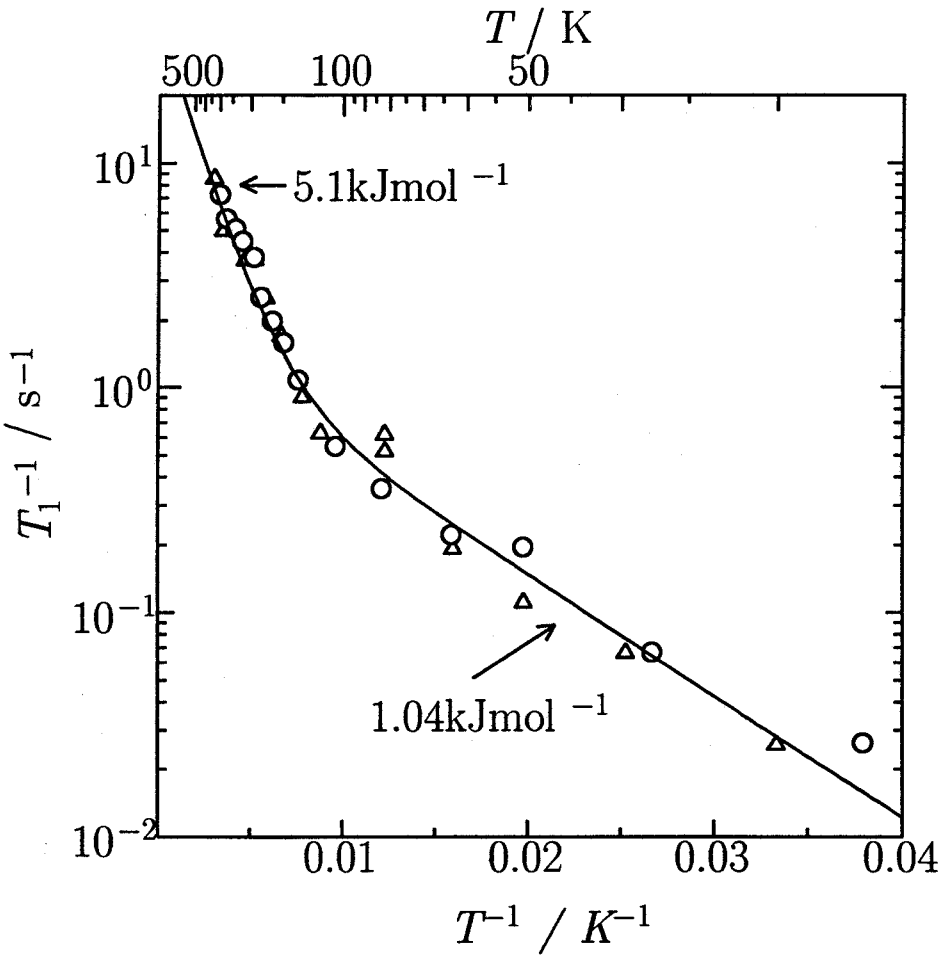

Figure 4.12: ^{87}Rb spin-lattice relaxation of RbH(adc):open circle and RbD(adc):open triangle, measured by inversion recovery method at $\nu_L = 65.485MHz$.

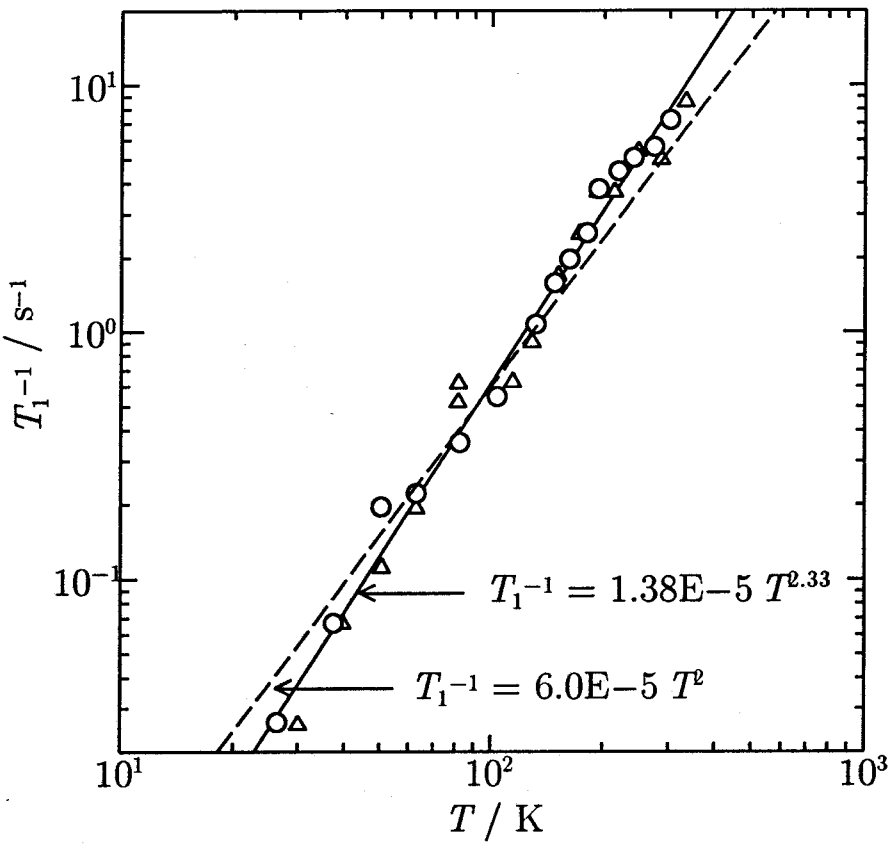

Figure 4.13: ^{87}Rb spin-lattice relaxation of RbH(adc):open circle and RbD(adc):open triangle, measured by inversion recovery method at $\nu_L = 65.485MHz$. The solid line is the result of the least square fitting of data by $T_1^{-1} \propto T^\alpha$. The dashed line is the guide line with the slope value $\alpha = 2$.

caused by the thermal motion of coordinating oxygens. The relaxation rate can roughly be represented by two straight lines which give rise to the activation energies of 5.1 kJ/mol in the high $T(> 100K)$ region and 1.03 kJ/mol in the low $T(< 100K)$ region. One possible explanation for this temperature dependence of T_1^{-1} is the molecular motions activated thermally with activation energies listed above. But the appropriate motional modes with effective fluctuation of EFG tensor and with activation energies listed above are required for this explanation. Another possible explanation for temperature dependence of T_1^{-1} is the contribution of the lattice vibration which also fluctuates electric field gradient. In this case the relation $T_1^{-1} \propto T^\alpha$ applies. α is a constant which depends on the process which works for the relaxation. When the T_1^{-1} is proportional to T^α the plot of logarithm of the T_1^{-1}against the logarithm of temperature T gives a straight line. And the slope of the line gives α. Such a plot is given in Fig. 4.13. A good linear relation is seen in Fig. 4.13. The least squares fitting gives the value of the exponent $\alpha = 2.33$ which resembles to $\alpha = 2$ in the case of the Raman process at higher temperatures than the Debye temperature. A line with $\alpha = 2$ is also drawn in Fig. 4.13. It can be concluded $T_1^{-1} \propto T^2$ applies to data in the present work.

Chapter 5

^{1}H spin-lattice relaxation and the dynamics of protons in one-dimensional hydrogen bonded chain

5.1 Effect of molecular motion on T_1

Measurement of the spin-lattice relaxation time (T_1) is a powerful tool for studying dynamic properties of solids. Random motion of nuclei gives rise to fluctuation of nuclear spin Hamiltonian. Fluctuating nuclear spin Hamiltonian causes the induced transitions between Zeeman-splitted nuclear spin energy levels. In ^{1}H-NMR the fluctuation of nuclear magnetic dipole-dipole interaction (hereafter it is called dipolar interaction for simplicity) is the largest and the most important cause for the nuclear spin relaxation. Because the dipolar interaction depends on the distance and orientation between nuclei, random molecular motion is very effective on the ^{1}H relaxation. The T_1^{-1} are proportional to the spectral density of the fluctuation of local dipolar field. In the weak-collision limit, *i.e.* when the purturbational theory is valid, the spin-lattice relaxation rate (T_1^{-1}) by the dipolar interaction between like spins is given by (see chapter VIII of Abragam's [34])

$$\frac{1}{T_1} = \frac{3}{2}\gamma^4\hbar^2 I(I+1)\{J^{(1)}(\omega_L) + J^{(2)}(2\omega_L)\}. \tag{5.1}$$

In Eq. (5.1) γ and I are the gyromagnetic ratio and the nuclear spin number of the probing spin. And $J^{(n)}(\omega)$ is the spectrum density of the fluctuation which is related to the time correlation function $G^{(n)}(\tau)$ of the $(\pm n)$th quantum state of the dipolar interaction, of the motion by

$$J^{(n)}(\omega) = \int_{-\infty}^{+\infty} G^{(n)}(\tau) e^{-i\omega\tau} d\tau. \tag{5.2}$$

It is convenient to use a reduced correlation function $g^{(n)}(\tau)$ normalized to 1 at $\tau = 0$ and its Fourier transform $j^{(n)}(\omega)$ instead of $G^{(n)}(\tau)$ and $J^{(n)}(\omega)$. Using this reduced $j^{(n)}(\omega)$ into Eq. (5.1),

$$\frac{1}{T_1} = C_{DD}\{j^{(1)}(\omega_L) + j^{(2)}(2\omega_L)\} \tag{5.3}$$

is obtained. C_{DD} expresses the magnitude of the dipolar interaction which is averaged out by a motional mode. Roughly speaking, the most effective relaxation occurs, *i.e.*, the T_1^{-1} takes the maximum value when a time scale of random motion (with the correlation time: τ_c) approaches to the inverse of Larmor frequency ($\nu_L = \omega_L/2\pi$). In the case of

some kind of molecule reorientating randomly, the correlation function of the motion is generally represented by

$$g(\tau) = \exp\left(-\left|\frac{\tau}{\tau_c}\right|\right), \tag{5.4}$$

and hence the spectral density is

$$j(\omega) = \frac{\tau_c}{1+\omega^2{\tau_c}^2}. \tag{5.5}$$

This single-exponential correlation function is attributed to the Markov character of the random molecular motion. Markov process is a process in which the probability of the motional event does not depend on any history. In Eqs. (5.4) and (5.5) τ_c is called the correlation time of the motion and its inverse correspond to the rate of the motion. These equations apply to the random thermal motion of molecules. The relaxation process obeying these equation is called Debye-type relaxation. Substitution of Eq. (5.5) to $j^{(n)}(\omega)$ of Eq. (5.3) leads to the famous BPP equation [52]:

$$\frac{1}{T_1} = C\left\{\frac{\tau_c}{1+{\omega_L}^2{\tau_c}^2} + \frac{4\tau_c}{1+4{\omega_L}^2{\tau_c}^2}\right\}, \tag{5.6}$$

where $j^{(1)}\omega : j^{(2)}(\omega) = 1 : 4$ for the dipolar interaction and for the powder specimen. It should be remarked that the T_1^{-1} depends on frequency as $T_1^{-1} \propto {\omega_L}^{-2}$ in the slow motion limit, *i.e.*, when $\omega_L\tau_c \geq 1$ holds.

Eq. (5.6) is derived by assuming a rapid $\tau_c(\tau_c \ll T_2)$ of isotropic motion of molecules or ionic spiecies. T_2 is the nuclear spin-spin relaxation time and is related to the spectral line width.

The temperature dependence of T_1^{-1} is evaluated by the use of the Arrhenius activation process according to which the correlation time is represented by

$$\tau_c = \tau_0 \exp\left(\frac{E_a}{RT}\right), \tag{5.7}$$

where E_a is the activation energy of the motion. Using Eq. (5.7) in Eq. (5.6) the plot of logarithm of the relaxation rate, $\log T_1^{-1}$, against the reciprocal temperature, $1/T$, gives a Λ-shape curve; its slope on the both sides of the maximum of T_1^{-1} gives the activation energy and the value of T_1^{-1} maximum is used to determine the coefficient C_{DD}. The analysis of C_{DD} by model calculation leads to the determination of $\tau_c$and τ_0 and the mode of the motion which contributes to the relaxation.

Most of classical motions such as molecular rotation or reorientation and translational diffusion contribute to the relaxation according to Eqs. (5.6) and (5.7), but there exist various specific motions which contribute to the proton relaxation in different ways from that predicted by Eq. (5.6). In such cases the spectral density and T_1^{-1}obey different equations from Eqs. (5.5) and (5.6), respectively [53,54]. An example of the effect of such specific motion on T_1^{-1} is described in the next section.

5.2 Effect of kink soliton on ^{1}H-T_1

5.2.1 The concept of the kink soliton in a hydrogen bonded chain

In a one-dimensional hydrogen bonded chain, the existence of a cooperative motion called a kink soliton has been pointed out. In this section the effect of the motion of the kink soliton on T_1 is discussed.

In the case that the neighboring hydrogen bonds interact strongly with each other, it is not appropriate to consider the positions of the acid hydrogen atoms in these hydrogen bonds are independent variables of each other because their movements are always closely linked together. The ice rule, which means that a water molecule must be electrically neutral in the network of hydrogen bond, is the most typical expression of such a situation. When a hydrogen atom jumps from its original site to another one in the double minimum hydrogen bond the electrical neutrality is broken. Hence, in order to meet the ice rule, the change of the hydrogen configurations in other hydrogen bonds has to take place. To keep the electrical neutrality in the one-dimensional network, an accidental jump of hydrogen atom in one hydrogen bond must induce the successive jump of hydrogens over the whole chain is needed. The probability of such a correlated motion of hydrogen atom is extremely small in the sense of linear interaction because it needs infinitely high energy.

When a hydrogen atom is displaced from its stable position in a hydrogen bond the resultant hydrogen bond having the hydrogen atom at the wrong site should be called "defect". The defect formation brings about the increase in the total energy of the chain. However, in the case that the coupling between hydrogen bonds is strong, the hydrogen atom in the neighboring hydrogen bond will respond to the change of situation and tend to move in phase with the motion of the defect. Thus the local motion transmit along the chain and if the system meet a condition which stabilizes this non-linear wave called "soliton", the total energy of the chain will be lowered.

The mechanism of the soliton formation can be described by a simple "ϕ^4" theory [1,55–58]. According to this theory the total Hamiltonian of the whole hydrogen bonded chain is given by

$$H_{\mathrm{T}} = \sum_i \left\{ \frac{m}{2}\dot{\phi}^2 + V(\phi) + \frac{1}{2}C(\phi_i - \phi_{i+1})^2 \right\}, \tag{5.8}$$

$$V(\phi) = -\frac{1}{2}A\phi^2 + \frac{1}{4}B\phi^4. \tag{5.9}$$

m and ϕ_i represents the mass and the position of hydrogen atom in the i-th hydrogen bond, respectively. The first term of Eq. (5.8) is the kinetic energy of the hydrogen atom, the second term is the potential energy at the hydrogen position, and the third term

represents the interaction between two neighboring hydrogen bonds. The name "ϕ^4" model comes from the ϕ^4 term in Eq. (5.9).

When the coupling constant C is strong $(\phi_i - \phi_{i+1})$ may remain small. In such a case Eq. (5.8) can be replaced by the continuous approximation,

$$H_{\mathrm{T}} \simeq \int \frac{dx}{l}\left\{\frac{p(x)^2}{2m} - \frac{1}{2}A\phi(x)^2 + \frac{1}{4}B\phi(x)^4 + Cl^2\left(\frac{d\phi}{dx}\right)\right\}, \tag{5.10}$$

where l is the lattice spacing and x represents the coordinate along the one-dimensional chain. From this H_{T} the Euler-Lagrange equation,

$$m\frac{\partial^2\phi}{\partial t^2} - Cl^2\frac{\partial^2\phi}{\partial t^2} + \frac{\partial V}{\partial \phi} = 0 \tag{5.11}$$

can be derived. This equation have a well-known (anti)kink solution,

$$\phi(x,t) = \tanh\left[\frac{x - vt}{\sqrt{2}\xi(1 - v^2/c_0^2)^2}\right], \tag{5.12}$$

where v is the kink velocity, $\xi = \sqrt{(C/A)}l$ is the kink width, and $c_0^2 = Cl^2/m$ is a relevant velocity. This solution is known to behave like a particle translating freely in the chain. And the formation energy (rest energy) of the static soliton is given by,

$$E = \frac{2\sqrt{2}}{3}\frac{A^{\frac{3}{2}}C^{\frac{1}{2}}}{B} \tag{5.13}$$

For a hydrogen bonded chain a improved model, two-component model, which takes into account of the dynamics of oxygen lattice was also proposed [2, 59]. Nature of the kink soliton by the two-component model is investigated mainly by computational method.

However, there is no NMR study of the dynamics of the kink soliton in the hydrogen bonded chain. In the next section the formulation of the spin-lattice relaxation rate due to the dynamics of the "kink soliton" is presented. The kink soliton can be generated in the limiting case of very strong interaction between neighboring hydrogen bonds in the chain as described above (Fig. 5.1 (c)). The ideal form of kink soliton will be partially destroyed when the interaction becomes intermediate strength. In such a case the soliton-like motion together with the local motion of the hydrogen atom in the local double minimum potential will occur (Fig. 5.1 (b)). This effect on the spin-lattice relaxation of proton is also discussed in the next section.

5.2.2 Spin relaxation by kink-promoted hydrogen atom motion

A kink soliton looks like a domain wall in a hydrogen bonded chain (see Fig. 5.1). In both side of a kink, hydrogen atom positions are reversed. Therefore as a kink soliton travels through a particular hydrogen bond the hydrogen jumps from its original position

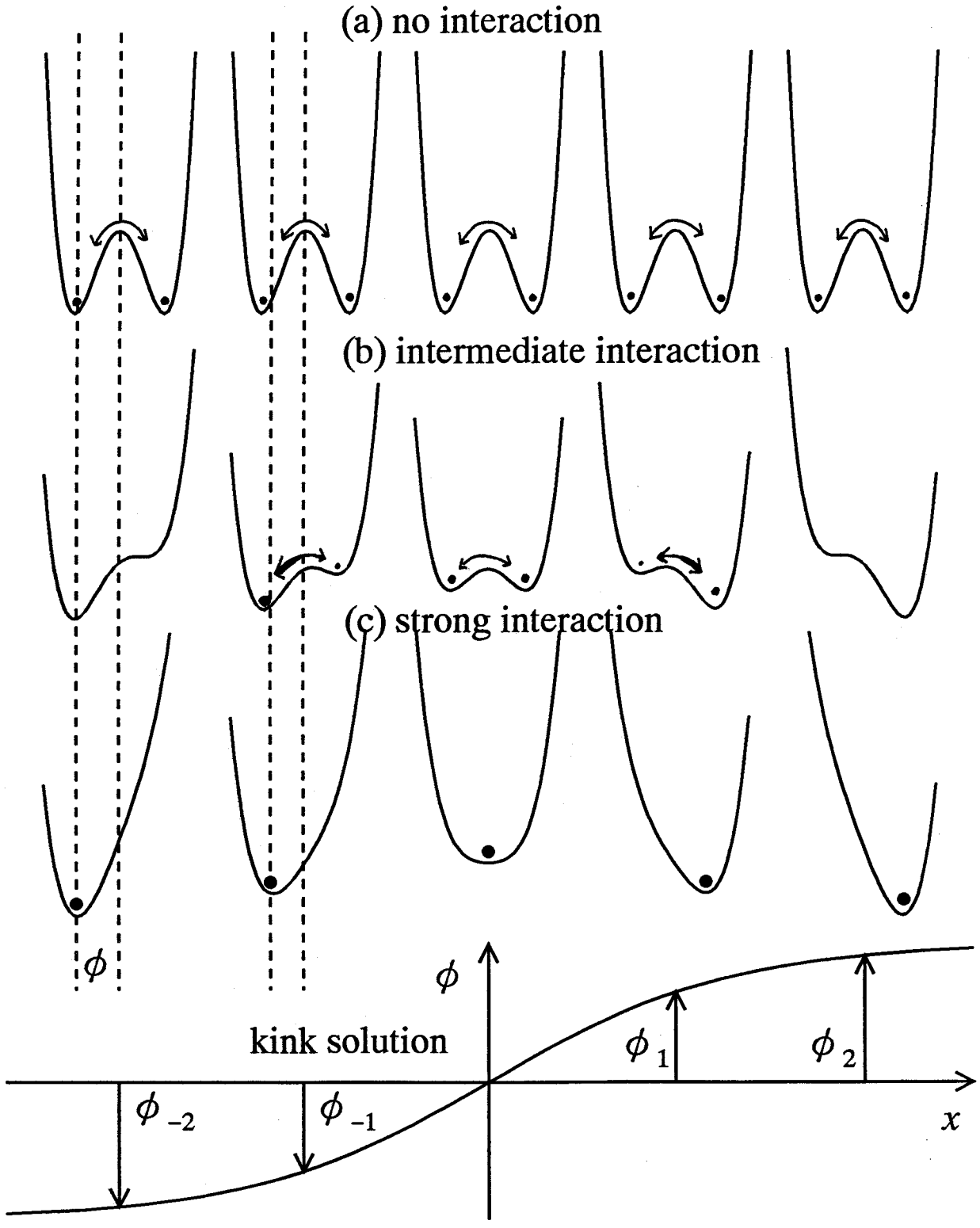

Figure 5.1: A comparison between the kink soliton (c) where $C \gg A$ in Eqs. 5.9 and 5.9, and local motion of the proton in local double minimum potential (a) where $C \ll A$. (b) is an intermediate situation where $C \sim A$ and local double minimum potential is strongly modulated by the interaction term in Eq. (5.8).

to another site in the double well.Such a kink-promoted hydrogen atom motion could be an effective mechanism of the proton spin-lattice relaxation, provided that the dipolar interactions of this proton with other spin species is strong enough. In this model a hydrogen atom motion is described by the use of the dynamics of the kink soliton.

Similar relaxation mechanism was also proposed in various situations. One of the most famous example is the electron and proton spin relaxations in *trans*-polyacetylene [60–63]. In this case the unpaired electron generated in defect in the polymer chain is regarded as a "kink" soliton (neutral soliton). Diffusion of electron spins accompanying the moving soliton causes an efficient spin relaxation in ESR and ^{1}H-NMR. It is noted that the relaxation is caused by the travelling electron spin in polymer chain. On the other hand the travelling soliton in one-dimensional hydrogen bonded chain consists of successive localized jumps of hydrogen atoms in their hydrogen bonds. And so the soliton dynamics brings about very local fluctuation in the dipolar interaction between protons which are localized in individual hydrogen bonds. Relaxation of a muon in *trans*-polyacetylene resembles the above situation. Sequential fluctuation of hyperfine interaction of the muon which is fixed at somewhere in the chain, leading to the muon spin relaxation [64]. In these studies it was pointed out that the relaxation rate has a characteristic frequency dependence, $T_1^{-1} \propto (D\omega_L)^{-1/2}$. This relation is regarded as the criterion for the evidence of soliton which undergoes one-dimensional Brownian motion with the diffusion constant D.

The soliton in one-dimensional hydrogen bonded chain resembles the defect motion in long alkyl chains [65, 66]. The defect means unusual *gauch* conformation which is produced in an alkyl chain which mostly assumes all *trans* conformations in solid state. When the defect happens to travel through the chain, the dipolar interaction between alkyl hydrogens fluctuates. It should be remarked that the spin-lattice relaxation in other various systems has been interpreted by soliton or soliton-like defect diffusion mechanism [67, 68]. However, the soliton mechanism has not yet been applied to the proton spin-lattice relaxation in one-dimensional hydrogen bonded chain system.

Skinner and Wolynes considered a system in which a number of kinks exist and their positions fluctuate randomly (Brownian motion) in the one-dimensional chain [69]. They described the Brownian motion of solitons phenomenologically and derived the following correlation function with respect to the hydrogen atom jump in the hydrogen bond:

$$g(\tau) = \exp\left\{-\frac{4n_0}{\gamma}\sqrt{\frac{\gamma t - 1 + \exp(-\gamma t)}{\beta m^* \pi}}\right\}, \tag{5.14}$$

where $\beta = (kT)^{-1}$, m^* is the effective mass of soliton, n_0 the density of the soliton, and γ expresses the strength of the friction. This complex equation can be reduced to a simple equation in two limiting cases, (i) no friction, *i.e.* $\gamma \to 0$, and (ii) strong friction, *i.e.*

$\gamma \to \infty$. In the case (i) Eq. (5.14) is reduced to a single exponential correlation function

$$g(\tau) = \exp\left(-\frac{t}{\tau_e}\right), \text{ with } \tau_e = \sqrt{\frac{\beta m^* \pi}{8 n_0^{-2}}}. \tag{5.15}$$

In the more interesting case (ii) of the strong friction limit Eq. (5.14) becomes

$$g(\tau) = \exp\left\{-\left(\frac{t}{\tau_s}\right)^{\frac{1}{2}}\right\}, \text{ with } \tau_s = \frac{\beta m^* \pi \gamma}{16 n_0^2}. \tag{5.16}$$

The correlation function in Eq. (5.15) assumes the same form as Eq. (5.4) and therefore gives rise to the relaxation rate T_1^{-1} of the same form as that predicted by the BPP theory (Eq. (5.6)). On the other hand Eq. (5.16) for the strong friction limit contains $t^{1/2}$ instead of t as in Eq. (5.15). Therefore the soliton-promoted motion with a strong friction provides a different relaxation mechanism from usual BPP process. A rigorous calculation of T_1^{-1} by the soliton mechanism as given in section 5.5 will show that the proton T_1^{-1} varies as ${\omega_L}^{-3/2}$. Such a novel result will be discussed later.

Skinner and Wolynes examined the equilibrium properties of the system when a number of solitons exists in a chain. Their results will be referred to in section 5.5 when the analysis of the spin-lattice relaxation data will be performed.

In the case that the interaction between the hydrogen bonds in one-dimensional chain has an intermediate strength *i.e.*, $C \sim A$ in Eqs. (5.8) and (5.9), the ideal structure of the kink soliton becomes partially destroyed and the local double minimum potential of the hydrogen bond remains near the center of the kink. (see Fig. 5.1 (b)). Therefore the motional mode of of protons in the hydrogen bonds becomes complicated. While the local motion is impossible and the ideal kink soliton propagates in the case of $C \gg A$ in Eqs. (5.8) and (5.9) (see Fig. 5.1 (c)), soliton like motions together with the local motion in the double minimum potential of individual hydrogen bond may occur. The correlation function of Eq. (5.16) does not anymore describe the motion of individual protons in the hydrogen bonds. However, it is hardly possible to obtain the analytical formula of the correlation function for such intermediate situation ($C \sim A$). Thus a phenomenological model which has almost the same concept as the above statement is used to represent the complicated situation of the system. The interaction term C modurates strongly the local double minimum potential, resulting in the distribution of the barrier height of the local double minimum potential energy function. For the present system it is appropriate to introduce the Cole-Cole distribution function to describe the correlated proton motion. The strength of the correlation is expressed by a parameter δ ($0 < \delta \leq 1$), where the smaller δ indicates the stronger correlation. The spectral density for the Cole-Cole distribution is given by [54, 70]

$$j(\omega) = \frac{2}{\omega} \sin\left(\frac{\delta\pi}{2}\right) \left\{ \frac{(\omega\tau_c)^\delta}{1 + (\omega\tau_c)^{2\delta} + 2\cos\left(\frac{\delta\pi}{2}\right)(\omega\tau_c)^\delta} \right\}. \tag{5.17}$$

This equation will be applied together with the model by Skinner and Wolynes to the analysis of the experimental T_1^{-1} in the next section.

Apart from the Skinner-type kink formation, the formation of trapped kink was suggested for the hydrogen bonded one-dimensional chain by an optical measurement by Moritomo *et al.* [5]. This kink is a kind of defect and is not mobile in the chain. The spin-lattice relaxation due to such a kink defect shows very different behavior from the mobile kink discussed above. A hydrogen bond near the kink have double minimum potential as can be seen in Fig. 5.1(b), while the hydrogen bonds far from the kink have almost single minimum potential. Therefore only the proton at the kink defect can move in the double minimum hydrogen bond and is directly responsible for the spin-lattice relaxation of proton. Other protons far from such frozen kink defect relax via the spin diffusion process. The spin-lattice relaxation rate of all protons in the crystal can be expressed by [71],

$$T_1^{-1} = 8.5NC^{\frac{1}{4}}D^{\frac{3}{4}}, \tag{5.18}$$

where D is the spin diffusion constant, N the concentration of the fast relaxation center (the number of the frozen kink defects in this case), and C the relaxation rate of the proton at the kink positions. This process of spin-lattice relaxation will be effective for the system in which the kink cannot travel freely in the hydrogen bonded chain by any trapping mechanism. The localized proton in the mixture of proton and deuteron in the one-dimmensional chain, for example, nay correspond to such case.

5.3 Experimental

In the present work the proton spin-lattice relaxation rates T_1^{-1}were measured for KH(adc), RbH(adc), and KH(tp). For NMR measurement on each material, powdered sample was sealed into a glass ampoule of diameter of 5mm together with a small amount of dry He gas (typically 10mmHg at room temperature) for heat exchange. Before sealing each specimen was dried in vacuo overnight.

A home-built pulse NMR apparatus and home-made cryostat with double-dewar vessel were used for the spin-lattice relaxation measurements at 18 and 37MHz, and a Bruker MSL-200 NMR system was used at 200.13MHz. Temperature was monitored by Chromel-P-Constantan thermocouple above 43K and by Au-Fe-Constantan thermocouple below it. The temperature of the sample was controlled to at least within 0.2K over whole temperature range of measurements. The spin-lattice relaxation measurement by the Bruker machine was carried out with an attached cryostat the temperature of which is controlled by passing cold N_2 gas or hot air into a probe head. The temperature was monitored by Cu-Constantan thermocouple and controlled to within 1K. Recoveries

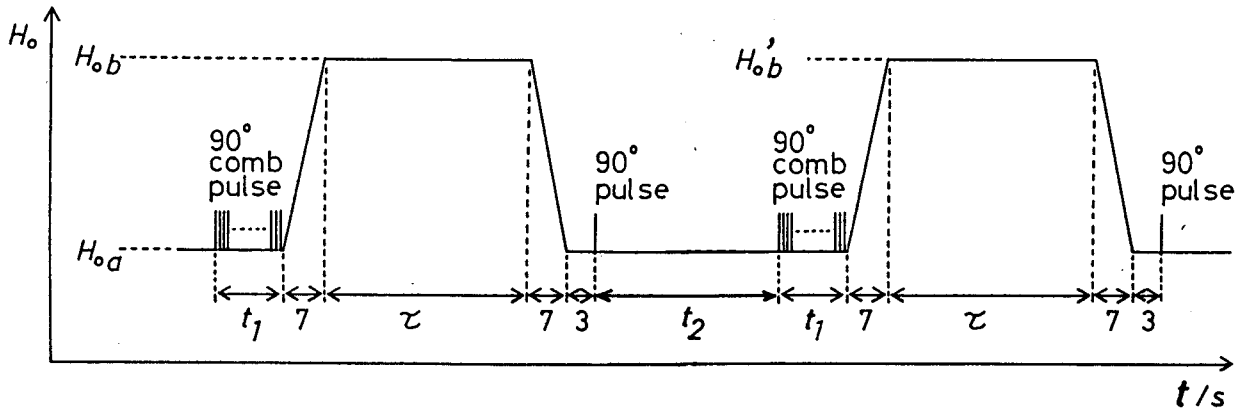

Figure 5.2: The procedures of the field cycling experiment for investigating the spin-lattice relaxation at the target field H_{0b} by measuring signals at the observing field H_{0a} (from Takeda(1982) [73]).

of the ^{1}H longitudinal magnetization were measured by the saturation recovery method (90°-train-τ-90° pulse sequence).

Field-cycling technique was also applied to investigate the detailed frequency dependence of $T_1^{-1}$for KH(tp) at 30K using the apparatus described in [72, 73]. In the present work about 20s was necessary for a field-cycling process. Therefore in the case that T_1 is shorter than 20s the spin temperature recovers to the lattice temperature during the field cycling. KH(tp) was appropriate for this experiment because of its relatively long T_1. Field cycling experiments was done at measuring frequencies of 18MHz and 37MHz.

5.4 Results

Typical magnetization recovery data are plotted in Figs. 5.3–5.5. Recoveries of ^{1}H longitudinal magnetization in each of samples did not obey the single exponential law over wide temperature range. The degree of non-exponentiality was small and depended on both the temperature (T) and the frequency (ν_L).

Analysis of experimental data has even ambiguity when the longitudinal magnetization returns non-exponentially to the equilibrium value. T_1 is usually applies as a time constant to a single exponential recovery of the longitudinal magnetization. But in the case of non-exponential recovery such a definition is meaningless. We can sometimes see such non-exponential recoveries of the magnetization. The most representative case is that two relaxation processes works simultaneously as is seen in the relaxation by dipolar coupling between unlike spins. The origin of these non-exponential recovery will be discussed in the next section.

As described above the longitudinal magnetization recovers non-exponentially to

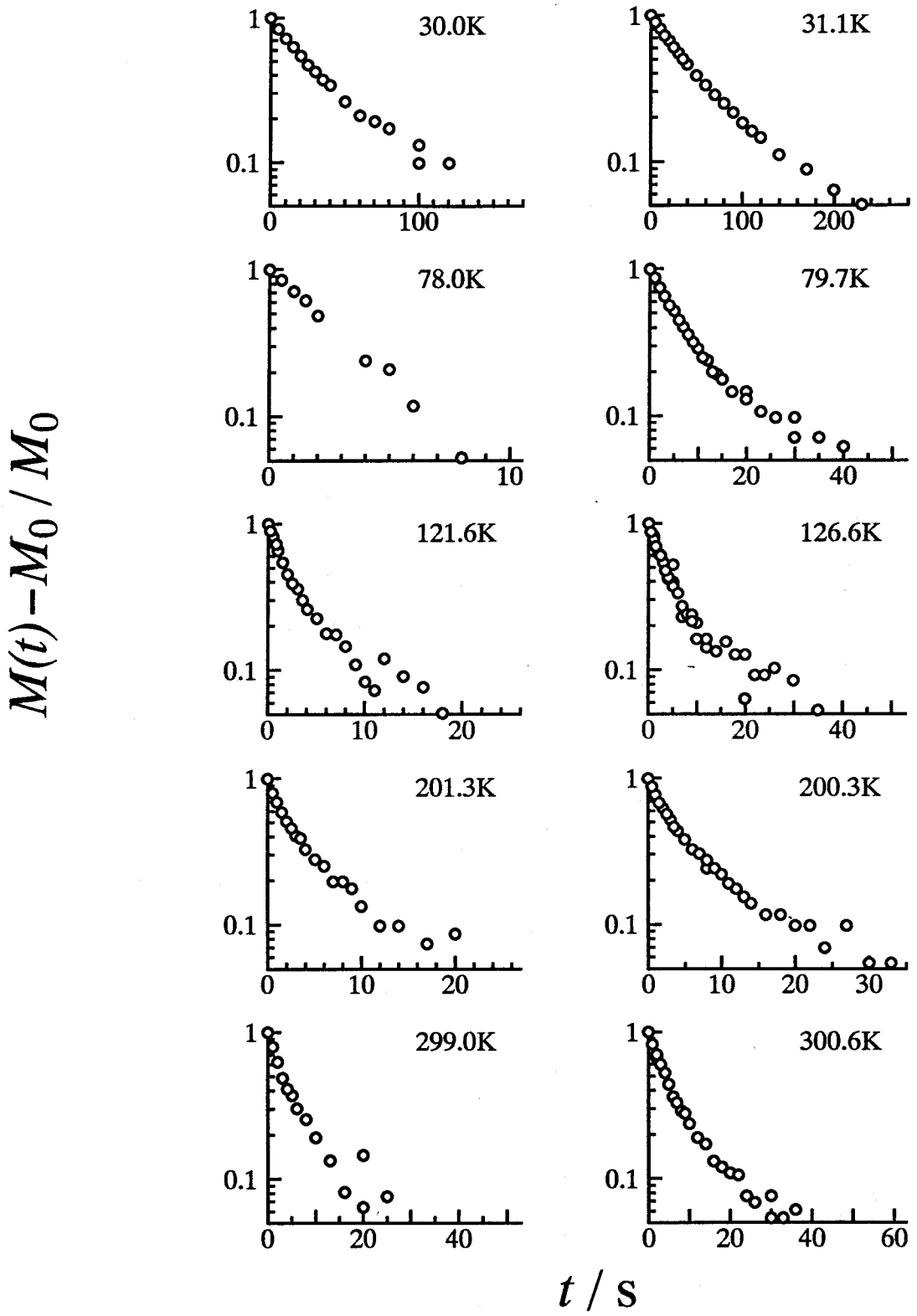

Figure 5.3: Recovery curves of ^{1}H magnetization of KH(tp) powder; the left column at 18MHz, the right column at 37MHz.

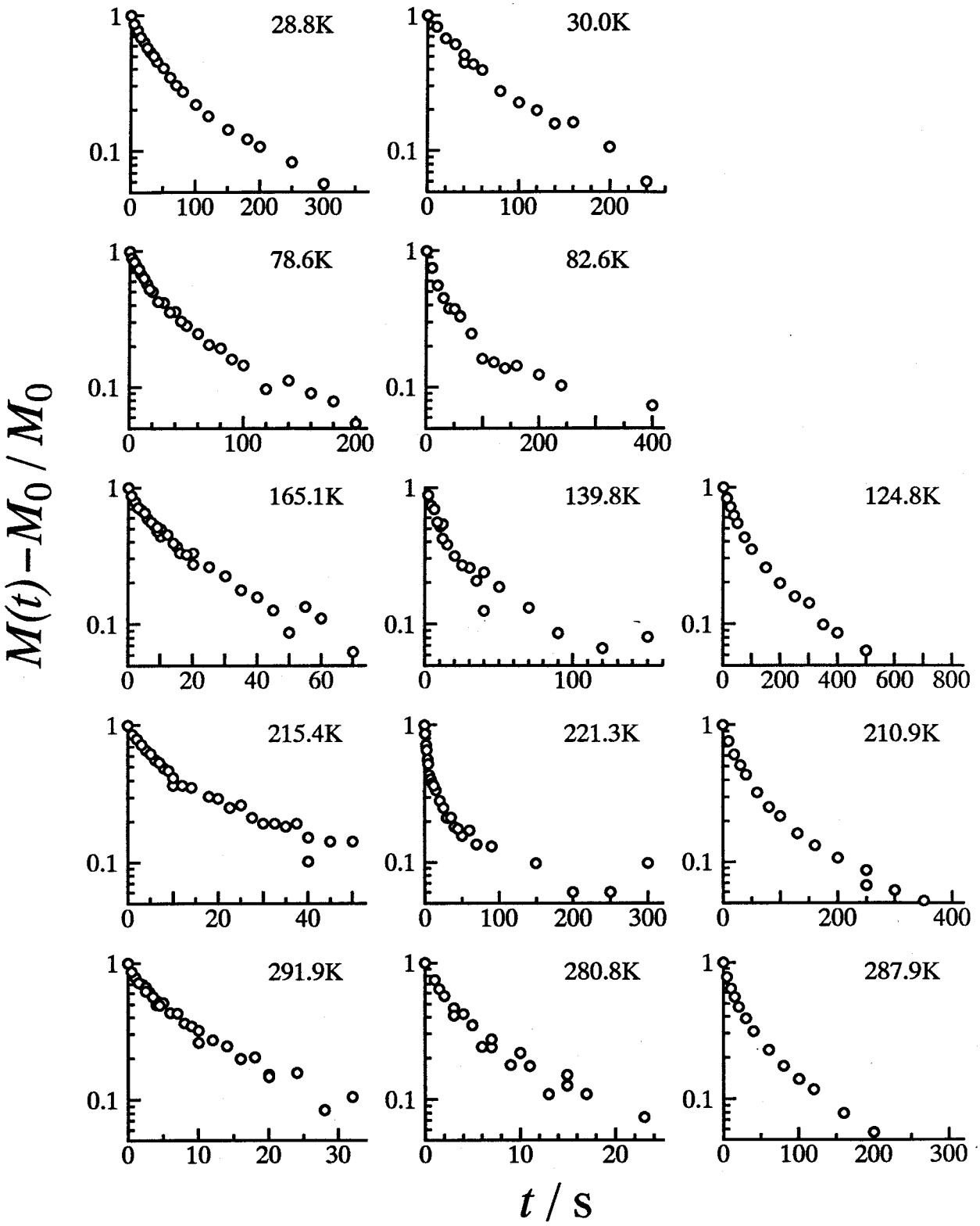

Figure 5.4: Recovery curves of ^{1}H magnetization of KH(adc) powder; the left column at 18MHz, the middle column at 37MHz, and the right column at 200MHz.

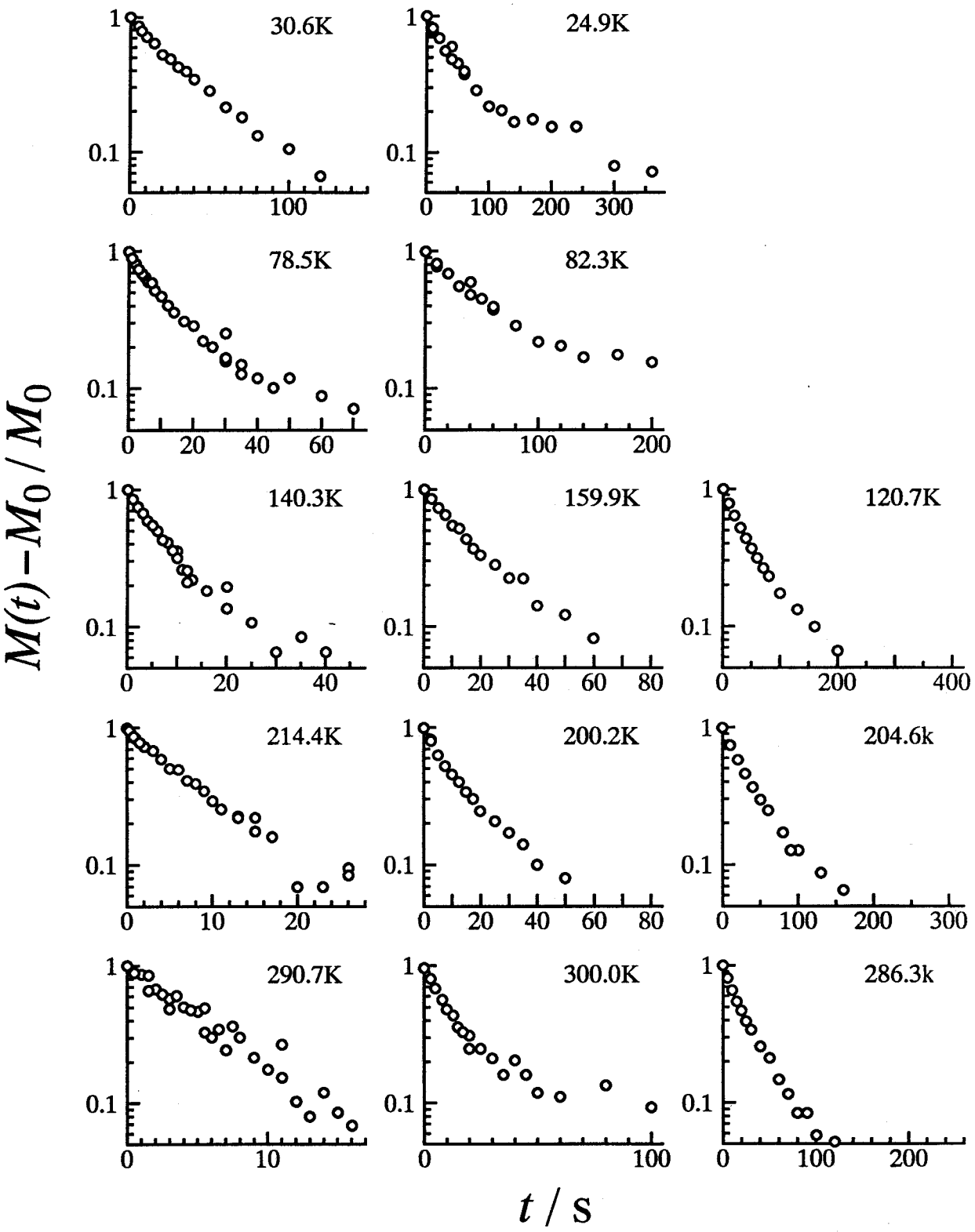

Figure 5.5: Recovery curves of ^{1}H magnetization of RbH(adc) powder; the left column at 18MHz, the middle column at 37MHz, and the right column at 200MHz.

the equilibrium magnetization in the present materials. Hence it was impossible to assign a single value to the T_1. Then the rate of spin-lattice relaxation $T_1^{-1}$was represented by an apparent T_1 which was deduced from the initial slope of the recovery curve. The resulted T_1^{-1} were plotted in Fig. 5.6 for KH(tp), in Fig. 5.7 for KH(adc), and in Fig. 5.8 for RbH(adc).

T_1^{-1} depends obviously on the Larmor frequency ($\omega_L = 2\pi\nu_L$) as can be seen in Figs. 5.7–5.6. The results of the field cycling experiment indicate that the T_1^{-1} of KH(tp) varies as ${\omega_L}^{-1/2}$ (Fig. 5.9) in the low temperature region. The T_1^{-1}'s of KH(adc) and RbH(adc) are nearly proportional to ${\omega_L}^{-\alpha}$ with $\alpha \sim 0.5 - 1.5$.

5.5 Discussion

The relaxation becomes faster with increasing temperature. This fact indicates that some thermally activated motional process governs the spin-lattice relaxation. The T_1^{-1} of ^{1}H of each compound depends only weakly on temperature in the lowest temperature region. One possible explanation for this fact is that different relaxation mechanism from simple fluctuation of the dipolar interaction between protons, for example, the contribution of paramagnetic impurities, works in these region. The variation of $R_{O\cdots O}$ which was suggested by the decrease of e^2Qq/h with decrease in temperature (subsection 4.1.3). Thus a relaxation mechanism originated in the change of the potential function may be proposed in the case of short hydrogen bonds. This change will be more remarkable at low temperature where $R_{O\cdots O}$ is very short.

In the high temperature region the T_1^{-1} shows strong temperature dependence (Figs. 5.10–5.12). The maximum value of T_1^{-1} of KH(tp) in Fig. 5.10 is interpreted reasonably by the fluctuation of the dipole interaction ($C_{DD} \sim 4.3 \times 10^7 s^{-2}$) between the phenyl protons and acid protons moving from one site to the other in the hydrogen bond in nearby hydrogen bonds The distance between the two sites of proton in the hydrogen bond was determined by single crystal X-ray diffraction experiment. No maximum of T_1^{-1} was observed for KH(adc) (Fig. 5.10) and RbH(adc) (Fig. 5.10). However, the values of $T_1^{-1}$of KH(adc) and RbH(adc) at the heighest temperatures of measurement (near 290K) are also interpreted by the fluctuation of the dipolar interaction ($C_{DD} \sim 4.0 \times 10^7 s^{-2}$) between protons, with the strength estimated from the crystal structure of RbH(adc). Much lower T_1^{-1} of protons of $KH_{0.5}D_{0.5}$(adc) than that of KH(adc) suggests that the relaxation in KH(adc) is caused by the fluctuation of the dipolar interacton between protons. From the view point of the similarity of T_1^{-1} as well as the crystal structures between KH(adc) and RbH(adc), it seems that the dipolar relaxation mechanism applies also to RbH(adc).

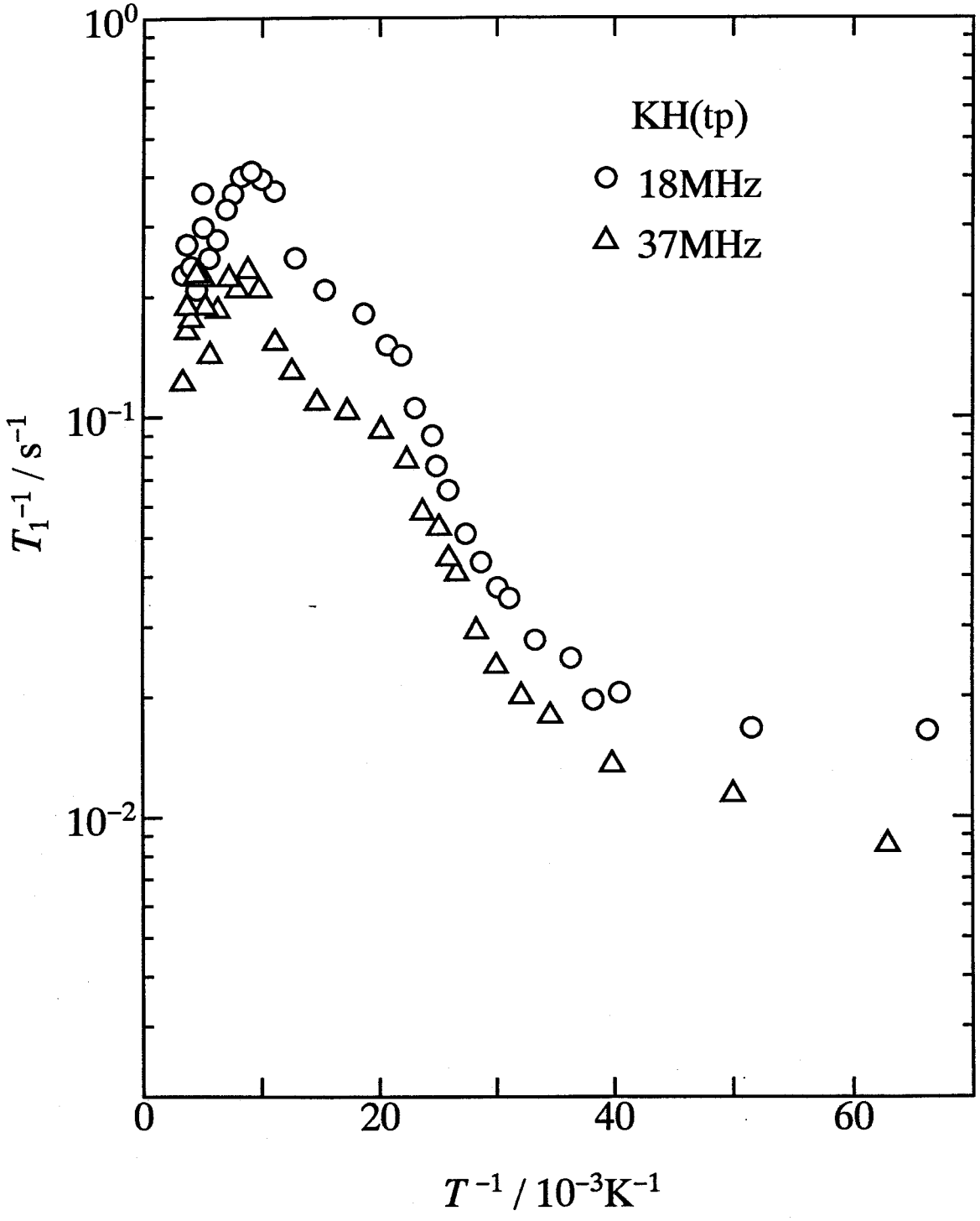

Figure 5.6: Arrhenius plot of T_1^{-1} of proton of KH(tp) at ν_L = 18MHz:open circle and 37MHz:open triangle.

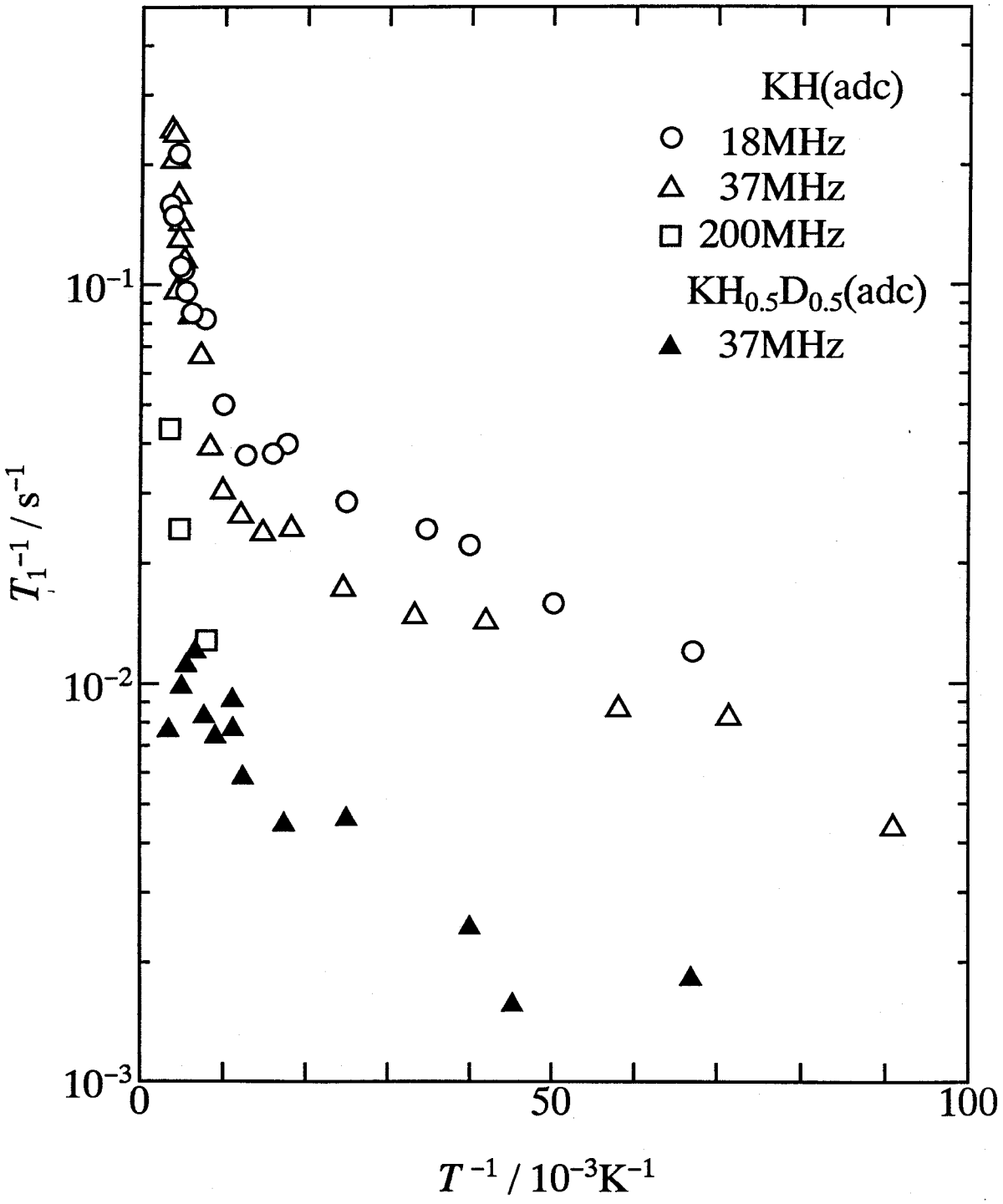

Figure 5.7: Arrhenius plot of T_1^{-1} of proton of KH(adc) at ν_L = 18MHz:open circle, 37MHz:open triangle, and 200MHz:open square, and $T_1^{-1}$of $KH_{0.5}D_{0.5}$(adc):closed triangle.

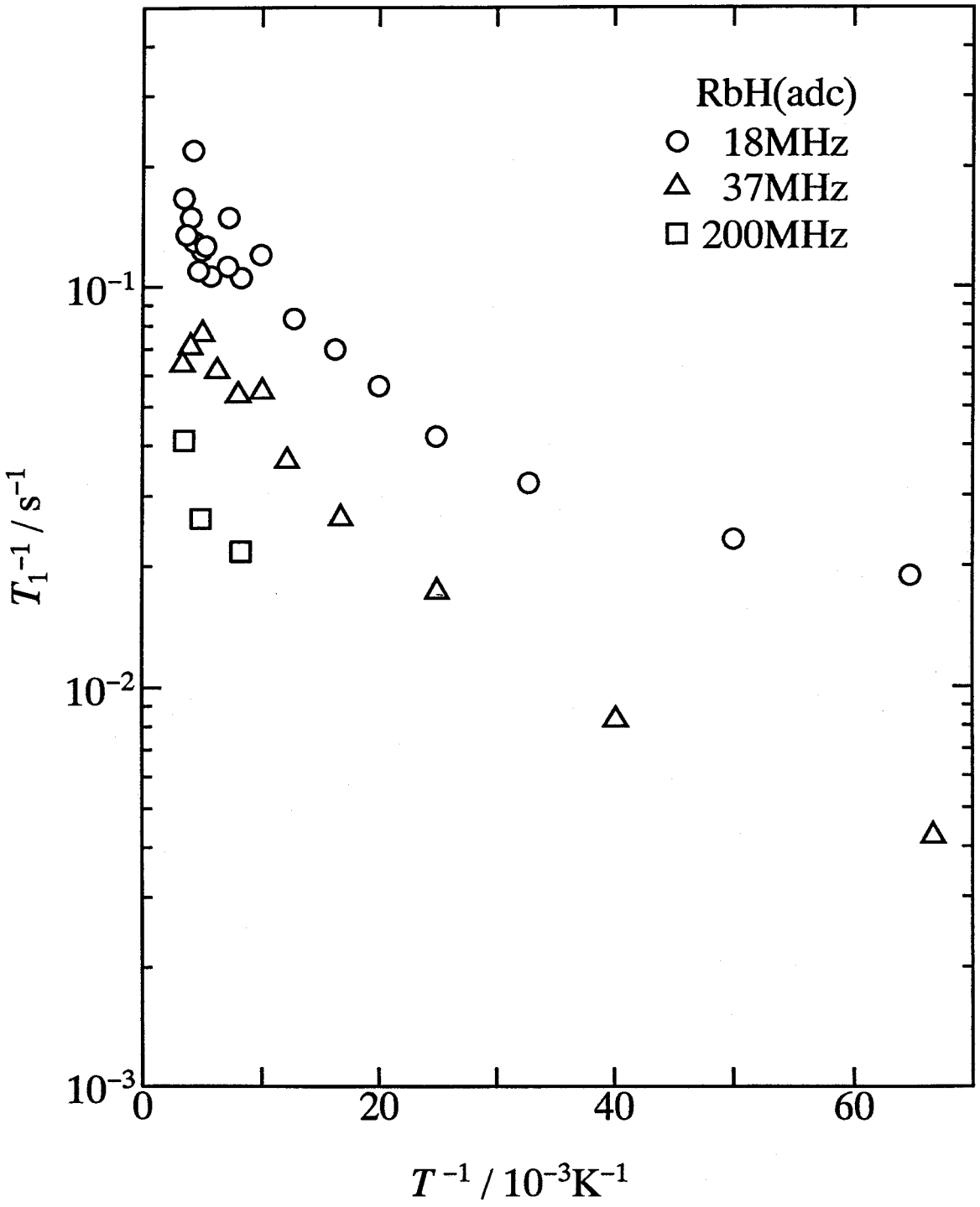

Figure 5.8: Arrhenius plot of T_1^{-1} of proton of RbH(adc) at ν_L = 18MHz:open circle, 37MHz:open triangle, and 200MHz:open square.

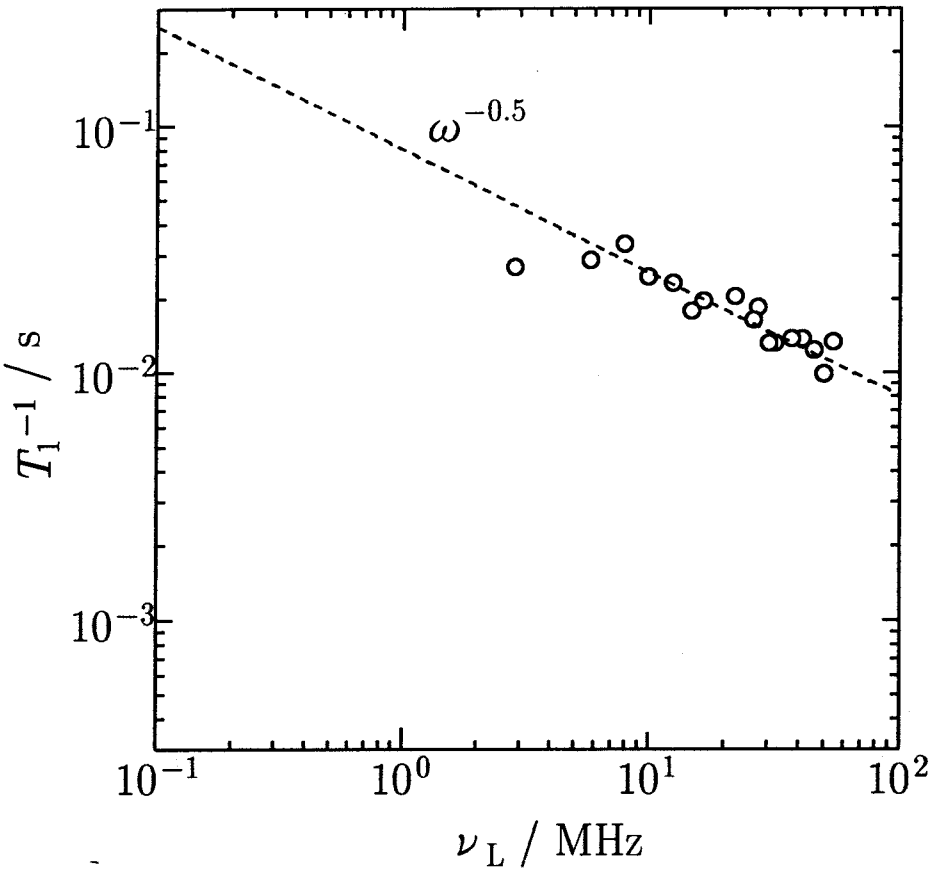

Figure 5.9: ν_L dependence of T_1^{-1} of KH(tp) by field cycling at 30K.

One tentative approach to interpret such relaxation behavior is to apply the well-known BBP equation (Eq. (5.6)) to the observed T_1^{-1} with τ_c obeying the Arrhenius activated process (Eq. (5.7)) as has been usually done in the presence of random molecular motion. But this approach does not apply to the present case because the BPP theory predicts that the T_1^{-1} is proportional to ω^{-2} in slow motional region, whereas the T_1^{-1} in the present work has weaker ω_L dependence than the case that $T_1^{-1} \propto {\omega_L}^{-2}$. Next, we introduce the effect of the interaction between neighboring hydrogen bonds as is described in section 5.2. Here two distinguishable models are considered.

1. Kink soliton model. In this case the interaction between the neighboring hydrogen bonds is very strong, *i.e.*, $C \gg A$ in Eqs. (5.8) and (5.9), and Skinner's correlation function described in the subsection 5.2.2 is applied.

2. Pseudo-kink soliton model. When the interaction between the neighboring hydrogen bonds becomes comparable with the barrier height of the local double minimum potential, *i.e.*, $C \sim A$ in Eqs. (5.8) and (5.9), the ideal shape of the kink soliton will be partially destroyed. The correlation between the motion of hydrogen atoms, however, remains to some extent.

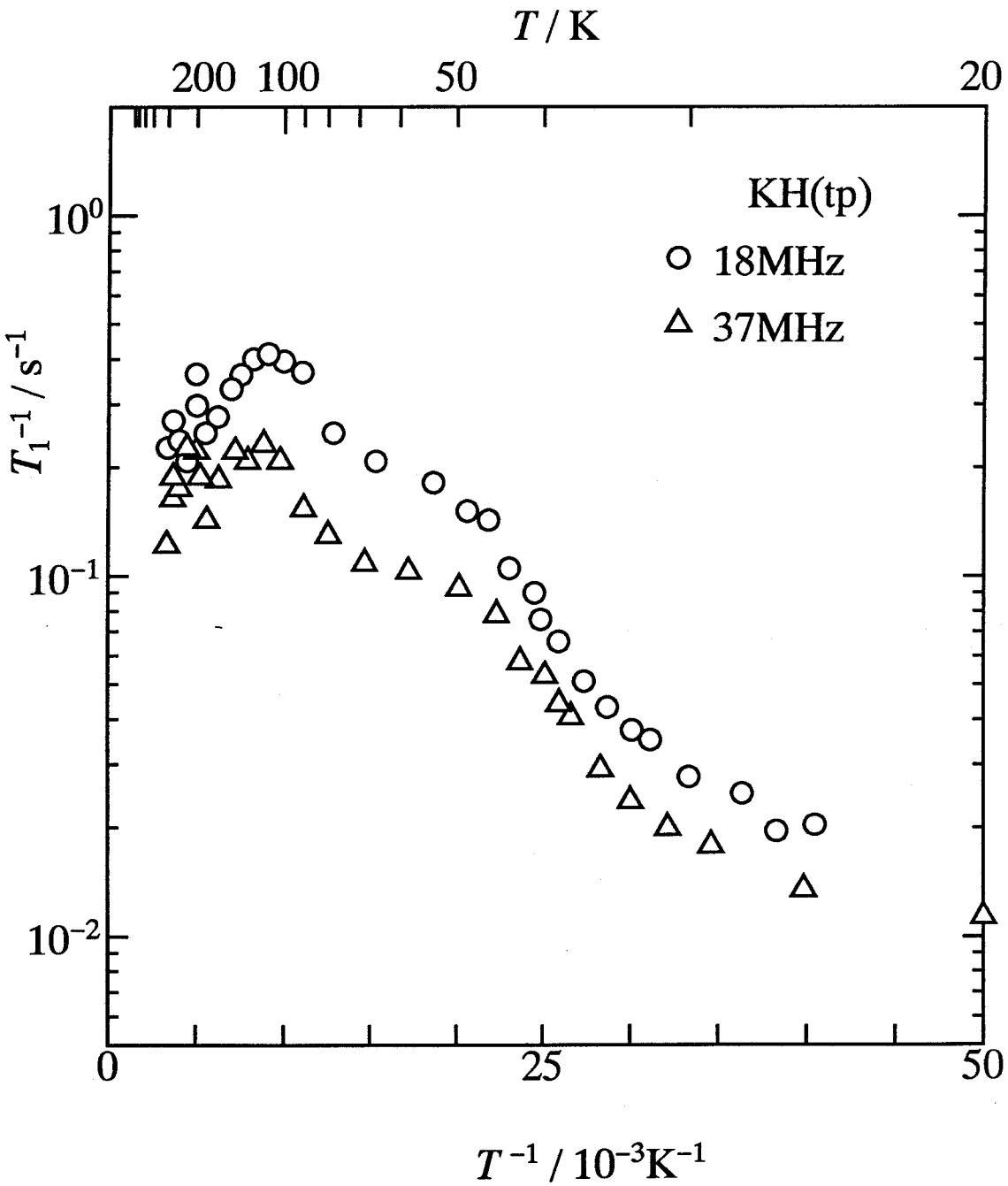

Figure 5.10: Arrhenius plot of T_1^{-1} of KH(tp) in high temperature region at ν_L = 18MHz:open circle and 37MHz:open triangle.

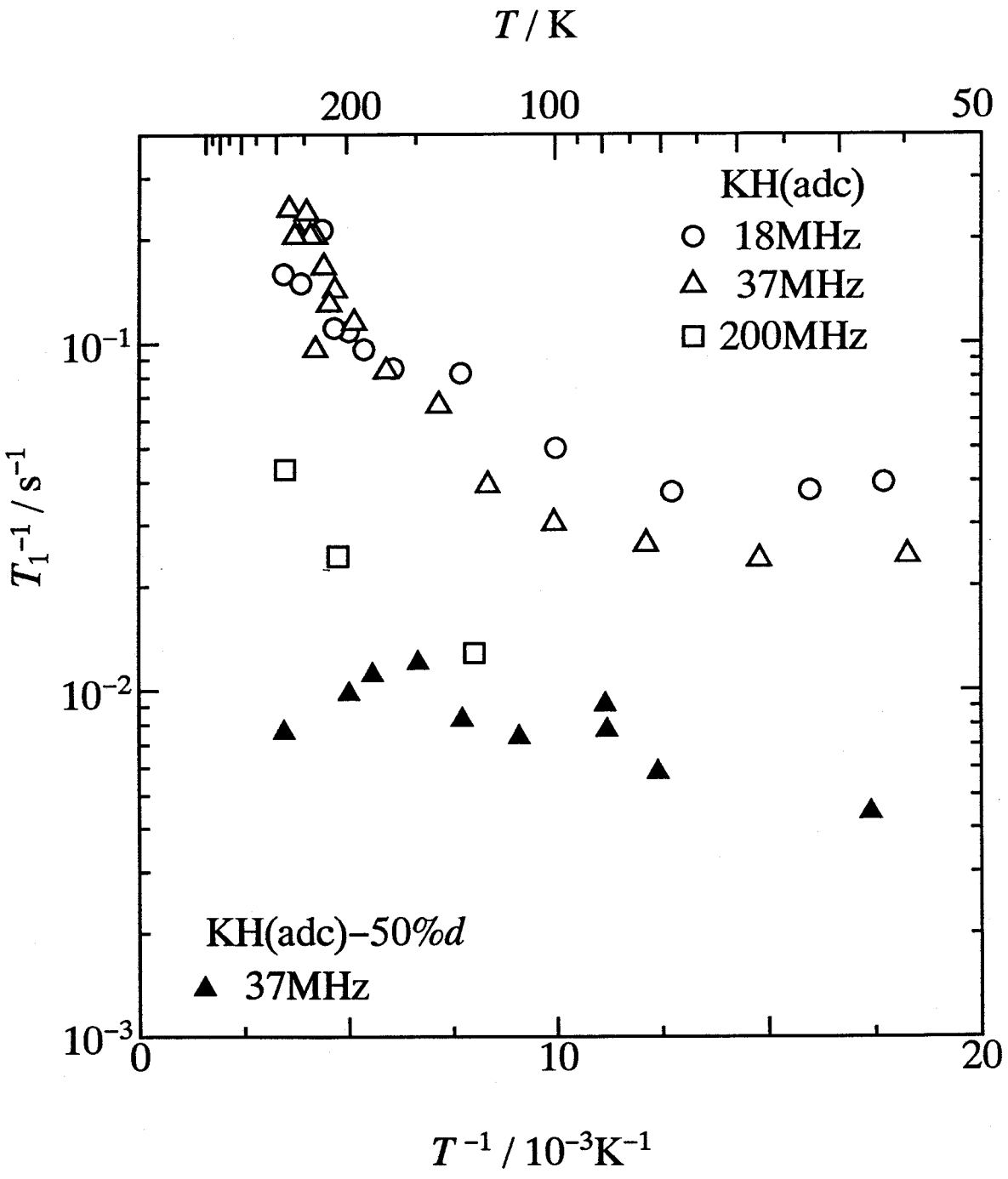

Figure 5.11: Arrhenius plot of T_1^{-1} of KH(adc) in high temperature region at ν_L = 18MHz:open circle, 37MHz:open triangle, 200MHz:open square, and $T_1^{-1}$of $KH_{0.5}D_{0.5}$(adc):closed triangle.

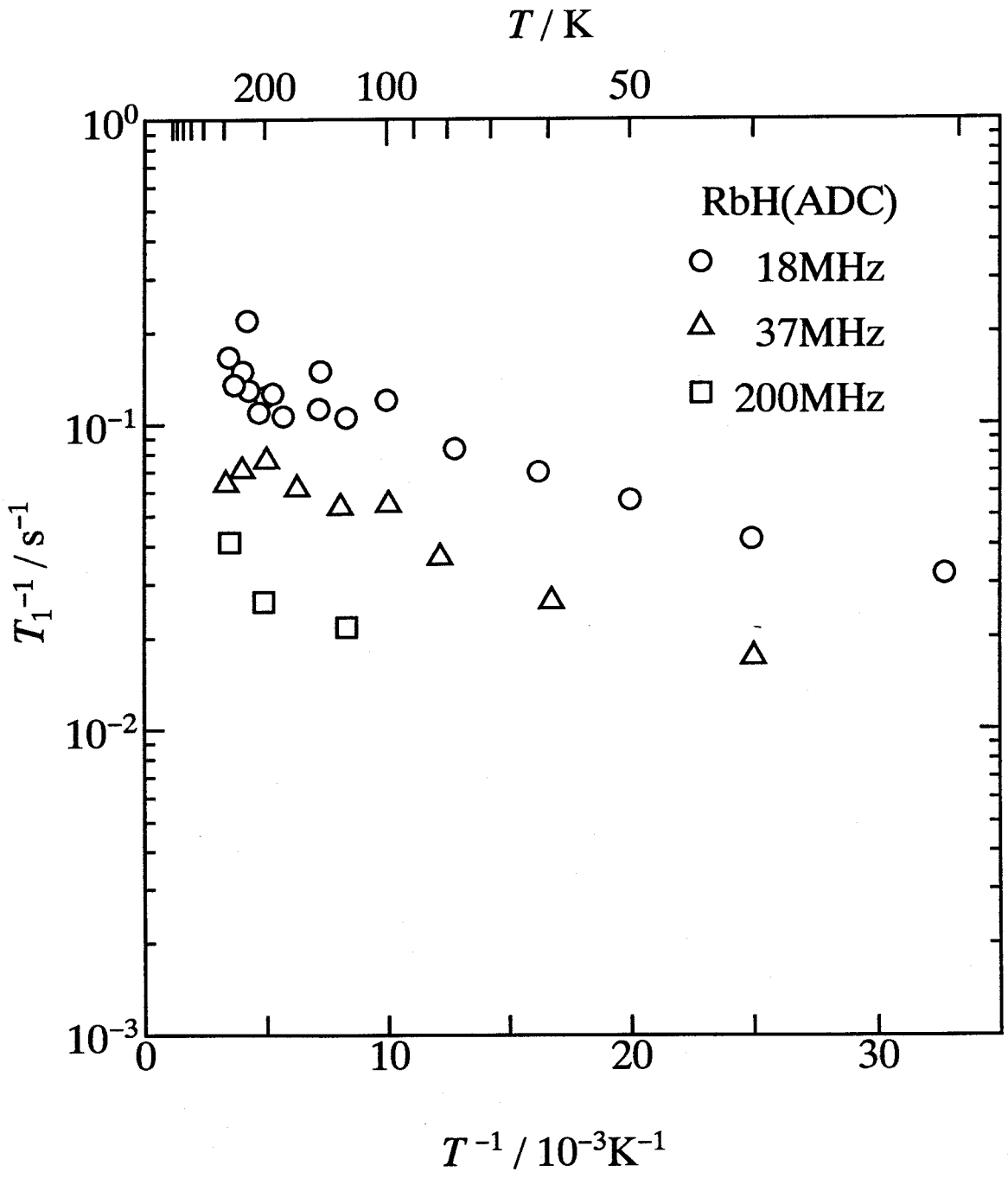

Figure 5.12: Arrhenius plot of T_1^{-1} of RbH(adc) in high temperature region at ν_L = 18MHz:open circle, 37MHz:open triangle, and 200MHz:open square.

5.5.1 Kink soliton model

In the analysis of the present T_1^{-1} data in three materials the Skinner's model considering a number of solitons diffusing in the chain is applied. But the correlation function of Eq. (5.15) in low friction limit is ruled out because it gives apparently the same result as BPP theory. Now we apply Skinner's correlation function in high friction limit (Eq. (5.16)) to derive the rigorous formulation of T_1^{-1}. As mentioned previously $J(\omega)$ is the Fourier transform of the time correlation function $g(\tau)$ in Eq. (5.16), *i.e.*

$$J(\omega) = \frac{\sqrt{2\pi}}{|\omega|}\frac{1}{\sqrt{\omega\tau_s}}g\left(\frac{1}{\sqrt{2\pi\omega\tau_s}}\right) \tag{5.19}$$

with

$$g(z) = \left[\frac{1}{2} - C(z)\right]\cos(\frac{\pi}{2}z^2) + \left[\frac{1}{2} - S(z)\right]\sin(\frac{\pi}{2}z^2). \tag{5.20}$$

In Eq. (5.19) C(z) and S(z) are Fresnel integrals

$$C(z) = \int_0^z \cos\left(\frac{\pi}{2}t^2\right)dt \text{ and } S(z) = \int_0^z \sin\left(\frac{\pi}{2}t^2\right)dt. \tag{5.21}$$

Replacing $1/\sqrt{2\pi\omega\tau_s}$ to p, $J(\omega)$ is approximated as

$$j(\omega) \simeq \frac{2\pi p}{\omega(2 + 4.142p + 3.492p^2 + 6.670p^3)} \xrightarrow{p\to 0} \sqrt{\frac{2\pi}{\omega^3\tau_s}} \tag{5.22}$$

(see Eqn 7.3.33 of ref. [74]). $j(\omega)$ in the slow motion (low temperature) limit can be obtained by putting $p \to 0$. Substituting this formula into Eq. (5.3) without any restriction to p and provided that

$$\tau_s = \tau_0 \exp(E_s/RT), \tag{5.23}$$

the T_1^{-1} can be calculated. Eq. (5.23) is appropriate for the linear slope of T_1^{-1} in Arrhenius plot. The above model was tentatively applied to the experimental results. The results of the fitting of the theoretical T_1^{-1} to the experimental T_1^{-1} are shown in Figs. 5.13–5.15. Using Skinner's correlation function the ${\omega_L}^{-3/2}$ dependence of the T_1^{-1} is expected in the low temperature limit. Obviously the theoretical frequency dependence does not agree with those of the actual T_1^{-1} in the present work.

The non-exponential recoveries may be also understood using kink-promoted motion model. Protons around kink solitons relax faster by the kink-promoted motion than other protons which are far from kink solitons and relax by the spin-diffusion. Such a nonuniform relaxation scheme may cause non-exponential recoveries. The gross feature of the spin-lattice relaxation and its temperature dependence due to the soliton motion can be understood in two ways. Firstly the increase of a number of solitons in a chain upon heating brings about the increase of the frequency of the intra-hydrogen bond jump of hydrogens which causes the dipolar relaxation. Secondly the mobility of the soliton

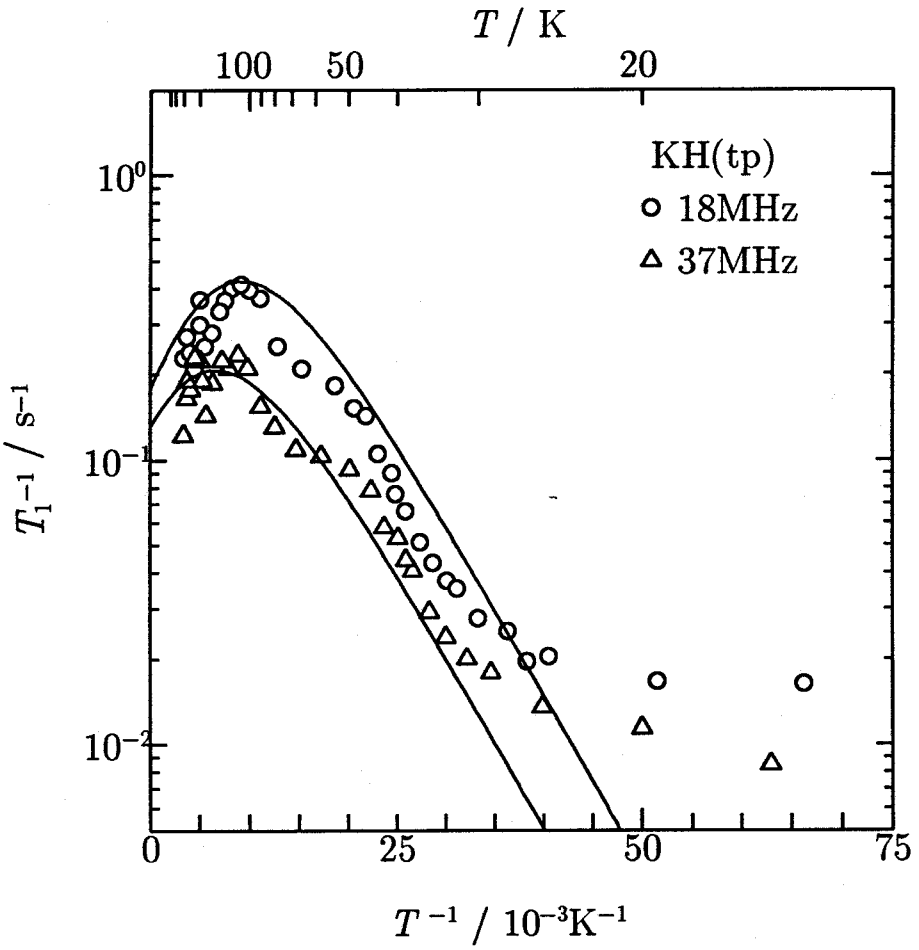

$E_s = 2.3$ kJmol^{-1}, $\tau_0 = 3.5\text{E}{-10}$s, $C_{DD} = 3.0\text{E}7$ s^{-2}

Figure 5.13: Fitting of T_1^{-1} of KH(tp) by soliton model at ν_L = 18MHz:open circle, 37MHz:open triangle

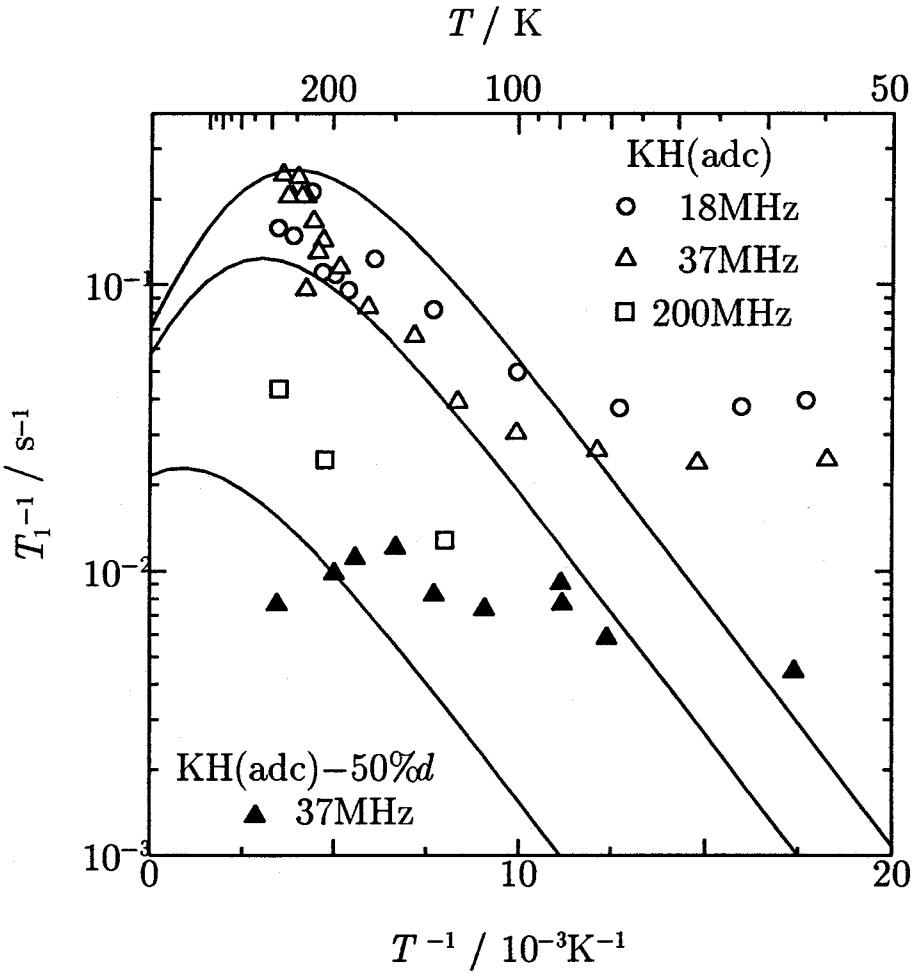

$E_a = 5.8$ kJmol^{-1}, $\tau_0 = 2.0\text{E}{-10}$ s, $C_{DD} = 1.8\text{E}7$ s^{-2}

Figure 5.14: Fitting of T_1^{-1} of KH(adc) by solitom model at ν_L = 18MHz:open circle, 37MHz:open triangle, 200MHz:open square, and $T_1^{-1}$of $KH_{0.5}D_{0.5}$(adc):closed triangle.

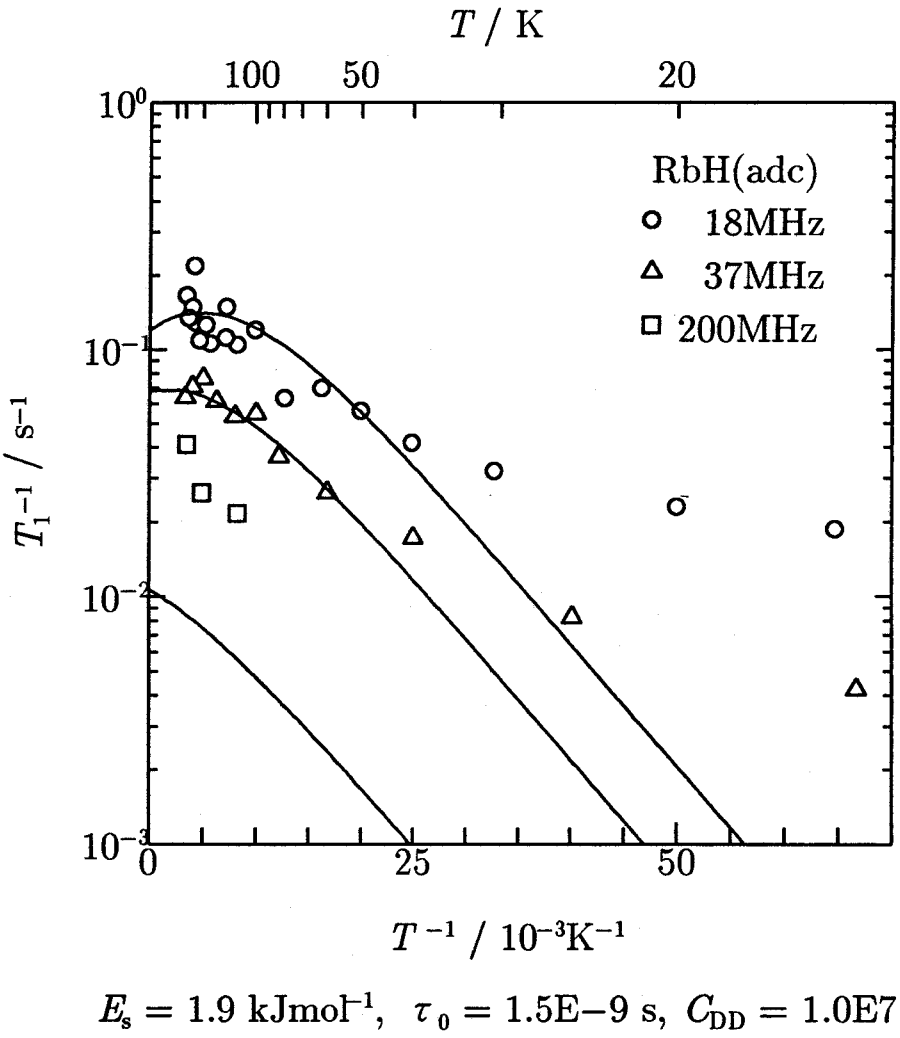

Figure 5.15: Fitting of T_1^{-1} of RbH(adc) by soliton model at ν_L = 18MHz:open circle, 37MHz:open triangle, and 200MHz:open square.

varies with increasing temperature. Comparing Eq. (5.23) with the second equation of Eq. (5.16), the temperature dependence of the T_1^{-1} seems to be derived quite naturally by assuming that n_0 increases according to Boltzmann factor. In this case E_s is interpreted as a twice of the formation energy of solitons ($2E$ in Eq. (5.13)). However, the formation energy of soliton depends on both the potential energy at the hydrogen bond and the interaction energy between neighboring hydrogen bonds. Therefore the formation energy of the soliton will strongly depend on the nature of the hydrogen bond and on the whole structure of the material. The tentatively estimated values of the formation energy of soliton for KH(tp), KH(adc) and RbH(adc) are 140K, 400K, and 115K respectively, which looks very small. The small value of the soliton formation energy is expected if the barrier height (A in Eq. (5.9)) of the double minimum potential of non interacting hydrogen bond is small (see Eq. (5.13) of the formation energy). The hydrogen bond lengths in KH(tp) (2.459Å), KH(adc) (2.446Å), and RbH(adc) (2.449Å) are short and thus barrier height A is expected to be small, yielding the small value of the soliton formation energy.

5.5.2 Pseudo kink soliton model

As can be seen in Figs. 5.13–5.15, there are some discrepancies between the model fitting and the observed T_1^{-1} for all compounds when the kink soliton model is adopted as the relaxation mechanism. We will to attempt to examine the validity of another model, the pseudo-kink model in which an intermediately strong interaction ($C \sim A$) works between the neighboring hydrogen bonds in the chain. In this case it is hardly possible to obtain the analytical formula of T_1^{-1} because the soliton like motions and the local motion of the proton in the double minimum hydrogen bond (see Fig. 5.1(b)). Thus a phenomenological model of Cole-Cole type which assumes the distribution of the correlation times is used for the analysis of the observed T_1^{-1} for all compounds.

When one watches the behavior of T_1^{-1} of KH(tp) in Fig. 5.10 two different motional modes seem to contribute to T_1^{-1}in the different temperature regions, *i.e.*, around 100K and near and lower 50K. Investigation of ω_L dependence of T_1^{-1} of KH(tp) at 30K over wide ω_L range by field cycling experiment shows that $T_1^{-1} \propto {\omega_L}^{-0.5}$. This ω_L dependence applies up to 50K. The motional mode dominating at low temperature mode was therefore assigned to the trapped kink defect in the hydrogen bonded chain. The spin-lattice relaxation process due to this mode was discussed previously in the subsection 5.2.2 and Eq. (5.18) is used for the analysis. In Eq. (5.18) the temperature dependence of C is substituted by Eq. (5.6), and is written as

$$T_1^{-1} = K_L \left\{ \frac{\tau_c}{1+{\omega_L}^2{\tau_c}^2} + \frac{4\tau_c}{1+{\omega_L}^2{\tau_c}^2} \right\}^{0.25}, \tag{5.24}$$

where K is the fitting parameter. The high temperature mode shows $\sim {\omega_L}^{-1.5}$ dependence

Table 5.1: Fitting parameters used in the fitting by pseudo kink model

sample	KH(tp)	KH(adc)	$KH_{0.5}D_{0.5}$(adc)	RbH(adc)
$R_{O\cdots O}$/Å	2.459	2.446	—	2.449
C_H/s^{-2}	2.5×10^7	4×10^7	—	4×10^7
τ_{0H}/s	3×10^{-11}	1×10^{-7}	—	2×10^{-10}
E_{aH}/K	570	2000	—	900
δ	0.65	0.3	—	0.25
$K_L/s^{-5/4}$	12	3.5	1.0	7
τ_{0L}/s	3×10^{-13}	8×10^{-9}	7×10^{-10}	2×10^{-9}
E_{aL}/K	520	100	190	100

and is assigned to the simultaneous excitation of the motion of pseudo kink soliton and the local motion of protons in the double minimum hydrogen bonds. This can be treated by Eq. (5.17) in the previous section. As shown in the following analysis of T_1^{-1} of KH(tp), KH(adc), RbH(adc), the two-modes model is rationalized for all compounds. Here it is noted that only the low temperature mode due to the trapped kink defects was observed in the proton-deuteron mixed system $KH_{0.5}D_{0.5}$(adc) (see Fig. 5.17). In this case the (pseudo) kink soliton cannot propagates even in the high temperature region, because a random distribution of proton and heavy deuteron prevent the (pseudo) kink soliton to propagate through the chain. The model calculations were performed on the three compounds and also on $KH_{0.5}D_{0.5}$(adc) . The results are shown in Figs 5.16–5.18. The solid curves are total profiles of T_1^{-1}, which can reproduce the observed T_1^{-1} satisfactory, particularly in the cases of KH(tp) and KH(adc).

The derived apparent activation energies and preexponential factors for the low temperature mode and the high temperature mode are listed in Table 5.1 together with the hydrogen bonded lengths. The parameter δ which measures the strength of the correlation between motions of protons for the high temperature mode are also tabulated. The values of δ for both KH(adc) and RbH(adc) are significantly smaller than that of KH(tp), indicating that the correlation between protons is stronger in the shorter hydrogen bonded systems in KH(adc) and RbH(adc) than in slightly longer hydrogen bonded system in KH(tp). In the longer hydrogen bonded system the local double minimum character is stronger because of its larger barrier height (A), provided that the interaction potential (C) assumes similar value in (adc) salts and (tp) salt. Thus the local mode of the proton in the double minimum hydrogen bond contributes more efficiently to T_1^{-1} in the high temperature region in the case of KH(tp) compared with the case of (adc) salts. Furthermore in the case of KH(tp) it is interesting to note that the apparent activation energy for the high temperature mode (570K) is close to 520K of the low temperature mode for the local proton motion at the trapped kink defect. In the case of (adc) salts the two

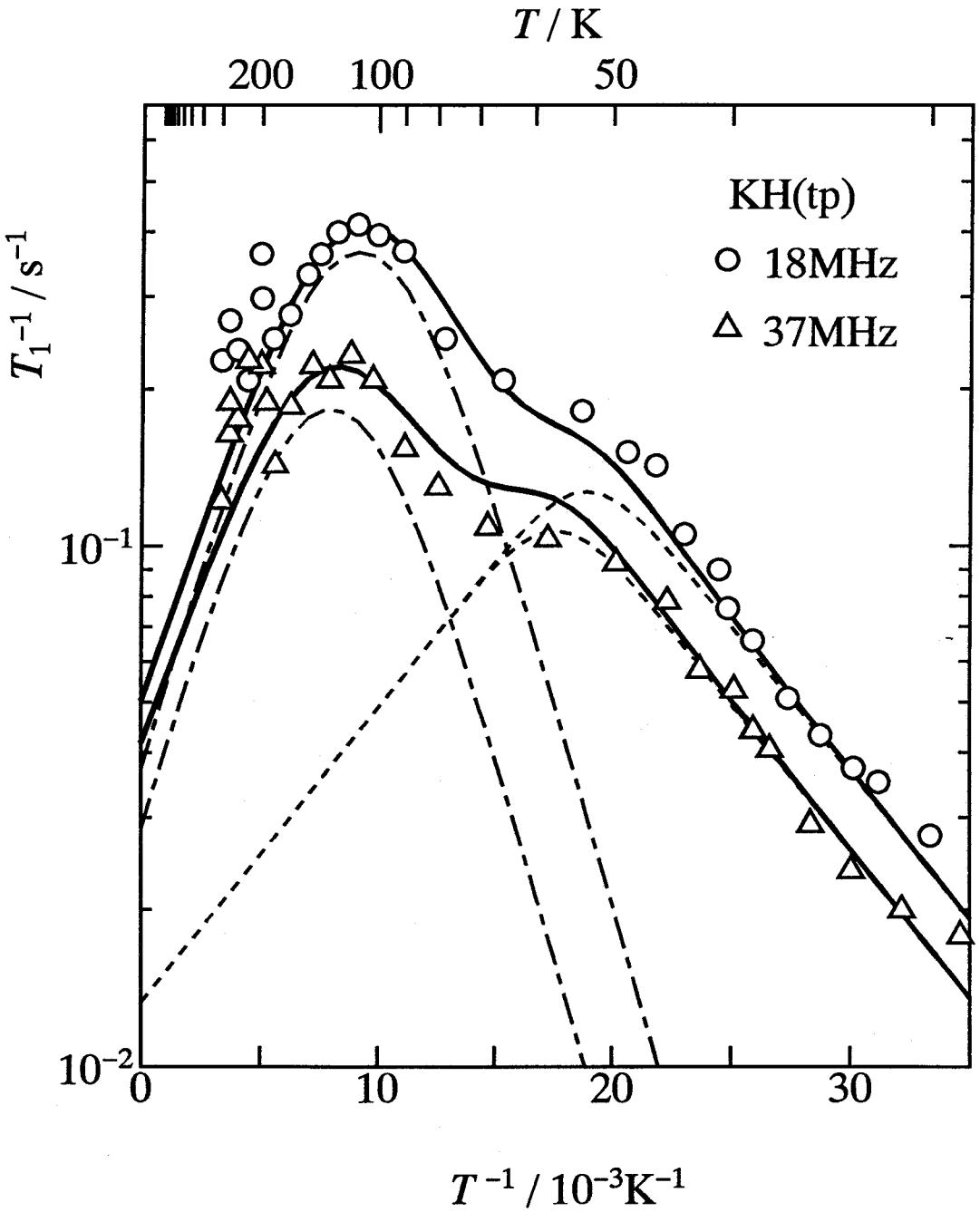

Figure 5.16: Fitting of T_1^{-1} of KH(tp) by pseudo soliton model using Eq. (5.18) and Eq. (5.17) at ν_L = 18MHz:open circle, 37MHz:open triangle

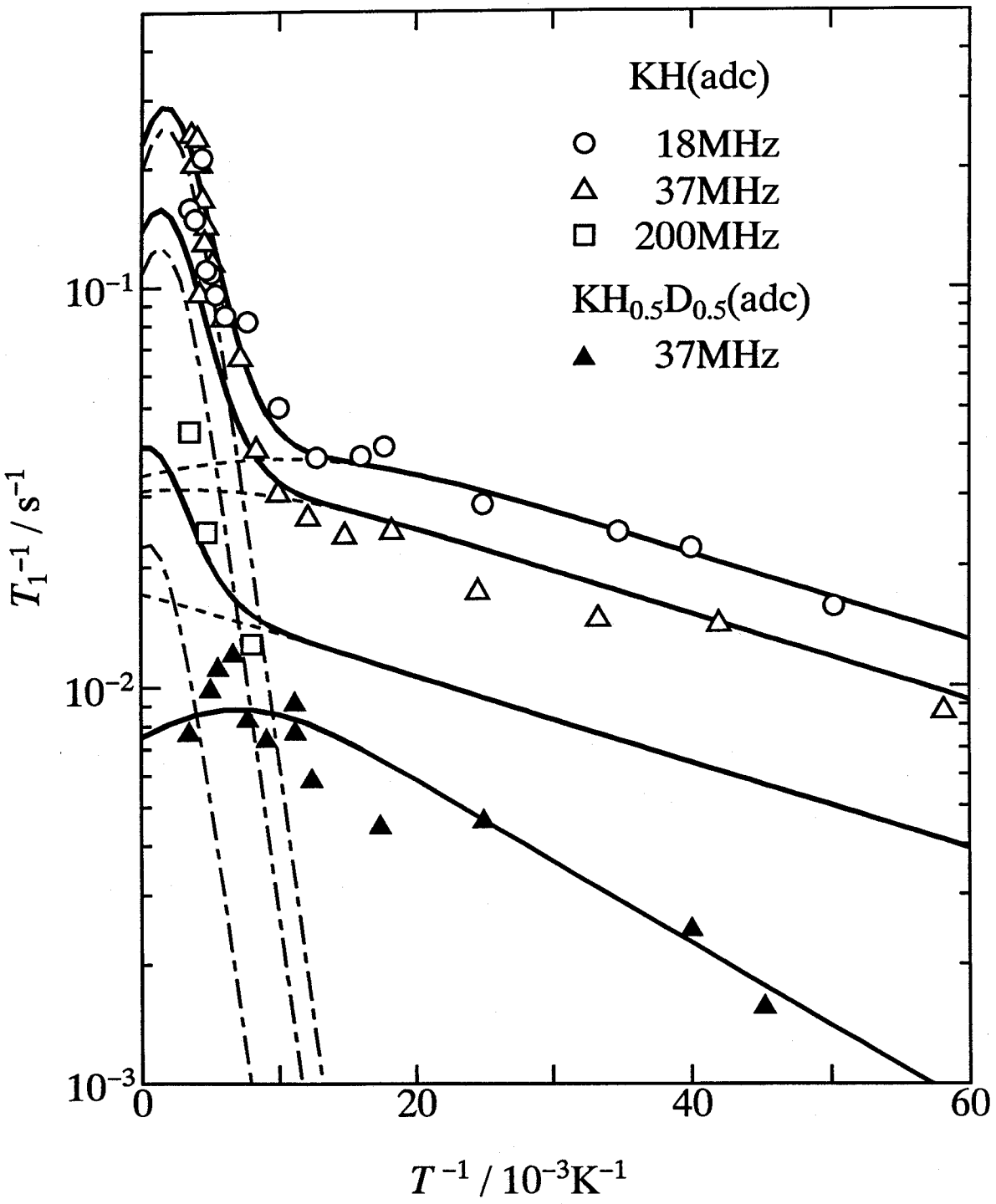

Figure 5.17: Fitting of T_1^{-1} of KH(adc) by pseudo soliton model using Eq. (5.18) and Eq. (5.17) at ν_L = 18MHz:open circle, 37MHz:open triangle, 200MHz:open square, and $T_1^{-1}$of $KH_{0.5}D_{0.5}$(adc):closed triangle.

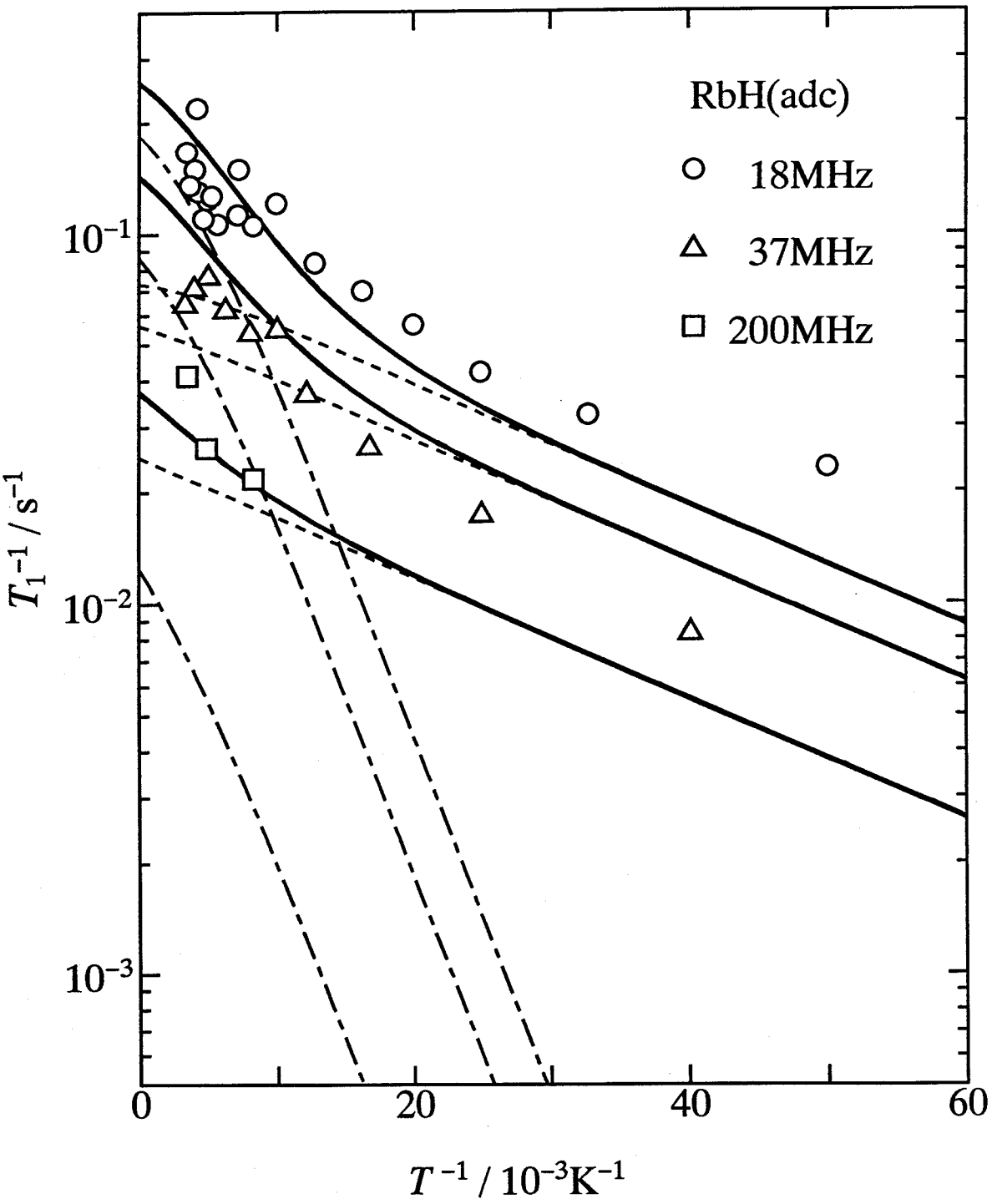

Figure 5.18: Fitting of T_1^{-1} of RbH(adc) by pseudo soliton model using Eq. (5.18) and Eq. (5.17) at ν_L = 18MHz:open circle, 37MHz:open triangle, and 200MHz:open square.

values are much different from each other, 2000K and 100K for KH(adc), and 900K and 150K for RbH(adc). Then the results probably suggest that the high temperature mode in (adc) salts contains much more pseudo kink soliton propagation than in KH(tp).

Bibliography

[1] Y. Kashimori, T. Kikuchi, and K. Nishimoto, *J. Chem. Phys.*, **77**, 1904 (1982).

[2] V. Y. Antonchenko, A. S. Davydov, and A. V. Zolotariuk, *Phys. Status Solid.*, **115b**, 631 (1983).

[3] M. Peyrard, S. Pnevmatikos, and N. Flytzanis, *Phys. Rev. A*, **36**, 903 (1987).

[4] G. B. Blanchet and C. R. Fincher, Jr., *Phys. Rev. Lett.*, **54**, 1310 (1985).

[5] Y. Moritomo, Y. Tokura, T. Oohashi, T. Kojima, and A. Itsubo, *J. Chem. Phys.*, **96**, 8507 (1992).

[6] F. Fillaux, A. Lautié, J. Tomkinson, and G. J. Kearley, *Chem. Phys.*, **154**, 135 (1991).

[7] F. Fillaux and J. Tomkinson, *Chem. Phys.*, **158**, 113 (1991).

[8] N. Kalsbeek and S. Larsen, *Acta Crystallogr.*, **C47**, 1005 (1991).

[9] N. Kalsbeek, *Acta Crystallogr.*, **C47**, 1649 (1991).

[10] N. Kalsbeek, *Acta Crystallogr.*, **C48**, 1389 (1992).

[11] P. R. Mallinson and C. S. Frampton, *Acta Crystallogr.*, **C48**, 1555 (1992).

[12] Y. Noda, H. Kasatani, Y. Watanabe, and H. Terauchi, *J. Phys. Soc. Jpn.*, **61**, 905 (1992).

[13] C. L. Perrin and J. D. Thoburn, *J. Am. Chem. Soc.*, **114**, 8559 (1992).

[14] P.Schuster, G.Zundel, and C. Sandorfy, ed., *Structure and Spectroscopy*, North-Holland, Amsterdam, 1976, Vol. II of *The Hydrogen Bond Recent developments in theory and experiments.*

[15] R. E. Cobbledick and R. W. H. Small, *Acta Crystallogr.*, **B28**, 2924 (1972).

[16] I. Leban, L. Golić, and J. C. Speakman, *J. Chem. Soc. Perkin Trans. 2*, **1973**, 703.

[17] J. Blain, J. C. Speakman, L. A. Stamp, I. Leban, and L. Golić, *J. Chem. Soc. Perkin Trans. 2*, **1973**, 706.

[18] J. L. Delarbre and L. Maury, *J. Raman Spec.*, **17**, 373 (1985).

[19] A. Novak, in *Structure and Bonding*, Springer, Berlin, 1974, Vol. 18, pp. 177–216.

[20] J. C. Speakman, in *Structure and Bonding*, Springer, Berlin, 1972, Vol. 12, pp. 141–199.

[21] J. Kroon and J. A. Kanters, *Acta Crystallogr.*, **B28**, 714 (1972).

[22] M. Currie, J. C. Speakman, J. A. Kanters, and J. Kroon, *J. Chem. Soc. Perkin Trans. 2*, **1975**, 1549.

[23] A. McAdam, M. Currie, and J. C. Speakman, *J. Chem. Soc. Perkin Trans. 2*, **1971**, 1994.

[24] M. Currie and J. C. Speakman, *J. Chem. Soc. (A)*, **1970**, 1923.

[25] A. L. Macdonald, J. C. Speakman, and D. Hadži, *J. Chem. Soc. Perkin Trans. 2*, **1972**, 825.

[26] S. Misaki, S. Kashino, and M. Haisa, *Acta Crystallogr.*, **C45**, 62 (1989).

[27] Molecular Structure Corporation. *TEXSAN - TEXRAY Structure Analysis Package*, 1980.

[28] C. J. Gilmore, *J. Appl. Cryst.*, **17**, 42 (1984).

[29] P. T. Beurskens, DIRDIF: Direct methods for difference structures - an automatic procedure for phase extension and refinement of difference structure factors, Technical Report 1984/1, Crystallography Laboratory, Toernooivekd, 6525 Ed Nijmegen, Netherlands, 1984.

[30] D. T. Cromer and J. T. Waber, *International Tables for X-ray Crystallography*, The Kinoch Press, Birmingham, England, 1974, Vol. IV.

[31] C. K. Johnson, ORTEP II, Report ORNL-5138, Oak Ridge National Laboratory, Oak Ridge, Tennessee, USA, 1976.

[32] I. Leban, *Cryst. Struc. Commun.*, **3**, 237 (1974).

[33] M. H. Cohen and F. Reif, in *Solid State Physics*, Academic Press, New York, 1957, Vol. 5, pp. 321–438.

[34] A. Abragam, *The Principles of Nuclear Magnetism*, Oxford University Press, 1961.

[35] T. Chiba, *J. Chem. Phys.*, **41**, 1352 (1964).

[36] R. Blinc and D. Hadži, *Nature*, **212**, 1307 (1966).

[37] T. Chiba and G. Soda, in *Magnetic Resonance and Relaxation. Proceedings of the XIVth Colloque Ampère, Ljubljana, 1966*, R. Blinc, D. Hadži, and M. Osredkar, ed., North-Holland, Amsterdam, 1967, pp. 722–727.

[38] G. Soda and T. Chiba, *J. Chem. Phys.*, **50**, 439 (1969).

[39] G. Soda and T. Chiba, *J. Phys. Soc. Japan*, **26**, 249 (1961).

[40] I. J. F. Poplett, M. Sabir, and J. A. S. Smith, *J. Chem. Soc., Faraday Trans. 2*, **77**, 1651 (1981).

[41] J. S. Waugh, L. M. Huber, and U. Haeberlen, *Phys. Rev. Lett.*, **20**, 180 (1968).

[42] U. Haeberlen and J. S. Waugh, *Phys. Rev.*, **175**, 453 (1968).

[43] U. Haeberlen, *High Resolution NMR in Solids Selective Averaging*, Academic Press, New York, 1976, Vol. Supplement 1 of *Advances in Magnetic Resonance.*

[44] B. C. Gerstein and C. R. Dybowski, *Transient Techniques in NMR of Solids*, Academic Press, Orlando, 1985.

[45] B. Berglund and R. W. Vaughan, *J. Chem. Phys.*, **73**, 2037 (1980).

[46] G. A. Jeffrey and Y. Yeon, *Acta Crystallogr.*, **B42**, 410 (1986).

[47] R. K. Harris, P. Jackson, L. H. Merwin, and B. J. Say, *J. Chem. Soc., Faraday Trans. 1*, **84**, 3649 (1988).

[48] R. Kaliaperumal, R. E. J. Sears, and J. E. Furst, *J. Chem. Phys.*, **91**, 7387 (1989).

[49] P. Jackson and R. K. Harris, *Magn. Reson. Chem.*, **26**, 1003 (1988).

[50] W.-K. Rhim, D. D. Elleman, and R. W. Vaughan, *J. Chem. Phys.*, **59**, 3740 (1973).

[51] L. González-Tovany and V. Beltrán-López, *J. Magn. Reson.*, **89**, 227 (1990).

[52] N. Bloembergen, E. M. Purcell, and R. V. Pound, *Phys. Rev.*, **73**, 679 (1948).

[53] F. Noack, in *NMR Basic Principles and Progress.*, Springer-Verlag, Berlin, 1971, Vol. 3, pp. 83–144.

[54] P. A. Beckmann, *Phys. Rep.*, **171**, 85 (1988).

[55] J. A. Krumhansl and J. R. Schrieffer, *Phys. Rev. B*, **11**, 3535 (1975).

[56] S. Aubry, *J. Chem. Phys.*, **62**, 3217 (1975).

[57] S. Aubry, *J. Chem. Phys.*, **62**, 3392 (1975).

[58] J. F. Currie, J. A. Krumhansl, A. R. Bishop, and S. E. Trullinger, *Phys. Rev. B*, **22**, 477 (1980).

[59] S. Pnevmatikos, *Phys. Rev. Lett.*, **60**, 1534 (1988).

[60] M. Nechtschein, F. Devreux, R. L. Greene, T. C. Clarke, and G. B. Street, *Phys. Rev. Lett.*, **44**, 356 (1980).

[61] K. Holczer, J. P. Boucher, F. Devreux, and M. Nechtschein, *Phys. Rev. B*, **23**, 1051 (1981).

[62] K. Mizoguchi, K. Kume, and H. Shirakawa, *Solid State Commun.*, **50**, 213 (1984).

[63] K. Mizoguchi, K. Kume, S. Masubuchi, and H. Shirakawa, *Solid State Commun.*, **59**, 465 (1986).

[64] R. Risch and K. W. Kehr, *Phys. Rev. B*, **46**, 5246 (1992).

[65] R. Kimmich, *Colloid Polymer Sci.*, **252**, 786 (1976). errata in *ibid.* **254**, 918 (1976).

[66] R. Kimmich and G. Voigt, *Z. Naturforsch.*, **33a**, 1294 (1978).

[67] W. H. Tanttila and D. J. Toms, *Solid State Commun.*, **33**, 693 (1980).

[68] E. Koivula, M. Punkkinen, W. H. Tanttila, and E. E. Ylinen, *Phys. Rev. B*, **32**, 4556 (1985).

[69] J. L. Skinner and P. G. Wolynes, *J. Chem. Phys.*, **73**, 4015 (1980).

[70] K. S. Cole and R. H. Cole, *J. Chem. Phys.*, **9**, 341 (1941).

[71] W. E. Blumberg, *Phys. Rev.*, **119**, 79 (1960).

[72] S. Takeda and H. Chihara, *J. Magn. Reson.*, **54**, 285 (1983).

[73] S. Takeda, Doctoral dissertation, Osaka University, Department of Chemistry, 1982.

[74] M. Abramowitz and I. Stegun, ed., *Handbook of Mathematical Functions*, Dover, New York, 1964.

Appendix A

Lists of structure factors

Table A.1: List of structure factors for KH(tp)

$10|F_c|$ vs. $10|F_o|$ for potassium hydrogen terephthalate, $C2/c$ Half hydrogens model (1 of 7)

k	l	Fo	Fc	sigF
^^^^^^^^ h = 0 ^^^^^^^^				
0	-14	206	204	4
0	-12	81	80	3
0	-10	307	311	5
0	-6	206	209	3
0	-4	331	338	5
0	-2	582	567	9
0	8	216	209	4
2	-12	56	47	3
2	-11	215	216	4
2	-8	128	128	3
2	-7	99	104	3
2	-5	221	225	4
2	-3	443	445	7
2	0	301	290	5
2	1	345	354	5
2	2	196	213	3
2	9	288	287	5
2	10	70	64	3
4	-9	96	96	3
4	-7	57	59	3
4	-1	139	139	3
4	0	220	217	4
4	2	57	53	3
4	5	134	130	3
4	6	156	153	3
4	10	37	25	4
^^^^^^^^ h = 1 ^^^^^^^^				
1	-15	139	134	3
1	-13	46	47	3
1	-12	181	182	3
1	-11	43	40	3
1	-10	47	45	2
1	-9	78	83	3
1	-8	57	66	2
1	-7	352	351	5
1	-6	398	396	6
1	-5	375	380	6
1	-4	273	271	4
1	-3	606	626	9
1	-2	495	506	7
1	-1	1079	1108	16
1	0	592	599	9
1	1	909	882	14
1	2	1128	1115	17
1	3	534	530	8
1	4	86	76	2
1	5	571	552	9
1	6	201	197	3
1	7	426	432	6
1	8	363	365	6
1	9	52	48	3
1	10	27	30	4
1	11	49	49	2
1	13	118	115	3
1	14	29	24	4
3	-12	78	80	3
3	-11	34	40	4
3	-9	44	52	3
3	-8	26	17	4
3	-7	96	98	3
3	-6	357	358	6
3	-5	55	53	3
3	-4	224	229	4
3	-3	30	21	3
3	-2	206	206	3
3	-1	160	153	3
3	0	62	70	2
3	1	28	8	4
3	2	219	214	4
3	3	30	25	3
3	4	233	230	4
3	5	155	148	3
3	7	95	86	3
3	8	343	341	5
3	9	49	53	3
3	11	33	34	4
5	-3	109	104	3
5	-2	56	49	3
5	-1	101	98	3
5	3	81	74	4
5	4	39	31	4
5	5	69	70	3
^^^^^^^^ h = 2 ^^^^^^^^				
0	-14	55	53	3
0	-10	482	484	7
0	-8	388	369	6
0	-6	49	78	2
0	-4	675	682	10
0	-2	177	177	3
0	0	431	408	7
0	2	1164	1135	18
0	4	1102	1071	17
0	6	28	16	2
0	8	130	132	3
0	10	410	409	6
0	12	135	134	3
0	14	31	26	4
2	-14	80	88	4
2	-13	78	72	3
2	-12	145	135	3
2	-11	94	93	3
2	-9	194	195	3
2	-8	193	196	3
2	-7	357	361	6
2	-5	87	89	2
2	-4	59	55	3
2	-3	154	161	3
2	-2	79	86	2
2	-1	132	145	2
2	0	51	33	2
2	1	1053	1049	16
2	2	647	650	10
2	4	139	133	3
2	5	157	158	3
2	6	205	203	3
2	7	374	369	6
2	8	155	162	3
2	9	126	126	3
2	10	131	125	3
2	11	150	150	3
2	12	86	77	3
2	13	111	110	3
4	-10	91	94	4
4	-9	92	89	3
4	-8	76	71	4
4	-7	130	134	3
4	-5	35	33	4
4	-4	159	157	3
4	-3	75	72	3
4	-2	79	77	3
4	-1	62	60	3
4	0	37	27	3
4	1	179	181	3
4	2	129	126	3
4	3	59	55	3
4	4	117	119	3
4	5	75	70	3
4	6	52	45	3
4	7	42	43	3
4	10	84	87	4
^^^^^^^^ h = 3 ^^^^^^^^				
1	-15	71	64	3

$10|F_c|$ vs. $10|F_o|$ for potassium hydrogen terephthalate, $C2/c$ Half hydrogens model (2 of 7)

k	l	Fo	Fc	sigF	k	l	Fo	Fc	sigF	k	l	Fo	Fc	sigF
1	-13	188	188	3	5	-1	85	76	4	4	-2	50	50	3
1	-12	178	182	3	5	1	78	72	4	4	-1	51	50	3
1	-11	143	141	3	5	3	62	57	3	4	0	89	90	3
1	-10	46	50	2						4	1	29	16	4
1	-9	46	44	2	^^^^^^^^ h = 4 ^^^^^^^^					4	2	149	149	3
1	-8	240	244	4						4	3	227	232	4
1	-7	49	28	2	0	-14	113	115	3	4	4	32	38	4
1	-6	36	39	2	0	-12	80	93	3	4	6	126	124	3
1	-5	716	701	11	0	-10	306	319	5	4	7	73	70	3
1	-4	262	266	4	0	-8	261	262	4	4	8	81	82	4
1	-3	376	385	6	0	-6	1085	1036	16					
1	-2	662	674	10	0	-4	91	63	2	^^^^^^^^ h = 5 ^^^^^^^^				
1	-1	743	754	11	0	-2	336	351	5					
1	0	453	458	7	0	0	453	443	7	1	-15	54	55	3
1	1	381	393	6	0	2	909	904	14	1	-14	91	91	3
1	2	159	143	3	0	4	709	682	11	1	-13	35	24	4
1	3	111	128	2	0	6	150	153	3	1	-12	73	79	3
1	4	24	16	2	0	8	551	554	8	1	-11	363	372	6
1	5	198	193	3	0	10	421	422	6	1	-10	112	110	3
1	6	481	471	7	0	12	280	279	5	1	-9	127	115	3
1	7	117	107	2	0	14	144	144	3	1	-8	195	197	3
1	8	67	64	3	2	-14	63	61	3	1	-7	114	118	2
1	9	587	583	9	2	-13	115	117	3	1	-6	160	153	3
1	10	174	184	3	2	-12	50	52	3	1	-5	34	60	2
1	11	111	113	3	2	-9	243	251	4	1	-4	580	571	9
1	12	66	71	3	2	-8	208	216	4	1	-3	510	514	8
1	15	67	64	3	2	-7	300	305	5	1	-2	70	64	2
3	-12	82	82	4	2	-6	115	118	3	1	-1	870	868	13
3	-11	96	94	3	2	-5	174	182	3	1	0	557	549	9
3	-10	119	118	3	2	-4	27	42	3	1	1	550	548	8
3	-8	55	56	3	2	-3	453	445	7	1	2	471	456	7
3	-6	115	114	3	2	-2	60	71	2	1	3	106	84	2
3	-5	86	83	3	2	-1	44	44	2	1	4	146	122	3
3	-4	219	229	4	2	0	23	24	3	1	5	287	268	4
3	-2	347	347	5	2	1	124	139	2	1	6	213	212	3
3	-1	53	48	3	2	2	226	225	4	1	7	158	152	3
3	0	349	349	5	2	3	713	698	11	1	8	40	35	3
3	2	213	210	4	2	4	115	114	2	1	9	35	37	3
3	3	197	201	3	2	5	228	241	4	1	10	315	315	5
3	4	333	327	5	2	6	178	175	3	1	11	285	287	5
3	5	63	64	2	2	7	109	112	3	1	12	109	114	3
3	6	125	126	3	2	11	184	181	3	1	13	36	23	4
3	8	130	126	3	2	12	65	58	3	1	14	51	56	3
3	9	78	79	3	2	14	32	21	5	3	-12	120	114	3
3	10	97	93	3	4	-9	45	40	3	3	-10	127	130	3
3	11	34	30	4	4	-8	117	118	3	3	-8	53	50	2
3	12	56	51	3	4	-7	53	47	3	3	-7	29	21	4
5	-5	92	86	4	4	-6	39	36	3	3	-6	188	185	3
5	-4	101	97	3	4	-5	171	177	3	3	-5	173	176	3
5	-3	44	37	4	4	-4	107	107	3	3	-4	94	94	3

$10|F_c|$ vs. $10|F_o|$ for potassium hydrogen terephthalate, $C2/c$ Half hydrogens model (3 of 7)

k	l	Fo	Fc	sigF
3	-3	145	145	3
3	-2	224	230	4
3	-1	162	160	3
3	0	308	318	5
3	2	285	289	5
3	5	106	109	3
3	6	80	76	3
3	8	113	107	3
3	10	190	180	4
5	-4	31	33	5
5	-3	75	69	3
5	-1	86	84	4
5	1	68	63	3
5	2	44	44	4
5	4	60	70	3
^^^^^^^^ h = 6 ^^^^^^^^				
0	-14	97	92	3
0	-12	252	261	4
0	-10	66	90	3
0	-8	242	258	4
0	-6	817	807	12
0	-4	395	375	6
0	-2	863	849	13
0	0	285	261	4
0	2	164	175	3
0	4	1144	1070	17
0	6	69	92	2
0	8	327	330	5
0	10	44	46	3
0	12	65	57	3
2	-14	52	49	3
2	-13	86	84	3
2	-12	47	53	3
2	-10	38	46	3
2	-9	176	182	3
2	-8	108	122	3
2	-7	260	257	4
2	-5	316	319	5
2	-4	514	521	8
2	-3	405	412	6
2	-2	232	224	4
2	-1	140	142	3
2	0	110	110	2
2	1	224	221	4
2	3	127	135	2
2	4	215	207	4
2	5	277	277	4
2	6	127	127	3
2	7	238	240	4
2	9	160	162	3
2	10	92	83	3
2	11	148	146	3
2	12	68	82	3
2	13	128	133	3
4	-9	75	71	4
4	-8	79	72	4
4	-7	118	113	3
4	-6	113	113	3
4	-5	58	57	3
4	-4	39	27	3
4	-3	85	82	3
4	-2	153	150	3
4	-1	107	108	3
4	2	65	61	3
4	3	28	17	5
4	4	124	127	3
4	5	157	157	3
4	7	49	37	3
4	8	43	41	3
4	9	59	47	3
^^^^^^^^ h = 7 ^^^^^^^^				
1	-15	123	119	3
1	-14	63	64	3
1	-13	75	75	3
1	-12	43	37	3
1	-11	102	96	3
1	-10	239	250	4
1	-9	358	372	6
1	-8	159	148	3
1	-7	232	225	4
1	-5	154	153	3
1	-4	472	471	7
1	-3	69	48	2
1	-2	327	312	5
1	-1	631	614	10
1	0	693	686	11
1	1	606	614	9
1	2	173	182	3
1	3	615	587	9
1	4	127	128	2
1	5	188	154	3
1	6	229	224	4
1	7	154	138	3
1	8	86	80	3
1	9	84	84	3
1	10	65	70	3
1	11	134	126	3
1	12	116	113	3
1	13	48	46	3
1	14	38	34	4
3	-12	49	39	3
3	-10	261	271	4
3	-9	47	49	3
3	-8	85	82	3
3	-7	48	47	3
3	-6	95	96	3
3	-5	44	48	2
3	-4	124	125	3
3	-3	192	183	3
3	-2	205	203	3
3	-1	36	39	3
3	0	178	186	3
3	2	263	261	4
3	3	56	59	3
3	4	133	136	3
3	5	30	41	4
3	6	85	76	3
3	8	42	38	3
5	-3	36	31	4
5	-2	53	55	3
5	-1	45	40	4
5	1	128	123	4
^^^^^^^^ h = 8 ^^^^^^^^				
0	-12	211	206	4
0	-10	157	154	3
0	-8	76	75	3
0	-6	462	454	7
0	-4	328	327	5
0	-2	1580	1528	24
0	0	349	295	5
0	2	312	304	5
0	4	68	36	2
0	6	463	442	7
0	8	323	326	5
0	10	64	63	2
0	12	28	23	4
0	14	65	63	3
2	-14	54	54	3
2	-13	156	158	3
2	-12	48	45	3
2	-11	186	193	3
2	-9	93	104	3
2	-8	43	42	3
2	-7	231	240	4

$10|F_c|$ vs. $10|F_o|$ for potassium hydrogen terephthalate, $C2/c$ Half hydrogens model (4 of 7)

k	l	Fo	Fc	sigF
2	-6	70	77	3
2	-5	391	391	6
2	-4	131	140	3
2	-3	208	221	3
2	-2	202	199	3
2	-1	385	390	6
2	0	158	166	3
2	1	150	149	3
2	2	115	119	2
2	3	40	42	2
2	4	33	35	3
2	5	313	299	5
2	6	203	203	3
2	7	45	59	2
2	9	161	166	3
2	10	78	68	3
2	11	107	107	3
2	12	41	38	3
2	13	77	68	4
4	-9	60	66	3
4	-8	31	28	5
4	-7	84	86	4
4	-6	75	67	4
4	-5	76	77	3
4	-4	90	79	3
4	-3	172	171	3
4	-2	95	91	3
4	0	107	107	3
4	1	45	46	3
4	3	96	94	3
4	4	114	114	3
4	7	82	81	4
4	8	75	69	4

^^^^^^^^ h = 9 ^^^^^^^^

k	l	Fo	Fc	sigF
1	-14	160	160	3
1	-13	94	86	3
1	-12	39	37	3
1	-11	112	115	3
1	-10	59	58	3
1	-9	313	313	5
1	-8	356	353	6
1	-7	277	275	4
1	-6	95	94	2
1	-5	209	212	3
1	-4	163	161	3
1	-3	386	377	6
1	-1	270	243	4
1	0	469	458	7
1	1	493	487	7
1	3	490	484	7
1	4	375	368	6
1	5	239	245	4
1	7	52	45	2
1	8	56	53	2
1	10	58	59	3
1	11	29	31	4
1	13	164	154	3
3	-12	67	69	3
3	-11	86	95	4
3	-9	53	53	3
3	-8	359	367	6
3	-7	47	46	3
3	-6	110	115	3
3	-4	110	111	3
3	-3	91	89	3
3	-2	67	65	2
3	0	155	155	3
3	1	34	33	3
3	2	278	277	4
3	3	82	88	3
3	4	90	85	3
3	5	128	125	3
3	6	120	123	3
3	7	166	176	3
3	8	60	54	3
3	9	57	50	3

^^^^^^^^ h = 10 ^^^^^^^^

k	l	Fo	Fc	sigF
0	-14	176	168	3
0	-12	327	331	5
0	-10	186	182	3
0	-8	52	57	2
0	-6	384	385	6
0	-4	346	339	5
0	-2	386	394	6
0	0	783	753	12
0	2	424	414	6
0	4	189	181	3
0	6	236	225	4
0	8	148	154	3
0	10	150	156	3
0	12	142	134	3
0	14	120	122	3
2	-11	139	133	3
2	-10	193	192	3
2	-9	344	349	5
2	-8	139	137	3

^^^^^^^^ h = 11 ^^^^^^^^

k	l	Fo	Fc	sigF
1	-13	85	86	4
1	-12	60	58	3
1	-10	208	209	4
1	-9	29	26	4
1	-8	77	79	3
1	-7	683	689	10
1	-6	350	356	5
1	-5	83	81	3
1	-4	208	211	3
1	-3	277	276	4
1	-2	159	149	3
1	-1	193	187	3
1	0	72	59	2
1	1	32	38	3
1	2	102	100	2
1	3	290	284	5
1	4	375	374	6
1	5	190	183	3
1	6	81	85	3
2	-7	118	127	3
2	-6	104	110	3
2	-5	254	261	4
2	-4	120	121	3
2	-3	236	242	4
2	-2	100	102	3
2	-1	509	519	8
2	0	267	269	4
2	1	85	93	3
2	2	93	97	3
2	3	48	48	2
2	4	151	147	3
2	5	175	184	3
2	6	138	155	3
2	7	32	15	3
2	8	184	186	3
2	9	153	156	3
2	10	38	35	3
2	11	59	60	3
4	-6	127	119	3
4	-5	67	62	3
4	-4	86	85	3
4	-1	211	214	4
4	0	171	171	3
4	2	43	44	3
4	5	42	36	4
4	6	60	71	3
4	7	81	75	4

$10|F_c|$ vs. $10|F_o|$ for potassium hydrogen terephthalate, $C2/c$ Half hydrogens model (5 of 7)

k	l	Fo	Fc	sigF
1	7	266	273	4
1	8	190	205	3
1	9	51	63	3
1	10	32	41	4
3	-11	34	34	4
3	-10	68	65	3
3	-9	29	31	5
3	-8	104	104	3
3	-7	83	85	3
3	-6	191	196	3
3	-5	59	58	3
3	-4	192	192	3
3	-3	37	36	3
3	-2	218	222	4
3	-1	139	139	3
3	0	153	160	3
3	1	37	30	3
3	2	253	256	4
3	4	155	156	3
3	5	47	56	3
3	6	110	103	3
3	10	44	41	3

^^^^^^^^ h = 12 ^^^^^^^^

k	l	Fo	Fc	sigF
0	-14	91	86	4
0	-12	112	110	3
0	-10	244	243	4
0	-8	709	701	11
0	-6	522	527	8
0	-4	508	510	8
0	-2	354	357	5
0	0	449	444	7
0	2	433	429	7
0	4	39	38	3
0	6	285	296	5
0	8	187	212	3
0	10	248	262	4
0	12	70	66	3
2	-13	182	181	4
2	-12	51	47	3
2	-11	143	148	3
2	-10	119	121	3
2	-9	141	141	3
2	-8	80	85	3
2	-7	95	93	3
2	-5	281	281	4
2	-3	32	31	3
2	-2	73	68	3
2	-1	110	111	3
2	0	252	257	4
2	1	576	582	9
2	3	36	31	3
2	4	72	71	3
2	7	75	83	3
2	9	81	72	3
2	10	29	17	5
2	11	31	40	5
2	12	48	44	3
4	-8	87	94	4
4	-7	31	33	5
4	-5	36	25	4
4	-4	74	69	4
4	-3	94	98	4
4	-2	133	125	3
4	1	183	185	4
4	2	62	58	3
4	3	32	14	4
4	4	61	63	3
4	6	44	42	4

^^^^^^^^ h = 13 ^^^^^^^^

k	l	Fo	Fc	sigF
1	-13	69	72	3
1	-12	35	32	4
1	-11	177	174	3
1	-10	66	64	3
1	-9	76	81	3
1	-7	50	54	2
1	-6	458	457	7
1	-5	540	546	8
1	-4	136	136	3
1	-3	323	322	5
1	-2	326	321	5
1	-1	173	175	3
1	0	262	268	4
1	1	129	137	3
1	2	236	235	4
1	3	257	257	4
1	4	231	236	4
1	5	171	172	3
1	6	31	35	4
1	7	39	36	3
1	8	149	151	3
1	9	175	182	3
1	10	60	59	3
1	12	46	51	3
3	-11	70	65	3
3	-10	46	40	3
3	-8	82	80	3
3	-6	227	234	4
3	-4	101	99	3
3	-3	103	104	3
3	-2	127	129	3
3	-1	96	92	3
3	0	264	265	4
3	1	111	117	3
3	2	116	125	3
3	4	111	111	3
3	6	121	116	3
3	8	112	109	3
3	9	48	53	3

^^^^^^^^ h = 14 ^^^^^^^^

k	l	Fo	Fc	sigF
0	-12	231	223	4
0	-10	80	89	3
0	-8	363	355	6
0	-6	284	287	5
0	-4	262	244	4
0	-2	142	137	3
0	0	237	227	4
0	2	800	803	12
0	4	148	144	3
0	6	147	148	3
0	8	67	65	3
2	-12	44	40	3
2	-11	94	94	3
2	-10	63	63	3
2	-9	245	244	4
2	-8	75	69	3
2	-7	286	293	5
2	-6	196	198	3
2	-5	116	123	3
2	-4	161	157	3
2	-3	260	265	4
2	-2	157	159	3
2	-1	206	213	4
2	0	73	81	3
2	1	60	60	3
2	2	275	273	4
2	3	345	352	5
2	4	31	19	4
2	5	88	86	3
2	7	48	50	3
2	8	35	39	4
2	9	73	78	3
2	11	104	101	3
4	-6	80	81	4
4	-4	69	70	3

$10|F_c|$ vs. $10|F_o|$ for potassium hydrogen terephthalate, $C2/c$ Half hydrogens model (6 of 7)

k	l	Fo	Fc	sigF
4	-3	74	75	3
4	-1	35	22	4
4	1	72	68	3
4	2	134	135	3
4	3	66	65	3
^^^^^^^^ h = 15 ^^^^^^^^				
1	-13	196	190	4
1	-12	92	98	3
1	-11	54	54	3
1	-10	172	166	3
1	-9	134	131	3
1	-8	39	33	3
1	-7	88	86	3
1	-6	67	58	3
1	-5	151	157	3
1	-4	175	193	3
1	-3	235	232	4
1	-2	270	262	4
1	-1	289	288	5
1	0	56	51	3
1	1	380	383	6
1	2	181	187	3
1	3	390	391	6
1	4	56	58	3
1	5	256	252	4
1	6	46	43	3
1	7	110	108	3
1	8	72	72	3
1	9	64	57	3
1	10	95	96	3
3	-10	116	114	3
3	-7	36	37	4
3	-5	74	75	4
3	-4	332	337	5
3	-3	90	84	3
3	-2	42	43	3
3	-1	72	73	3
3	0	142	148	3
3	1	66	68	3
3	2	32	35	4
3	3	77	63	3
3	4	81	75	4
3	5	54	62	3
3	6	49	45	3
3	8	32	31	5
^^^^^^^^ h = 16 ^^^^^^^^				
0	-10	166	175	3
0	-8	335	330	5
0	-6	251	252	4
0	-4	216	196	4
0	-2	109	126	3
0	0	201	203	3
0	2	232	238	4
0	4	646	651	10
0	6	38	30	3
0	8	34	38	4
2	-11	108	105	3
2	-10	69	69	3
2	-8	52	52	3
2	-7	248	245	4
2	-6	122	126	3
2	-5	270	291	4
2	-4	31	20	4
2	-2	72	78	3
2	-1	77	82	3
2	0	48	52	3
2	1	71	73	3
2	2	66	58	3
2	3	290	295	5
2	4	127	125	3
2	5	81	82	3
2	7	114	118	3
2	8	65	55	3
2	9	119	117	3
2	10	89	89	4
4	-3	37	43	4
4	-2	144	146	3
4	-1	58	60	3
4	3	75	71	3
^^^^^^^^ h = 17 ^^^^^^^^				
1	-12	124	125	3
1	-11	203	206	4
1	-10	51	48	3
1	-9	171	166	3
1	-8	123	127	3
1	-6	83	87	3
1	-5	57	47	3
1	-4	29	31	4
1	-3	261	280	4
1	-2	201	210	3
1	-1	110	98	3
1	0	70	75	3
1	1	201	200	3
1	2	230	236	4
1	3	196	194	3
1	4	224	220	4
1	5	80	87	3
1	6	188	192	3
1	8	34	25	4
1	10	81	80	4
3	-8	85	95	4
3	-7	48	51	3
3	-6	54	58	3
3	-5	40	42	4
3	-3	67	66	3
3	-2	138	140	3
3	-1	49	49	3
3	0	181	178	3
3	2	99	100	3
3	4	76	82	4
3	5	50	65	3
3	6	93	95	4
3	7	81	74	4
^^^^^^^^ h = 18 ^^^^^^^^				
0	-12	70	68	3
0	-10	77	76	4
0	-8	51	45	3
0	-6	330	333	5
0	-4	380	398	6
0	-2	56	85	3
0	0	255	259	4
0	2	44	45	3
0	4	176	174	3
0	6	34	30	4
0	8	141	146	3
0	10	108	105	4
2	-10	125	125	3
2	-8	127	130	3
2	-7	190	191	4
2	-6	61	60	3
2	-5	118	115	3
2	-4	97	103	3
2	-3	175	182	3
2	-2	34	28	4
2	-1	148	155	3
2	1	46	48	3
2	2	70	66	3
2	5	260	262	4
2	6	134	134	3
2	8	33	39	4
^^^^^^^^ h = 19 ^^^^^^^^				

$10|F_c|$ vs. $10|F_o|$ for potassium hydrogen terephthalate, $C2/c$ Half hydrogens model (7 of 7)

k	l	Fo	Fc	sigF
1	-11	50	44	3
1	-9	300	296	5
1	-8	242	239	4
1	-7	78	86	4
1	-6	34	34	4
1	-5	88	82	3
1	-4	69	73	3
1	-3	36	51	3
1	-2	125	125	3
1	-1	200	209	4
1	0	71	69	3
1	1	162	161	3
1	2	218	226	4
1	3	104	102	3
1	4	45	46	3
1	7	54	49	3
1	9	33	17	4
3	-7	36	34	4
3	-6	71	75	3
3	-5	35	35	4
3	-4	69	65	3
3	-2	37	33	4
3	-1	36	25	4
3	0	75	70	4
3	2	103	99	3
3	4	144	144	3

^^^^^^^^ h = 20 ^^^^^^^^

k	l	Fo	Fc	sigF
0	-10	273	268	5
0	-8	215	203	4
0	-6	301	292	5
0	-4	139	137	3
0	-2	268	286	4
0	0	161	151	3
0	2	129	129	3
0	4	97	96	3
0	6	137	132	3
2	-9	84	74	4
2	-7	45	50	3
2	-5	124	128	3
2	-4	100	100	3
2	-3	154	163	3
2	-2	135	130	3
2	-1	76	70	4
2	0	66	69	3
2	1	113	115	3
2	2	63	59	3
2	4	41	49	4
2	5	39	42	4
2	6	87	81	4
2	7	114	110	3

^^^^^^^^ h = 21 ^^^^^^^^

k	l	Fo	Fc	sigF
1	-8	165	171	3
1	-7	303	293	5
1	-5	68	74	3
1	-4	122	124	3
1	-3	45	46	3
1	1	90	78	3
1	2	109	106	3
1	3	154	150	3
1	5	113	112	3
1	6	95	96	4
1	7	92	92	4
1	8	31	17	5
3	-3	47	43	3
3	-2	115	105	3
3	-1	136	142	3
3	1	117	112	3
3	2	63	57	3

^^^^^^^^ h = 22 ^^^^^^^^

k	l	Fo	Fc	sigF
0	-8	149	137	3
0	-4	66	63	3
0	-2	197	205	4
0	0	201	193	4
0	2	31	40	4
0	6	94	103	4
2	-7	71	67	3
2	-6	45	50	4
2	-5	116	111	3
2	-4	98	99	3
2	-3	141	138	3
2	-2	48	56	3
2	0	197	192	4
2	1	184	181	4
2	2	53	58	3
2	3	36	38	4

^^^^^^^^ h = 23 ^^^^^^^^

k	l	Fo	Fc	sigF
1	-7	91	98	4
1	-6	154	146	3
1	-5	159	160	3
1	-4	70	80	3
1	-3	53	49	3
1	-2	54	53	3
1	-1	135	128	3
1	0	139	136	3
1	1	151	146	3
1	2	77	74	4
1	3	145	136	3
1	4	65	69	3
1	5	58	50	3
1	6	67	67	3

^^^^^^^^ h = 24 ^^^^^^^^

k	l	Fo	Fc	sigF
0	-6	35	38	4
0	-4	43	30	4
0	-2	153	160	3
0	0	93	88	3
0	2	342	341	5
0	4	79	85	4
2	-4	78	73	3
2	-3	120	119	3
2	-1	57	55	3
2	0	36	40	4
2	1	89	100	4

^^^^^^^^ h = 25 ^^^^^^^^

k	l	Fo	Fc	sigF
1	-5	256	247	4
1	-4	216	209	4
1	-1	68	65	3
1	0	88	95	4
1	1	93	81	4
1	2	93	93	4
1	3	81	82	4

^^^^^^^^ h = 26 ^^^^^^^^

k	l	Fo	Fc	sigF
0	-4	273	259	5
0	-2	249	237	4

Table A.2: List of structure factors for RbH(adc) $C2/c$, Half hydrogen model

$10|F_c|$ vs. $10|F_o|$ for rubidium hydrogen acetylenedicarboxylate, $C2/c$ Half hydrogens model (1 of 6)

k	l	Fo	Fc	sigF
^^^^^^^^	h =	0	^^^^^^^^	
0	2	1177	1162	18
0	4	804	779	12
0	6	546	532	8
2	-7	194	193	6
2	-6	201	204	5
2	-5	87	95	4
2	-3	780	815	12
2	-2	904	950	14
2	0	502	475	8
2	1	581	588	9
2	4	467	462	7
4	-5	475	486	7
4	-4	254	259	4
4	-3	239	247	4
4	-2	450	442	7
4	0	1374	1299	21
4	1	693	694	11
4	6	193	189	5
4	7	181	177	6
6	-6	336	339	6
6	-5	111	110	4
6	-4	649	668	10
6	-2	1113	1126	17
6	0	757	747	11
6	1	126	78	3
6	3	49	51	5
8	-5	290	294	5
8	-4	354	364	6
8	-3	250	257	4
8	-2	405	404	6
8	0	544	543	8
8	1	332	328	5
8	6	216	214	5
10	-6	118	112	6
10	-5	222	225	5
10	-4	167	164	5
10	-3	309	310	5
10	-1	316	312	5
10	0	143	141	4
10	2	160	149	4
12	-4	305	307	5
12	-2	402	399	6
12	-1	127	130	5
12	0	387	377	6
14	-4	120	117	6
14	-3	67	72	7
14	-2	223	226	5
14	-1	179	171	5
14	0	259	260	5
16	-1	160	162	6
16	2	84	77	6
^^^^^^^^	h =	1	^^^^^^^^	
1	-8	117	111	6
1	-7	221	217	6
1	-6	376	388	6
1	-5	497	507	8
1	-4	151	156	4
1	-3	813	854	12
1	-2	587	627	9
1	-1	417	417	6
1	0	664	669	10
1	1	1224	1311	19
1	2	73	54	3
1	3	824	802	13
1	4	579	566	9
1	5	455	447	7
1	6	150	143	6
1	7	329	316	6
3	-6	444	454	7
3	-5	51	48	6
3	-4	684	709	10
3	-3	201	195	3
3	-2	1048	1067	16
3	-1	1089	1031	17
3	0	912	871	14
3	1	204	197	3
3	2	845	852	13
3	4	602	596	9
3	5	95	90	4
3	6	297	286	6
3	7	85	85	7
5	-7	210	206	6
5	-6	106	110	5
5	-5	422	429	7
5	-4	487	502	7
5	-3	401	412	6
5	-2	523	526	8
5	-1	937	937	14
5	0	687	665	10
5	1	743	731	11
5	2	649	640	10
5	3	528	512	8
5	4	51	54	6
5	5	438	437	7
5	6	155	155	6
5	7	190	181	7
7	-7	171	181	6
7	-6	69	65	6
7	-5	243	244	5
7	-4	236	235	4
7	-3	539	552	8
7	-2	275	272	4
7	-1	958	919	15
7	0	95	98	3
7	1	679	661	10
7	2	384	381	6
7	3	545	544	8
7	4	120	119	5
7	5	303	300	5
7	6	107	90	5
9	-6	234	234	5
9	-4	397	402	6
9	-3	115	119	5
9	-2	540	547	8
9	0	776	767	12
9	1	103	104	4
9	2	434	428	7
9	3	120	119	5
9	4	243	243	5
9	5	56	45	8
9	6	182	187	6
11	-6	149	148	7
11	-5	96	102	5
11	-4	246	253	5
11	-3	330	339	5
11	-2	243	243	4
11	-1	376	372	6
11	0	267	260	5
11	1	324	324	5
11	2	258	256	5
11	3	271	270	5
11	4	165	162	6
11	5	112	108	5
13	-5	170	174	6
13	-4	88	70	5
13	-3	202	199	5
13	-2	56	56	7
13	-1	315	319	5
13	0	169	165	5
13	1	256	253	5
13	2	68	77	6
13	3	249	245	5
15	-4	181	180	6
15	-2	173	169	6
15	0	158	150	6
15	1	84	89	6

$10|F_c|$ vs. $10|F_o|$ for rubidium hydrogen acetylenedicarboxylate, $C2/c$ Half hydrogens model (2 of 6)

k	l	Fo	Fc	sigF	k	l	Fo	Fc	sigF	k	l	Fo	Fc	sigF
15	2	220	213	5	6	2	550	553	8	16	1	172	178	6
17	-1	93	87	6	6	3	196	189	4					
17	0	94	97	6	6	4	302	300	5	^^^^^^^^ h = 3 ^^^^^^^^				
					6	6	273	266	6					
^^^^^^^^ h = 2 ^^^^^^^^					8	-7	233	231	5	1	-8	150	156	6
					8	-6	256	257	5	1	-7	353	358	6
0	-8	205	211	6	8	-5	337	346	6	1	-6	195	199	5
0	-6	271	279	5	8	-4	93	90	4	1	-5	535	541	8
0	-4	354	374	6	8	-3	507	500	8	1	-4	290	289	5
0	-2	1414	1493	21	8	-2	292	287	5	1	-3	577	608	9
0	0	542	530	8	8	-1	562	552	9	1	-2	510	517	8
0	2	512	502	8	8	0	329	315	5	1	-1	865	875	13
0	4	492	467	8	8	1	535	520	8	1	0	218	234	4
0	6	136	128	6	8	2	128	122	4	1	1	736	719	11
2	-8	93	96	7	8	3	521	519	8	1	2	656	631	10
2	-7	228	222	5	8	4	319	319	6	1	3	518	516	8
2	-6	159	167	5	8	5	271	260	5	1	4	318	313	5
2	-5	655	677	10	8	6	113	112	6	1	5	345	333	6
2	-4	396	403	6	10	-6	120	115	5	1	6	128	125	5
2	-3	980	989	15	10	-5	313	320	5	3	-8	197	198	6
2	-2	59	63	3	10	-4	50	42	7	3	-6	406	413	6
2	-1	1590	1584	24	10	-3	531	541	8	3	-4	706	716	11
2	0	404	390	6	10	-2	79	82	4	3	-3	378	365	6
2	1	1485	1573	23	10	-1	375	376	6	3	-2	634	627	10
2	2	432	415	7	10	0	112	112	5	3	-1	174	155	3
2	3	429	424	7	10	1	602	601	9	3	0	1152	1135	18
2	4	150	144	5	10	2	77	72	4	3	1	74	67	3
2	5	431	426	7	10	3	432	432	7	3	2	861	863	13
2	6	188	183	6	10	4	158	156	6	3	3	49	37	6
4	-8	84	80	7	10	5	217	211	6	3	4	475	473	7
4	-7	376	387	6	12	-6	186	185	6	3	5	93	85	6
4	-5	495	505	8	12	-4	171	172	5	3	6	338	340	6
4	-4	228	236	4	12	-3	55	69	7	5	-8	76	75	7
4	-3	886	892	13	12	-2	237	233	5	5	-7	308	315	5
4	-2	587	576	9	12	-1	243	250	5	5	-6	183	182	4
4	-1	1541	1482	23	12	0	322	317	5	5	-5	266	268	5
4	0	182	182	3	12	2	194	194	5	5	-4	327	332	5
4	1	766	767	12	12	4	206	203	6	5	-3	663	664	10
4	2	287	292	5	14	-5	98	98	6	5	-2	631	612	10
4	3	872	880	13	14	-4	156	157	6	5	-1	717	711	11
4	4	97	87	5	14	-3	202	210	5	5	0	633	614	10
4	5	432	436	7	14	-2	159	163	5	5	1	310	315	5
6	-6	292	284	5	14	-1	195	188	5	5	2	236	231	4
6	-5	63	66	5	14	0	147	147	6	5	3	549	559	8
6	-4	512	519	8	14	1	160	165	6	5	4	250	253	5
6	-3	165	168	3	14	2	156	157	6	5	5	192	198	6
6	-2	235	256	4	14	3	199	189	6	5	6	146	143	6
6	-1	274	262	4	16	-3	153	151	7	7	-7	162	162	6
6	0	571	569	9	16	-1	247	254	5	7	-6	145	140	5
6	1	208	204	4	16	0	74	67	7	7	-5	462	471	7

$10|F_c|$ vs. $10|F_o|$ for rubidium hydrogen acetylenedicarboxylate, $C2/c$ Half hydrogens model (3 of 6)

k	l	Fo	Fc	sigF
7	-4	293	298	5
7	-3	626	616	9
7	-2	45	39	4
7	-1	630	616	10
7	0	468	466	7
7	1	622	622	9
7	2	210	202	4
7	3	210	207	5
7	4	72	77	6
7	5	176	178	6
9	-6	221	220	5
9	-5	128	136	5
9	-4	319	327	5
9	-3	54	57	5
9	-2	790	789	12
9	-1	56	54	5
9	0	428	434	7
9	1	183	172	4
9	2	364	368	6
9	4	346	347	6
9	5	61	50	9
11	-6	135	135	7
11	-5	264	270	5
11	-4	160	161	5
11	-3	254	253	5
11	-2	227	230	4
11	-1	255	257	5
11	0	259	255	5
11	1	368	371	6
11	2	230	237	5
11	3	62	46	8
11	4	179	179	6
13	-5	165	166	6
13	-3	255	252	5
13	-2	220	226	5
13	-1	251	245	5
13	1	210	217	5
13	3	221	220	6
15	-4	157	153	7
15	-2	120	125	5
15	-1	85	75	6
15	0	219	216	5
15	2	173	172	7

^^^^^^^^ h = 4 ^^^^^^^^

k	l	Fo	Fc	sigF
0	-8	258	258	6
0	-6	494	507	8
0	-4	985	1007	15
0	-2	1509	1524	23
0	0	1041	1043	16
0	2	796	771	12
0	4	428	433	7
2	-8	128	128	5
2	-7	177	175	5
2	-6	325	330	5
2	-5	402	414	6
2	-4	385	392	6
2	-3	572	582	9
2	-2	509	510	8
2	-1	597	597	9
2	0	808	784	12
2	1	360	359	6
2	2	343	337	6
2	3	255	243	5
2	4	298	289	5
2	5	190	191	6
4	-8	66	58	7
4	-7	244	243	5
4	-6	250	259	5
4	-5	269	264	5
4	-4	353	353	6
4	-3	584	601	9
4	-2	561	546	9
4	-1	300	308	5
4	0	534	523	8
4	1	480	473	7
4	2	124	119	5
4	3	450	449	7
4	4	166	168	6
4	5	156	151	7
6	-8	224	220	5
6	-7	76	66	6
6	-6	449	450	7
6	-5	103	94	5
6	-4	580	587	9
6	-3	256	264	4
6	-2	706	710	11
6	-1	208	187	4
6	0	944	938	14
6	1	113	100	5
6	2	581	583	9
6	4	426	427	7
6	5	137	129	6
8	-7	173	170	5
8	-6	115	115	5
8	-5	211	206	4
8	-4	357	361	6
8	-3	218	221	4
8	-2	444	445	7
8	-1	298	304	5
8	0	195	201	4
8	1	328	332	5
8	2	535	539	9
8	3	244	250	5
8	4	179	180	6
8	5	147	146	8
10	-7	153	149	6
10	-6	60	52	7
10	-5	275	271	5
10	-4	120	127	5
10	-3	113	114	5
10	-2	128	130	5
10	-1	408	406	6
10	0	84	77	4
10	1	301	301	5
10	2	250	242	5
10	3	155	156	6
10	4	83	92	7
12	-6	168	159	6
12	-4	302	293	5
12	-3	184	190	5
12	-2	363	359	6
12	0	274	276	5
12	2	341	351	6
12	3	78	55	7
14	-5	102	93	5
14	-4	162	154	6
14	-3	110	95	5
14	-2	185	185	5
14	-1	148	143	6
14	0	238	243	5
14	1	124	119	6
16	-1	103	107	6

^^^^^^^^ h = 5 ^^^^^^^^

k	l	Fo	Fc	sigF
1	-8	185	178	5
1	-7	267	264	5
1	-6	126	121	5
1	-5	459	467	7
1	-4	299	307	5
1	-3	477	477	7
1	-2	296	302	5
1	-1	807	791	12
1	0	240	241	4
1	1	742	730	11
1	2	424	424	7
1	3	453	434	7
1	4	127	126	6

$10|F_c|$ vs. $10|F_o|$ for rubidium hydrogen acetylenedicarboxylate, $C2/c$ Half hydrogens model (4 of 6)

k	l	Fo	Fc	sigF	k	l	Fo	Fc	sigF	k	l	Fo	Fc	sigF
1	5	267	272	6	11	1	80	70	6	6	-1	63	69	5
3	-8	267	265	5	11	2	166	158	6	6	0	364	377	6
3	-6	421	424	7	11	3	178	175	6	6	1	86	86	5
3	-4	432	441	7	13	-5	153	149	6	6	2	269	276	5
3	-3	315	300	5	13	-4	136	128	6	6	3	142	139	7
3	-2	776	773	12	13	-3	209	214	5	6	4	225	232	6
3	-1	140	129	4	13	-1	199	193	5	8	-7	168	169	6
3	0	611	619	9	13	1	246	249	6	8	-6	146	145	6
3	2	427	431	7	15	-2	161	145	6	8	-5	245	247	5
3	4	345	350	6	15	0	149	162	7	8	-4	177	162	4
5	-8	80	75	6						8	-3	365	369	6
5	-7	175	167	5	^^^^^^^^ h = 6 ^^^^^^^^					8	-2	109	90	4
5	-6	266	273	5						8	-1	345	352	6
5	-5	394	398	6	0	-8	183	183	6	8	0	343	343	6
5	-4	410	413	6	0	-6	268	271	5	8	1	389	390	6
5	-3	557	572	8	0	-4	753	748	11	8	2	131	137	7
5	-2	360	363	6	0	-2	302	314	5	8	3	233	234	6
5	-1	361	368	6	0	0	362	360	6	10	-7	196	187	6
5	0	357	357	6	0	2	410	410	7	10	-6	74	60	6
5	1	676	680	10	0	4	131	130	6	10	-5	211	205	5
5	2	127	116	5	2	-8	115	118	5	10	-3	385	385	6
5	3	316	322	6	2	-7	367	371	6	10	-1	361	366	6
5	4	109	110	5	2	-6	188	178	5	10	0	167	181	5
5	5	161	167	8	2	-5	515	519	8	10	1	280	297	5
7	-7	250	241	5	2	-4	110	111	5	10	2	84	83	6
7	-6	156	156	5	2	-3	625	635	9	10	3	268	278	6
7	-5	312	315	5	2	-2	381	374	6	12	-6	138	132	5
7	-3	560	555	9	2	-1	839	837	13	12	-5	121	120	5
7	-2	270	268	5	2	0	201	195	4	12	-4	150	147	6
7	-1	603	604	9	2	1	293	287	5	12	-3	69	58	7
7	0	177	189	4	2	2	174	167	5	12	-2	181	178	5
7	1	268	270	5	2	3	337	338	6	12	0	231	237	5
7	2	94	37	5	2	4	174	168	7	12	2	122	119	6
7	3	325	331	6	4	-8	83	86	6	14	-4	102	104	6
7	4	160	171	7	4	-7	238	234	5	14	-3	153	150	7
9	-6	213	219	5	4	-6	88	90	4	14	-2	136	141	5
9	-4	516	519	8	4	-5	509	522	8	14	-1	93	103	6
9	-2	311	318	5	4	-4	333	332	5					
9	-1	142	135	5	4	-3	595	605	9	^^^^^^^^ h = 7 ^^^^^^^^				
9	0	337	339	6	4	-2	192	203	4					
9	2	286	291	5	4	-1	545	546	8	1	-7	280	278	5
9	3	81	75	6	4	1	708	709	11	1	-6	181	185	5
9	4	71	76	8	4	2	168	169	5	1	-5	239	236	5
11	-6	148	142	6	4	3	285	293	6	1	-4	259	261	5
11	-5	169	171	5	6	-8	172	165	6	1	-3	513	508	8
11	-4	189	178	5	6	-6	277	271	5	1	-2	111	110	5
11	-3	253	258	5	6	-5	60	67	6	1	-1	484	483	8
11	-2	198	200	5	6	-4	203	207	4	1	0	550	541	8
11	-1	368	375	6	6	-3	135	124	4	1	1	293	291	5
11	0	221	216	5	6	-2	475	481	7	1	2	188	178	6

$10|F_c|$ vs. $10|F_o|$ for rubidium hydrogen acetylenedicarboxylate, $C2/c$ Half hydrogens model (5 of 6)

k	l	Fo	Fc	sigF	k	l	Fo	Fc	sigF	k	l	Fo	Fc	sigF
1	3	284	292	6	13	-4	85	65	6	10	-5	122	117	6
3	-6	199	193	6	13	-3	124	122	6	10	-3	186	191	6
3	-6	307	303	5	13	-2	82	71	7	10	-2	106	109	5
3	-5	250	244	5	13	-1	174	179	6	10	-1	190	199	6
3	-4	477	480	7						10	0	105	111	6
3	-3	78	82	4	^^^^^^^^		h =	8	^^^^^^^^	10	1	144	146	6
3	-2	541	546	8						12	-5	76	54	8
3	0	553	559	9	0	-8	199	192	6	12	-4	204	203	6
3	1	79	88	6	0	-6	548	544	9	12	-2	177	190	6
3	2	436	428	7	0	-4	406	401	6					
3	3	135	120	6	0	-2	501	498	8	^^^^^^^^		h =	9	^^^^^^^^
5	-8	134	135	7	0	0	549	540	9					
5	-7	191	183	5	0	2	159	157	7	1	-8	93	89	7
5	-6	190	186	5	2	-8	137	135	6	1	-7	133	137	5
5	-5	300	303	5	2	-7	174	172	6	1	-6	119	117	5
5	-4	231	231	5	2	-6	134	131	6	1	-5	323	310	6
5	-3	262	263	5	2	-5	263	264	5	1	-3	358	347	6
5	-2	392	391	6	2	-4	307	308	5	1	-2	342	334	6
5	-1	378	368	6	2	-3	443	443	7	1	-1	343	332	6
5	0	76	70	5	2	-2	302	299	5	1	0	126	123	6
5	1	271	286	5	2	-1	51	62	8	1	1	363	352	6
5	2	180	185	6	2	0	205	197	5	3	-8	156	168	7
5	3	125	135	6	2	1	242	246	5	3	-7	100	96	6
7	-7	190	184	5	2	2	245	245	6	3	-6	213	209	5
7	-6	90	85	5	2	3	232	225	7	3	-4	317	318	6
7	-5	379	378	6	4	-8	79	79	7	3	-2	356	356	6
7	-4	152	153	5	4	-7	186	182	6	3	0	241	244	5
7	-3	351	354	6	4	-6	236	239	5	3	1	130	126	6
7	-2	219	231	5	4	-5	269	265	5	3	2	188	189	7
7	-1	230	233	5	4	-4	149	157	5	5	-7	180	172	6
7	0	91	93	5	4	-3	183	176	5	5	-6	168	166	6
7	1	247	249	5	4	-2	158	165	5	5	-5	229	227	5
7	2	159	162	6	4	-1	426	429	7	5	-4	232	234	5
7	3	120	130	5	4	0	160	169	6	5	-3	234	241	5
9	-6	252	259	5	4	1	208	211	6	5	-2	53	40	8
9	-4	297	301	5	6	-6	203	207	5	5	-1	341	352	6
9	-3	88	85	5	6	-4	419	420	7	5	0	137	139	7
9	-2	322	332	6	6	-2	446	449	7	5	1	181	183	7
9	-1	56	55	8	6	-1	113	97	5	7	-7	182	184	6
9	0	261	267	5	6	0	320	328	6	7	-5	208	207	5
9	1	60	46	8	6	2	336	343	6	7	-4	124	132	5
9	2	166	177	7	8	-7	106	97	5	7	-3	263	259	5
11	-6	83	79	7	8	-6	137	135	7	7	-1	189	192	6
11	-5	162	160	6	8	-5	148	148	6	7	1	145	157	6
11	-4	122	129	5	8	-4	204	191	5	9	-6	198	205	6
11	-3	188	190	5	8	-3	151	153	6	9	-4	168	168	6
11	-2	179	173	5	8	-2	237	234	5	9	-2	139	137	7
11	-1	82	86	6	8	-1	250	264	5	9	0	158	161	7
11	0	156	151	6	8	0	250	252	5	11	-4	114	110	5
11	1	106	106	6	8	1	154	166	7	11	-3	156	162	7

$10|F_c|$ vs. $10|F_o|$ for rubidium hydrogen acetylenedicarboxylate, $C2/c$ Half hydrogens model (6 of 6)

k	l	Fo	Fc	sigF	k	l	Fo	Fc	sigF	k	l	Fo	Fc	sigF
11	-2	113	103	5										
					^^^^^^^^ h = 12 ^^^^^^^^									
^^^^^^^^ h = 10 ^^^^^^^^														
					0	-4	180	162	7					
0	-6	190	180	6	2	-5	119	112	6					
0	-4	220	222	5	2	-4	101	84	7					
0	-2	239	237	6	2	-3	74	75	9					
0	0	96	89	7										
2	-7	211	207	6										
2	-6	111	101	5										
2	-5	292	293	6										
2	-4	158	147	6										
2	-3	173	163	6										
2	-2	86	81	6										
2	-1	247	249	6										
2	0	150	153	8										
4	-7	192	191	6										
4	-5	185	184	6										
4	-4	106	118	5										
4	-3	331	338	6										
4	-1	276	284	6										
6	-6	157	146	7										
6	-5	74	59	7										
6	-4	208	213	6										
6	-3	82	82	6										
6	-2	167	169	6										
6	0	222	221	6										
8	-6	93	84	6										
8	-5	142	137	7										
8	-3	192	206	6										
8	-2	187	195	6										
8	-1	173	171	7										
^^^^^^^^ h = 11 ^^^^^^^^														
1	-7	138	124	6										
1	-5	175	168	7										
1	-4	167	161	7										
1	-3	215	213	6										
1	-2	154	156	8										
1	-1	203	185	7										
3	-6	207	200	6										
3	-4	249	238	6										
3	-2	208	215	6										
5	-6	92	96	7										
5	-5	90	86	7										
5	-4	74	74	8										
5	-3	215	219	6										
5	-2	92	91	7										
7	-4	85	72	7										